CENTRIFUGE STUDIES OF CYCLIC LATERAL LOAD-DISPLACEMENT BEHAVIOR OF SINGLE PILES

Ronald F. Scott

Report Through May 30, 1978
Research Program

for

American Petroleum Institute
OSAPR Project 8

June 15, 1978

Soil Mechanics Laboratory
Division of Engineering and Applied Science
California Institute of Technology
Pasadena, California 91125

TABLE OF CONTENTS

FIGURE CAPTIONS

FIGURE CAPTIONS (continued)

1. Introduction

In the period following the completion of the previous report of December 1977 and the end of the contract on OSAPR Project 8 with California Institute of Technology, additional pile loading tests were conducted.

Two different test series were followed through: additional load-unload cyclic tests again in simulation of the Mustang Island (MI) tests and pile vibration tests. The reasons for the first series were: (a) the model pile dimensions originally chosen for the Mustang Island simulation did not correctly represent either the El of the prototype pile, nor its width; and (b) it was desired to perform the tests in a soil more closely resembling the fine-grained MI sand, at higher relative densities than had been achieved in the earlier tests. It is worth pointing out here that it is not easy to produce a model pile with the correctly scaled EI, since, although the dimensions can be correctly calculated, they are based on an assumed E for the material which may be slightly different in the metal actually machined, and the strain gauges, leads and moisture-protection coating employed increase the EI in the final product. A further deficiency of the first test pile was that, although the model pile had been instrumented with 5 strain gauges, they had been installed in locations and at intervals that proved inconvenient in the actual centrifuge tests. Only three gauges could be positioned below ground surface. On the model pile whose use is described here, 6 strain gauges were bonded, closer together near the top, at sites such that all six gauges were at or below the soil surface. As will be seen later, this enabled much better curves of moment in the pile as a function of depth to be plotted.

The dynamic test series was designed to explore resonant behavior in a model pile-soil system at model frequencies representative of those produced in a prototype earthquake. The centrifuge scaling laws for frequency (see first report, Table 2.1) require that the model frequencies be 100 times those of the prototype at 100 g acceleration. Since earthquake frequencies of interest to structures lie generally in the range 0.2 to 20 Hertz, model frequencies of 20 to 200 Hertz are required. Earthquake strong motion durations of 10 to 50 seconds at full scale correspond to model durations of 0.1 to 0.5 seconds. Prototype earthquakes have peak strong motion lateral acceleration in the range 0.3 to 1.0 g; model simulation therefore requires 30 to 100 g equivalent accelerations. Ideally, therefore, a centrifuge earthquake to apply to a structural model would consist of a 0.1 to 0.5 second burst of essentially random vibration containing frequencies of tens to hundreds Hertz, at peak lateral g's of 30 to 100 g. Equipment to do this has not yet been developed, and a different approach was adopted for the preliminary work.

One method of treating the effects of earthquakes on a prototype structure is modal analysis which requires a knowledge of the modes of vibration of a structure in the frequency range of interest. Since an electrical signal generator was available with the capability of sweeping through a selected range of frequencies at a constant amplitude, as well as emitting a burst of signal at constant frequency for a preselected duration, it was employed to find, first, the resonant frequencies of a pile-mass system, and second, to vibrate the system at one of these frequencies for a short time.

The results of both of these studies are reported here. In addition, some time was devoted previously to analytical studies of pile-soil behavior under load; an appendix is attached describing the technique of the analysis.

2. Soils Tested

For this test sequence, a fine-grained soil named "Nevada 130 Sand" was employed. Its grain size distribution is shown in Figure 2.1, from which it can be seen to be somewhat finer than the Mustang Island sand, although possessing approximately the same uniformity. The maximum and minimum sand dry unit-weights were found to be 84.6 and 98.4 pcf, respectively. The unit weight employed in each test is given with the test description.

3. Equipment and Instrumentation

3.1 Test Apparatus

Except for the pile, the equipment and instrumentation used in pile load-unload cyclic tests were the same as described in the first report.

In order to simulate more closely the full-scale pile tests performed by Cox and Reese at Mustang Island, a new pile was machined out of aluminum with dimensions 0.240" x 0.136" x 8.00", as shown in Figure 3.1.1. Laboratory tests on the pile with strain gauges and waterproof coating installed gave 500 lb in^2 for EI, smaller than the intended prototype MI simulation value of 600 lb in^2. The impact of this difference is probably small. It means that the pile thickness was too small by 6%. It had been deliberately chosen small because of the stiffening effect of the coating, but apparently the modulus was smaller than assumed.

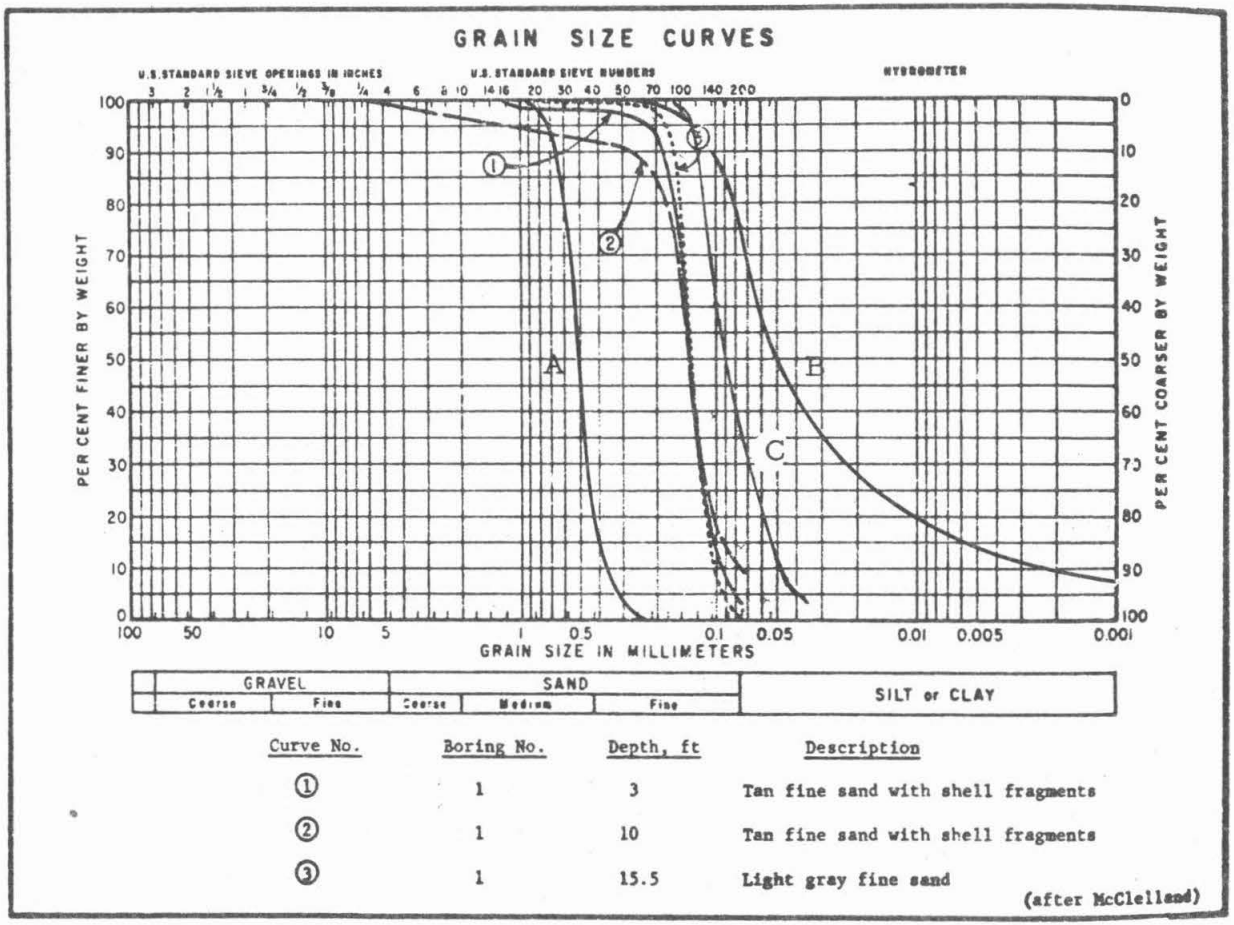

Fig. 2.1 Grain size distribution curves of soils
A. Ottawa Sand B. Santa Barbara Silt
C. Nevada Sand

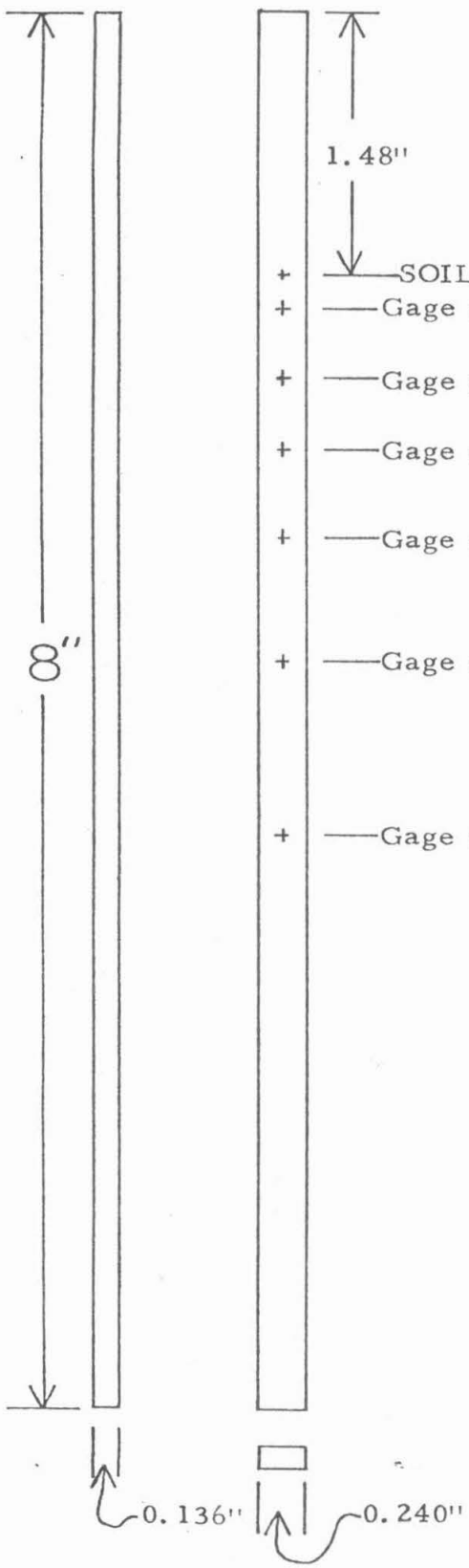

PILE- 0.240 x 0.136 x 8.00"
Aluminum

EI = 500 (with gages and protective coating) lb-in^2

Gages- Micro-Measurements
CEA-13-062UV-350
Resistance = 350.0 Ohms
Gage Factor = 2.15
Bonding Agent =BLH epy 150 two part epoxy resin

Bridge completion resistors= 350 Ohm 1% precision resistors

Fig. 3.1.1 Dimensions of model pile and instrumentation details

As can be seen in that figure, the strain gauges were closely spaced near the proposed soil level to obtain as many significant data points as possible. These gauges constituted the active arm of a Wheatstone bridge, the other three arms being composed of inactive 350 ohm precision resistors. The excitation voltage was 5.00 Vdc. In use the pile was displaced perpendicular to its 0.240" dimension so that the effective prototype diameter presented to the soil would be 24", as in the MI tests.

The vibration of the pile was achieved with a magnet/coil arrangement which can be seen in cross section in Figure 3.1.2. The magnet of cylindrical re-entrant configuration was obtained from a long-period seismometer. The magnet was mounted in a rigid aluminum framework which was bolted to the centrifuge soil container, parallel to and above the soil surface. The coil core was composed of a piece of machined plexiglass around which was wound 17 turns of 0.056" diameter copper wire in two layers. The mass of the coil and plexiglass was 72.0 gm.

A 1.00" x 0.75" x 0.35" piece of aluminum with a 0.25" slot to accommodate the pile was used to attach the pile rigidly to the coil. Bolted to this piece of aluminum was an adjustable counterweight and a visible light source whose mass was 73.5 gm, so that the total mass added to the pile top was 145.5 gm. The mass of the pile alone was 15.0 gm. The pile top, coil and magnet assembly are shown in the photographs, Figures 3.1.3, 3.1.4, and 3.1.5.

To supply the necessary current to the coil, an amplifier capable of delivering 4 amperes from DC to 1000 Hz was designed by the Caltech Electrical Engineering Department and built in the soil mechanics laboratory.

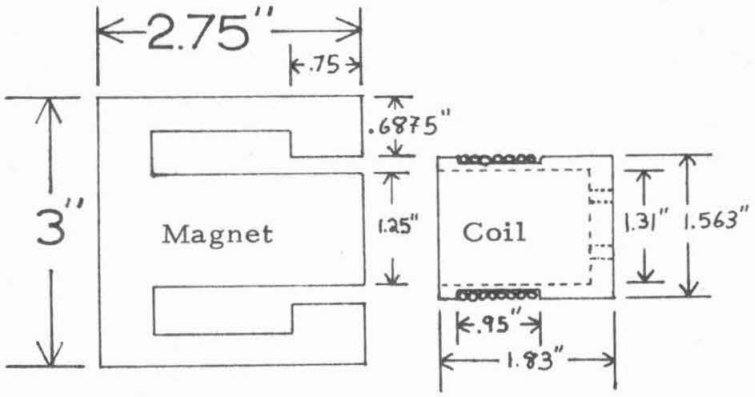

Fig. 3.1.2 Cross section of magnet and coil used in vibration tests

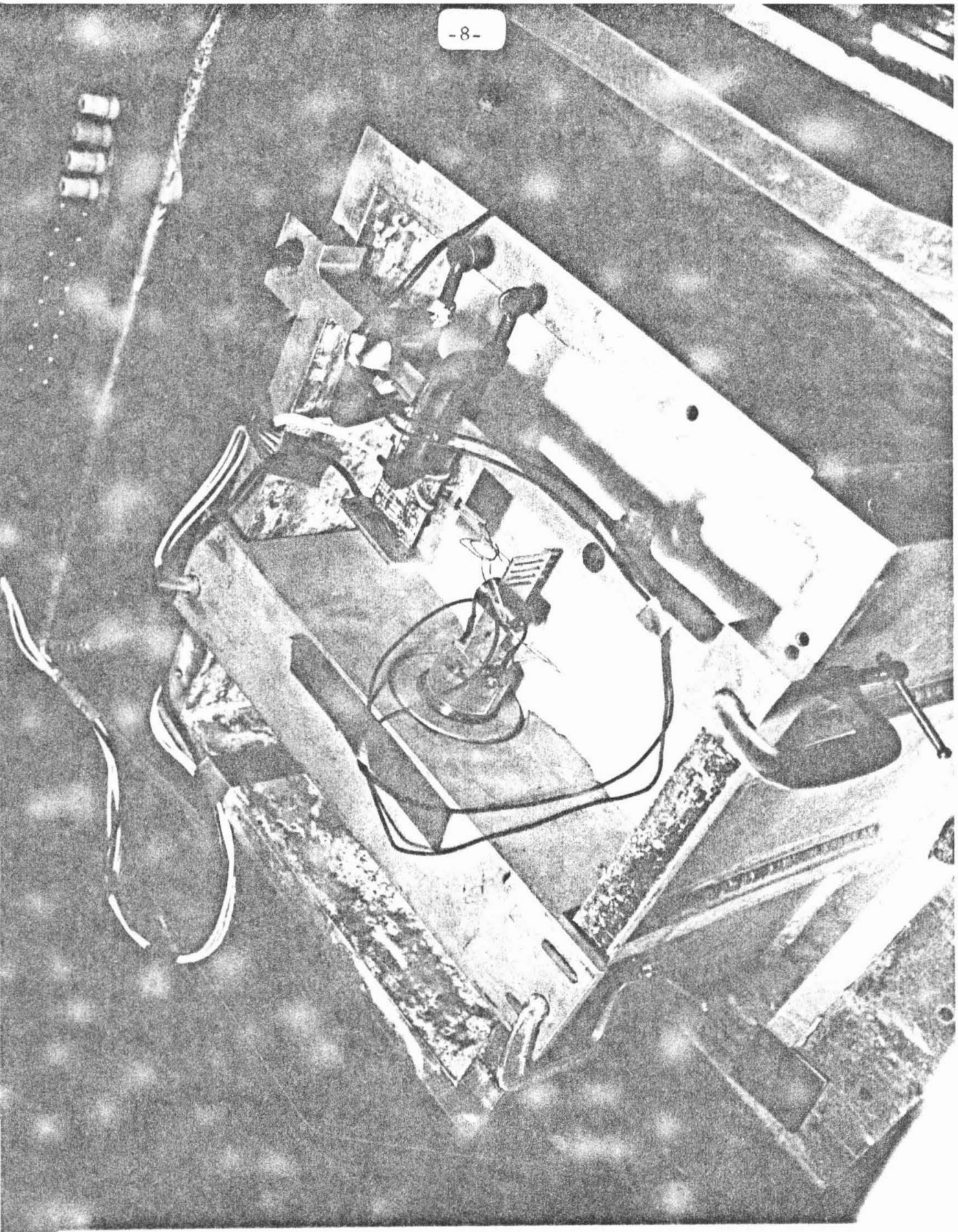

Fig. 3.1.3 View of soil container mounted on the centrifuge arm. Installation for vibration tests.

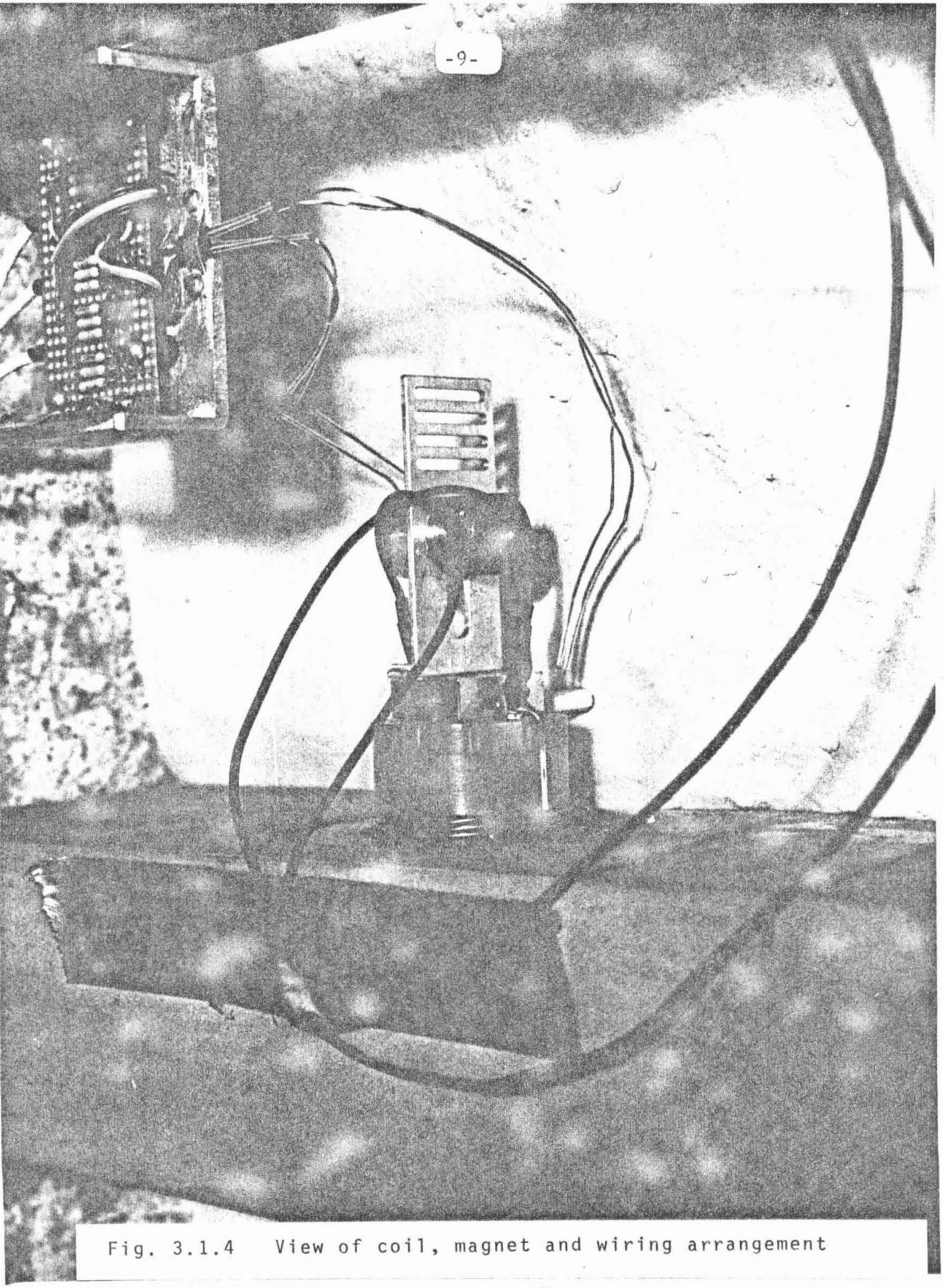

Fig. 3.1.4 View of coil, magnet and wiring arrangement

Fig. 3.1.5 Close-up of magnet and top of pile

A schematic is provided in Figure 3.1.6. A function/sweep generator Exact Model #126 was used to provide the sine wave input to the amplifier. This generator is also capable of frequency sweeps and was employed in this mode quickly to find the resonant frequencies of the pile/coil system.

To measure the dynamic pile top movement without influencing the mechanical characteristics of the system, it was decided to design and build an optical displacement detecting device to replace the cantilever beam arrangement used in the static tests. United Detector Technology in Santa Monica, California, manufactures a position-sensing detector PIN-SC/10D composed of planar diffused PIN photo diodes. When illuminated with a light spot, these detectors can detect its position with a sensitivity in both the X and Y axes of 0.0001". Schematic and dimensional drawings are provided in Figure 3.1.7. The light spot consisted of a 3.0 volt incandescent light bulb (CM 253) mounted inside a 1/2" cube of aluminum, and emitting light through a pin hole 0.0156" in diameter. The detector is insensitive to changes in the size of the light spot, making possible the use of a pin hole light source; however, the detector does respond to changes in intensity of the light. Therefore, a power supply (Hewlett-Packard #6214A) with constant current and voltage provided power to light the bulb.

3.2 Data Acquisition Systems

For the load-unload cyclic tests, the equipment was the same as was employed previously. This recording equipment was also used for the dynamic tests, but it was necessary to modify the system used to obtain signals from the pile strain gauges.

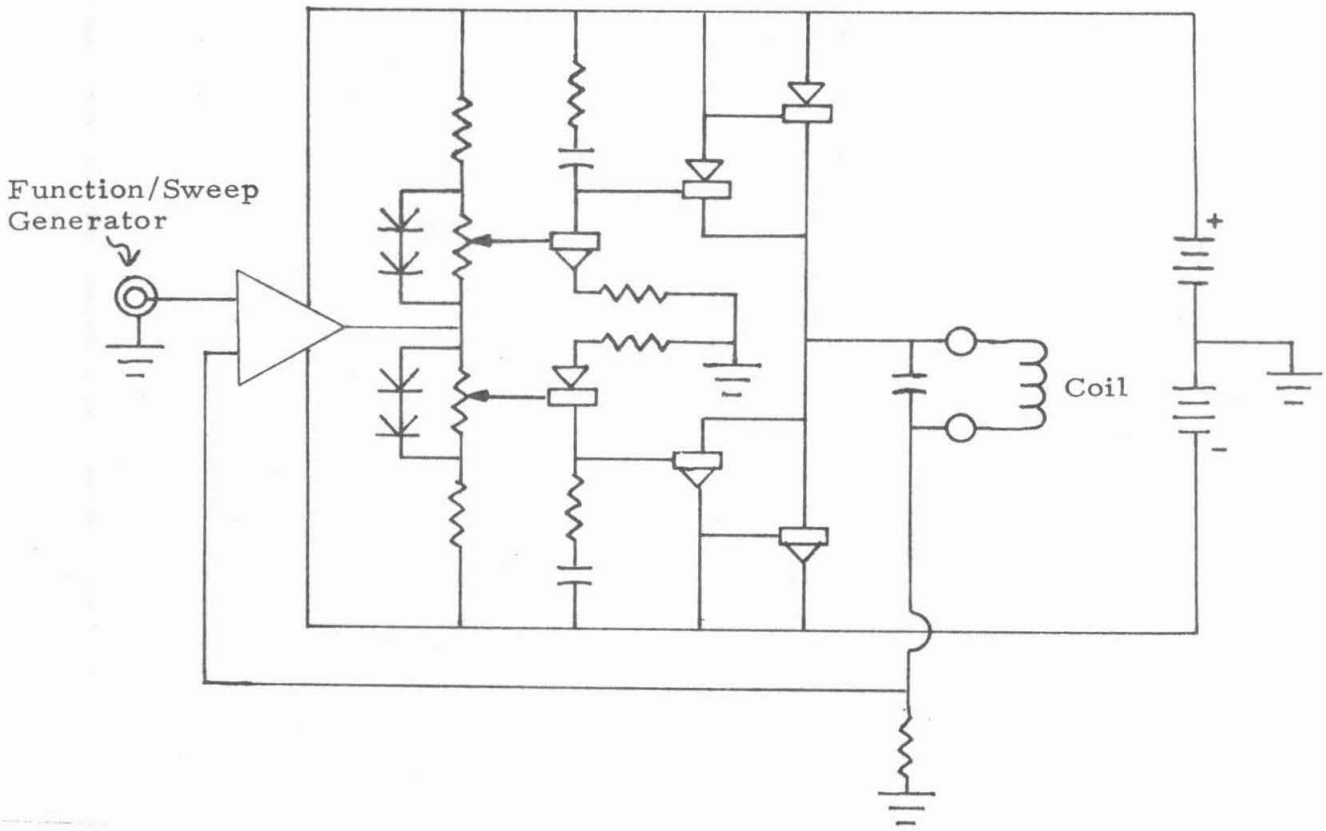

Fig. 3.1.6 Wiring schematic of 4 amp power amplifier

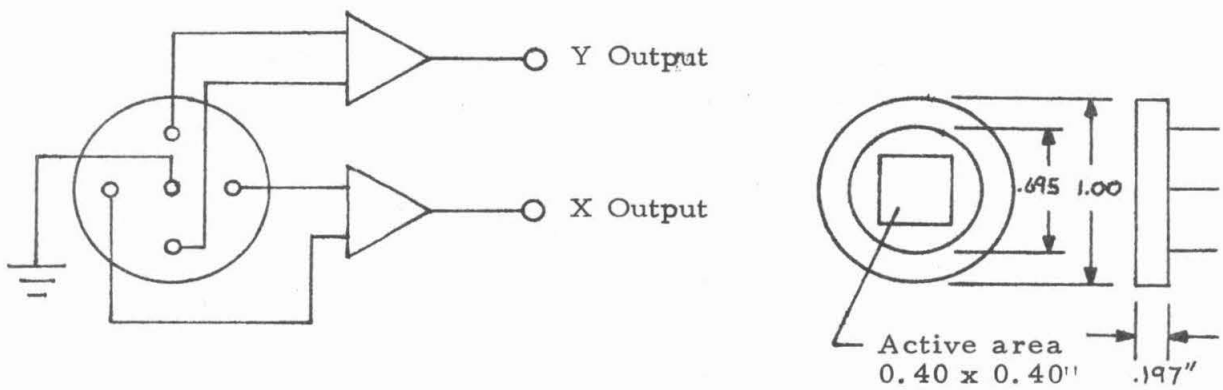

Fig. 3.1.7 Wiring schematic and dimensional drawing of optical displacement detector

For the pile vibration studies, it was realized that the already minute signal levels from the pile strain gauges would diminish further so that they would be indistinguishable from the noise level of the system. Thus a new amplifier with higher amplification and more signal channels was designed and built by the Electrical Engineering Department at Caltech. A schematic is provided in Figure 3.2.1. This new amplifier also necessitated the construction of a redesigned bridge power supply, since in the new equipment the amplifier input rather than the bridge voltage would float above the instrument ground potential. This scheme allowed the single power supply to drive all of the transducers and strain gauge bridges simultaneously. It was therefore possible to mount the power supply and the amplifier on the centrifuge arm. The advantages of this arrangement were: (a) a reduction in the number of sliprings needed; and (b) a decrease in electronic noise by elimination of the ground loops which had plagued the previous system.

3.3 Test Procedures

The procedure for testing the pile under load-unload cyclic conditions was described in the previous report. The present test series differed only in that more strain gauges were monitored at closer intervals on the pile than before.

For the dynamic tests, the procedure was as follows. After densification of the sand with a vibrator, the pile was inserted to the proper depth at 1 g. For the last inch of insertion, it was necessary to use a small hammer as the sand was quite dense. The dry unit weight was 95.2 pcf, so that the relative density was 79%. The coil was then positioned on the

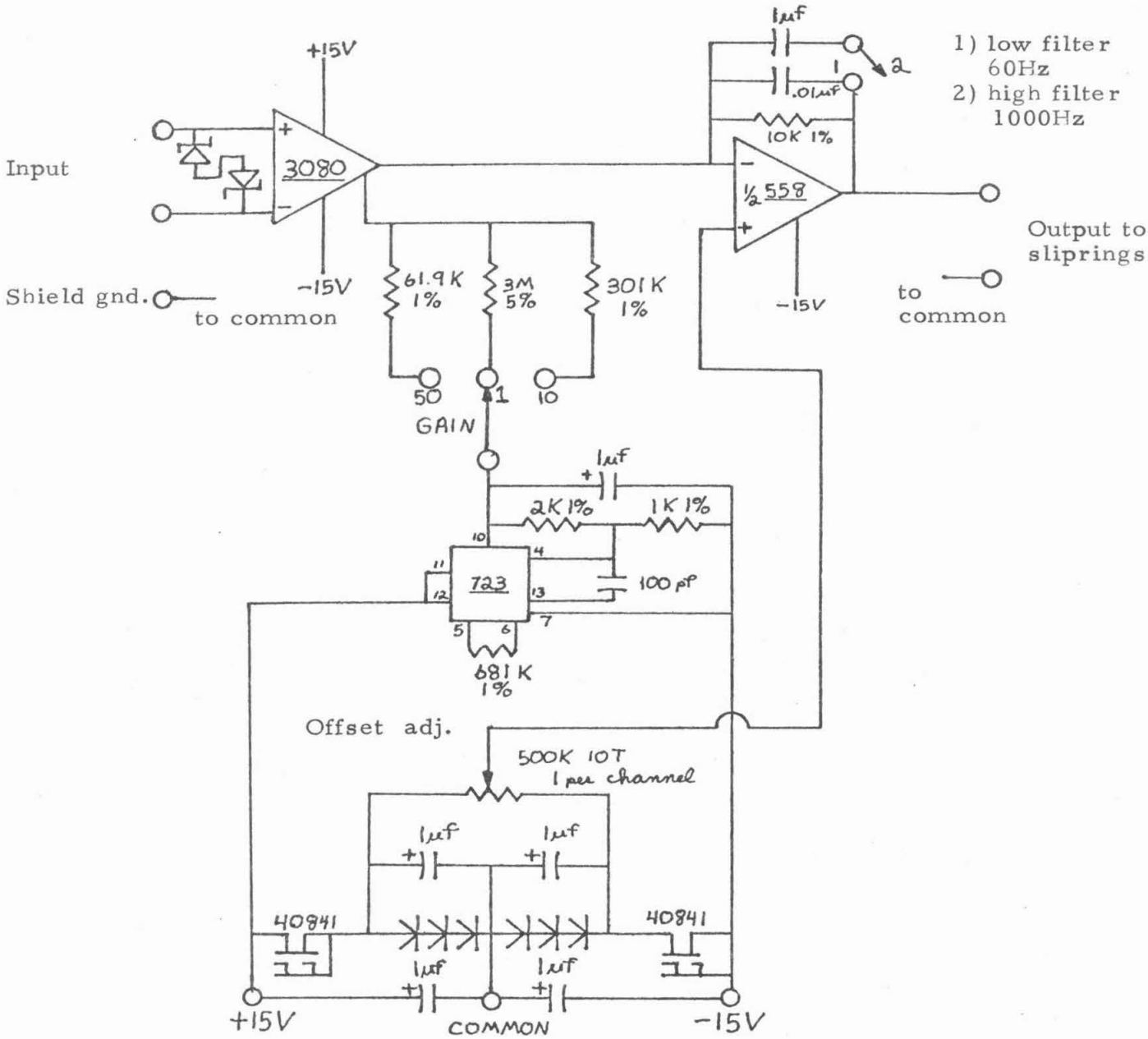

Fig. 3.2.1 Wiring schematic of 13 channel amplifier (only 1 channel shown)

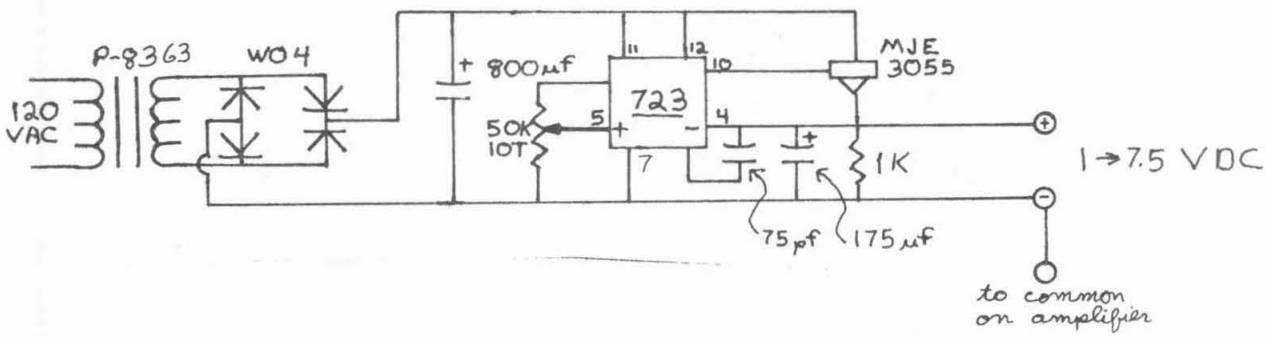

Fig. 3.2.2 Wiring schematic of bridge power supply

pile and the magnet mounted on the soil container such that the coil was in the field of the magnet (Figures 3.1.3 through 3.1.5), without making physical contact. The centrifuge was then brought to 300 rpm (100 g's). With the Visicorder oscillograph operating, the function generator was used to give several wide-range frequency sweeps, to reveal the resonance peaks. Thereafter, the range of the frequency sweeps was narrowed to include more of the region at resonance. The function generator could also be used in a burst mode so that the ring-down characteristics of the system could be observed. A representation of a section of the data record is shown in Figure 3.3.1, which illustrates a resonance peak occurring as the generator swept from 30 to 50 Hz.

3.4 Data Reduction

The load-unload test was digitized as described previously. No special data reduction procedures have yet been applied to the dynamic tests.

4. Tests: Description and Results

4.1 Load-Unload Cyclic Tests

The new pile with six strain gauges was installed in relatively dense dry Nevada sand (unit weight 97 pcf, relative density 91%), so that all strain gauges were below the soil surface. Care was taken to apply the lateral load just at ground surface so that the moment there was known to be zero. Load-unload tests were performed to different load levels, as shown by the load-displacement plot of Figure 4.1.1. The strain gauge data on the Visicorder records were digitized for plotting

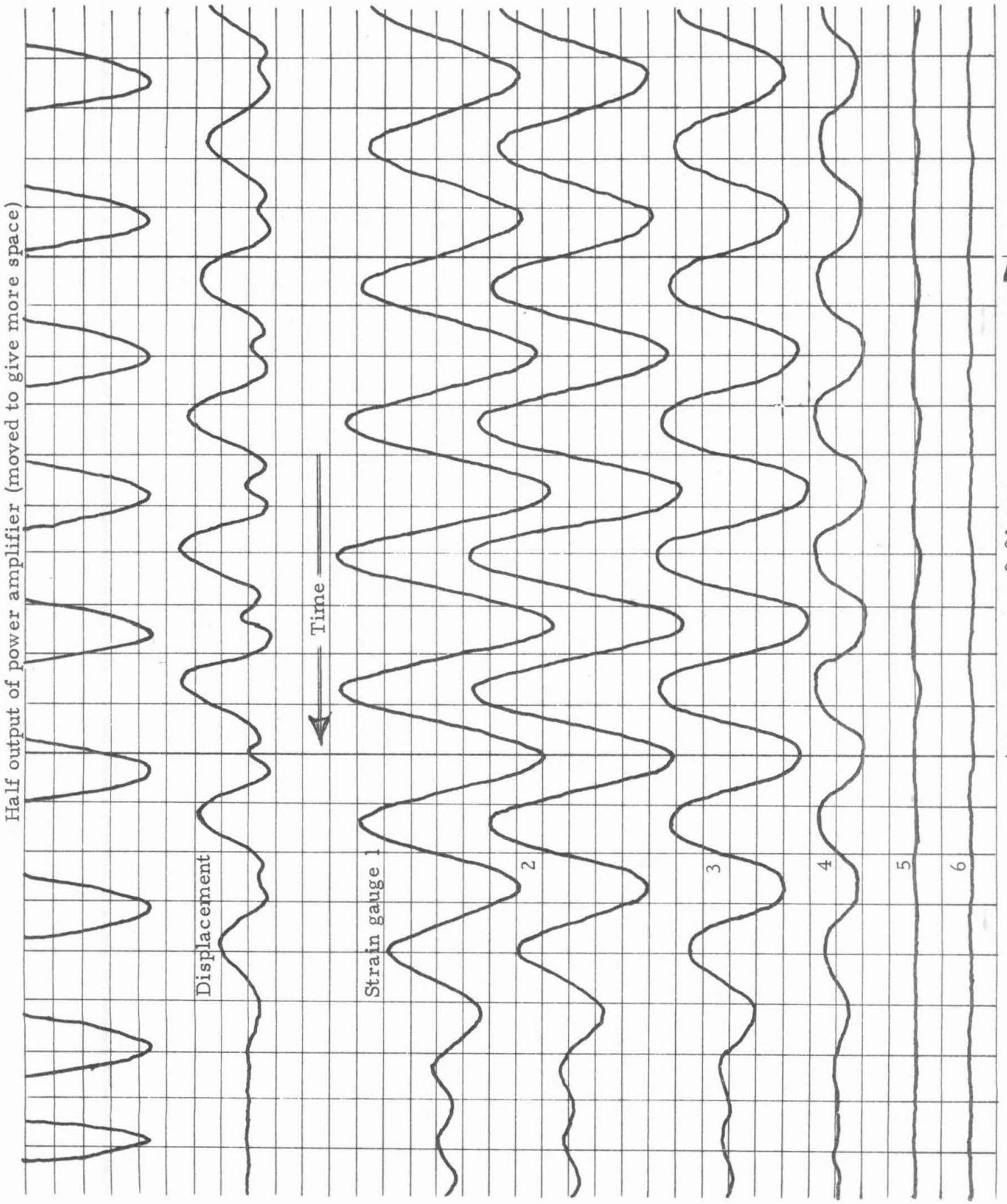

Fig. 3.3.1 Tracing of a portion of Visicorder recording of dynamic pile test

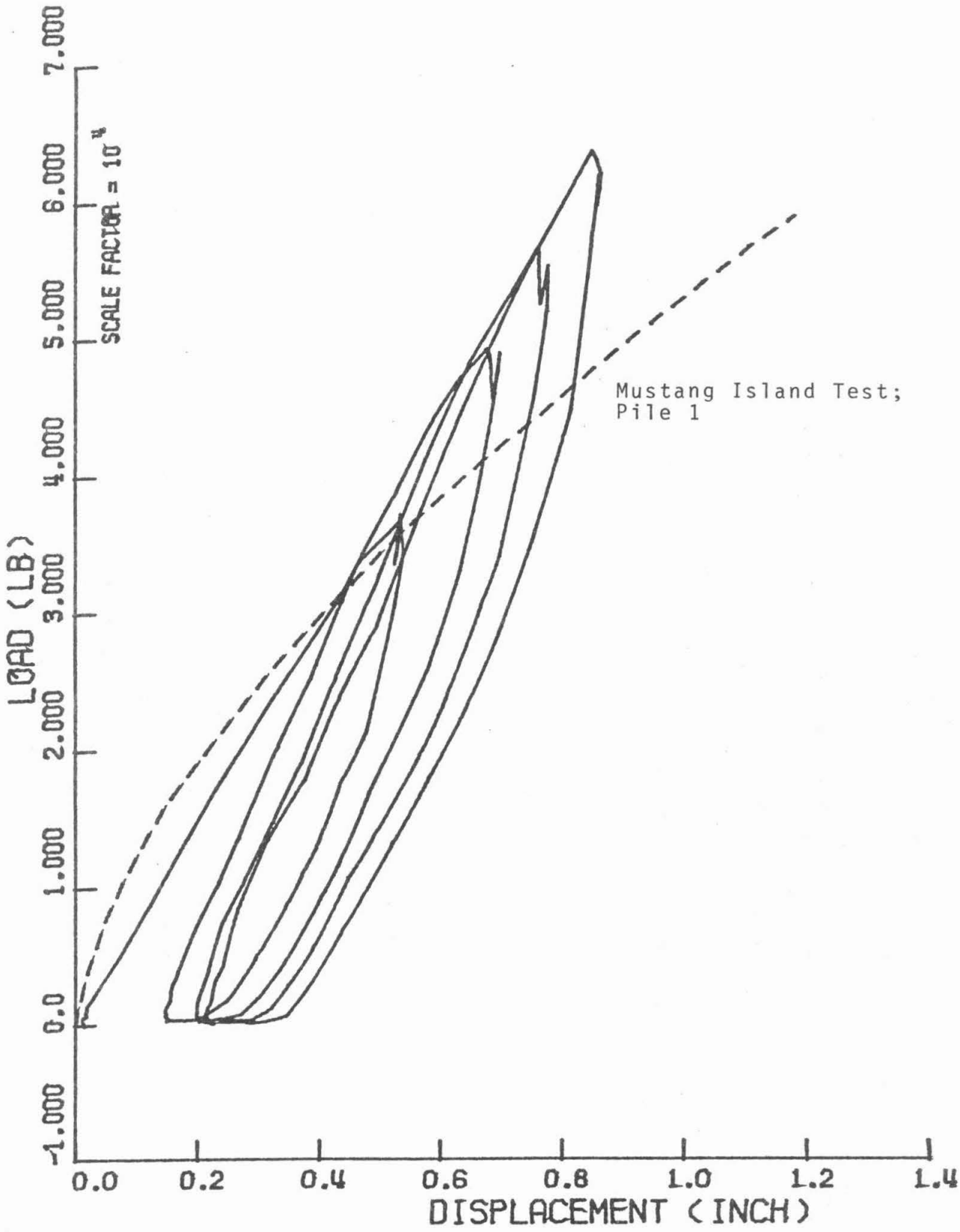

Fig. 4.4.1 Lateral load versus top displacement for dry load-unload cyclic tests. Static Mustang Island Pile 1 prototype test also shown

on a scale of moment versus depth, and a typical resulting diagram is shown in Figure 4.1.2.

Another test was performed on the pile imbedded in saturated Nevada sand at a dry unit weight of 96 pcf which corresponds to a relative density of 85%. The water table was maintained at the ground surface. Photographs of dry and wet tests are included as Figures 4.1.3 and 4.1.4. After digitization the curves of moment versus depth at various lateral loads during loading and unloading were prepared and shown in Figure 4.1.5. In particular one curve on that diagram represents the moment distribution in the pile when the load has returned essentially to zero. It can be seen that the point at which the maximum moment occurs increases in depth both as the load is increased and as it is reduced. The actual value of the maximum moment at zero load after unloading stays at a surprisingly high proportion of the maximum moment attained at the peak lateral loads, and at a depth well below that of the peak moment. Because of the high residual stresses left in prototype piles after driving, field lateral load tests do not properly indicate these zero load moments after a loading cycle. As shown in the previous report, this first bias moment has an effect which persists through many positive and negative portions of complete cycles of load.

When the original Visicorder strain gauge test data have been digitized at different times (corresponding to different applied loads), the result is in the form of curvatures or moments in the pile at discrete depth intervals for various applied loads. These points are plotted by computer to make moment diagrams such as Figures 4.1.2 and 4.1.5. In

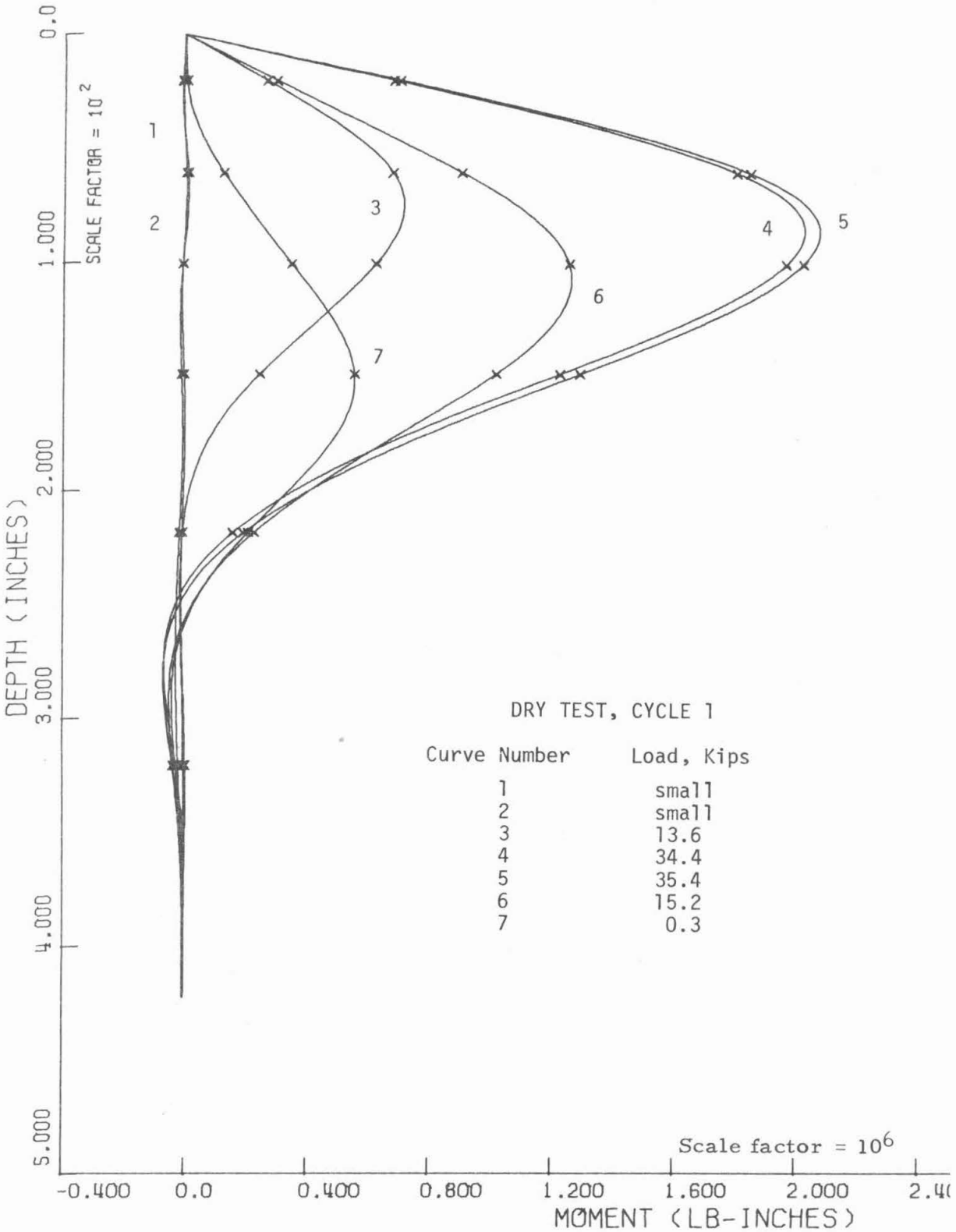

Fig. 4.1.2 Raw strain gauge data of moment versus depth at different loads; load-unload first cycle dry soil. Spline function fitted curves

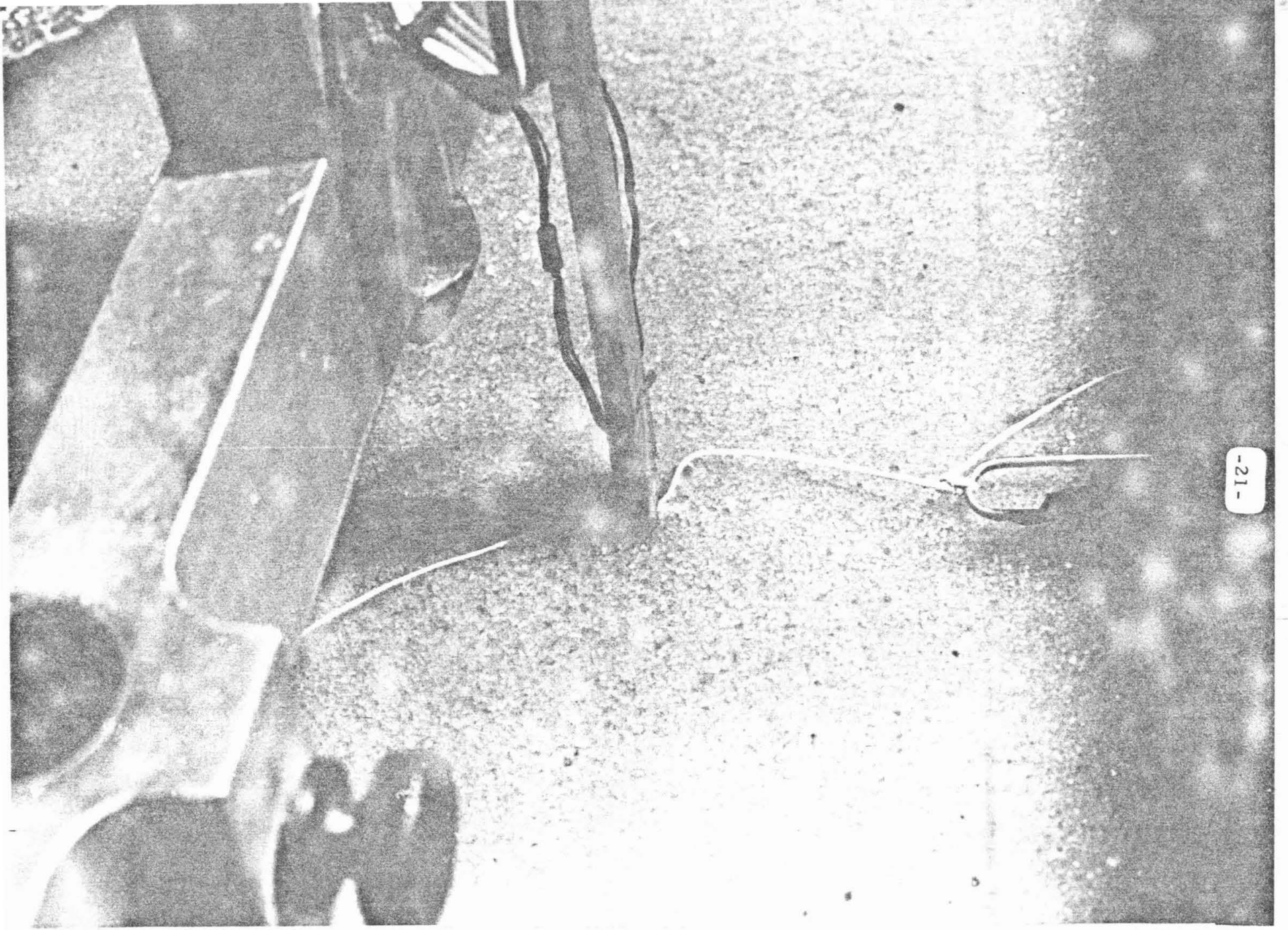

Fig. 4.1.3 Cyclic load-unload test apparatus; dry soil (Ottawa Sand is shown here)

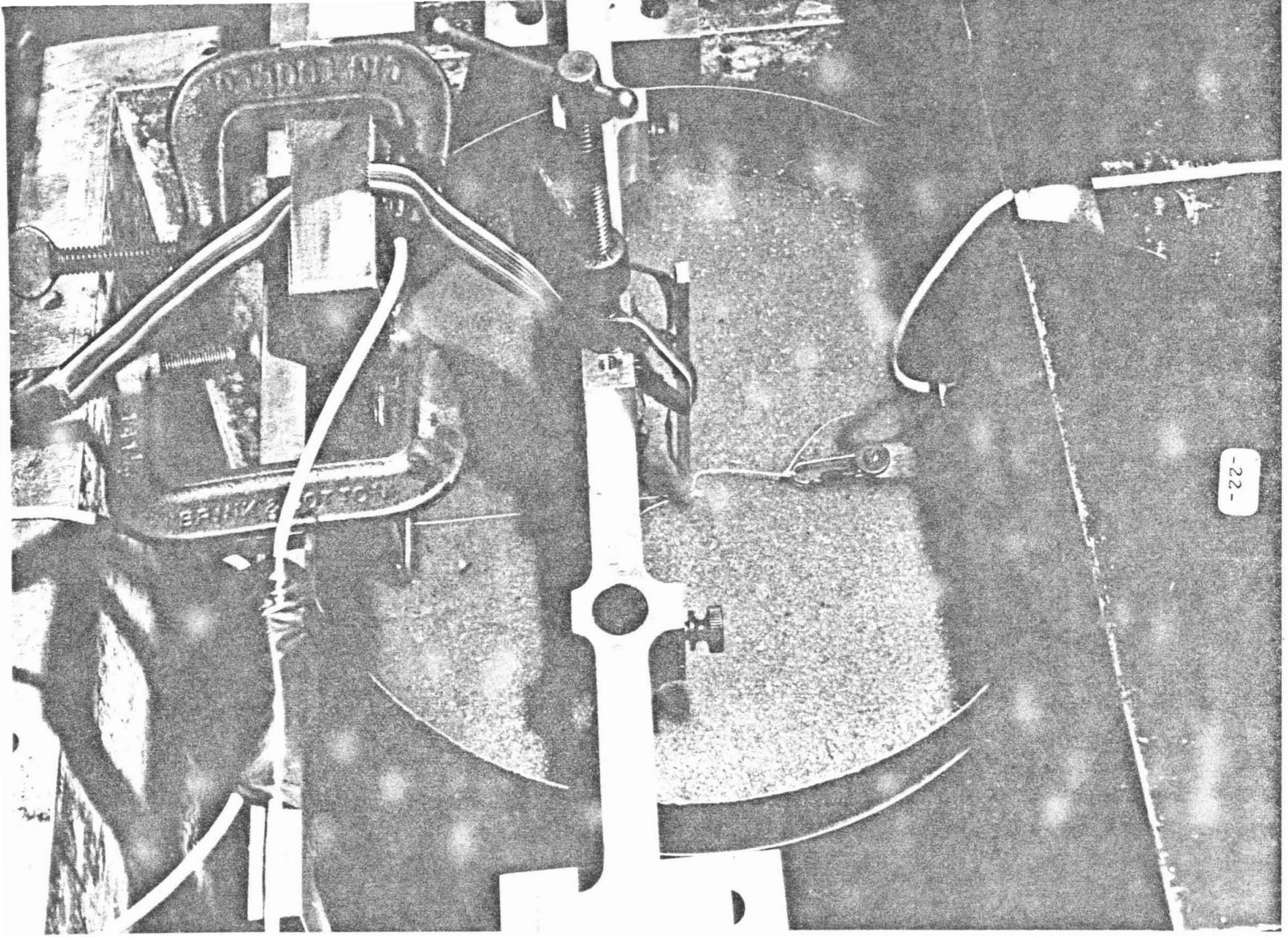

Fig. 4.1.4 Cyclic load-unload test apparatus and container; saturated soil (Ottawa Sand)

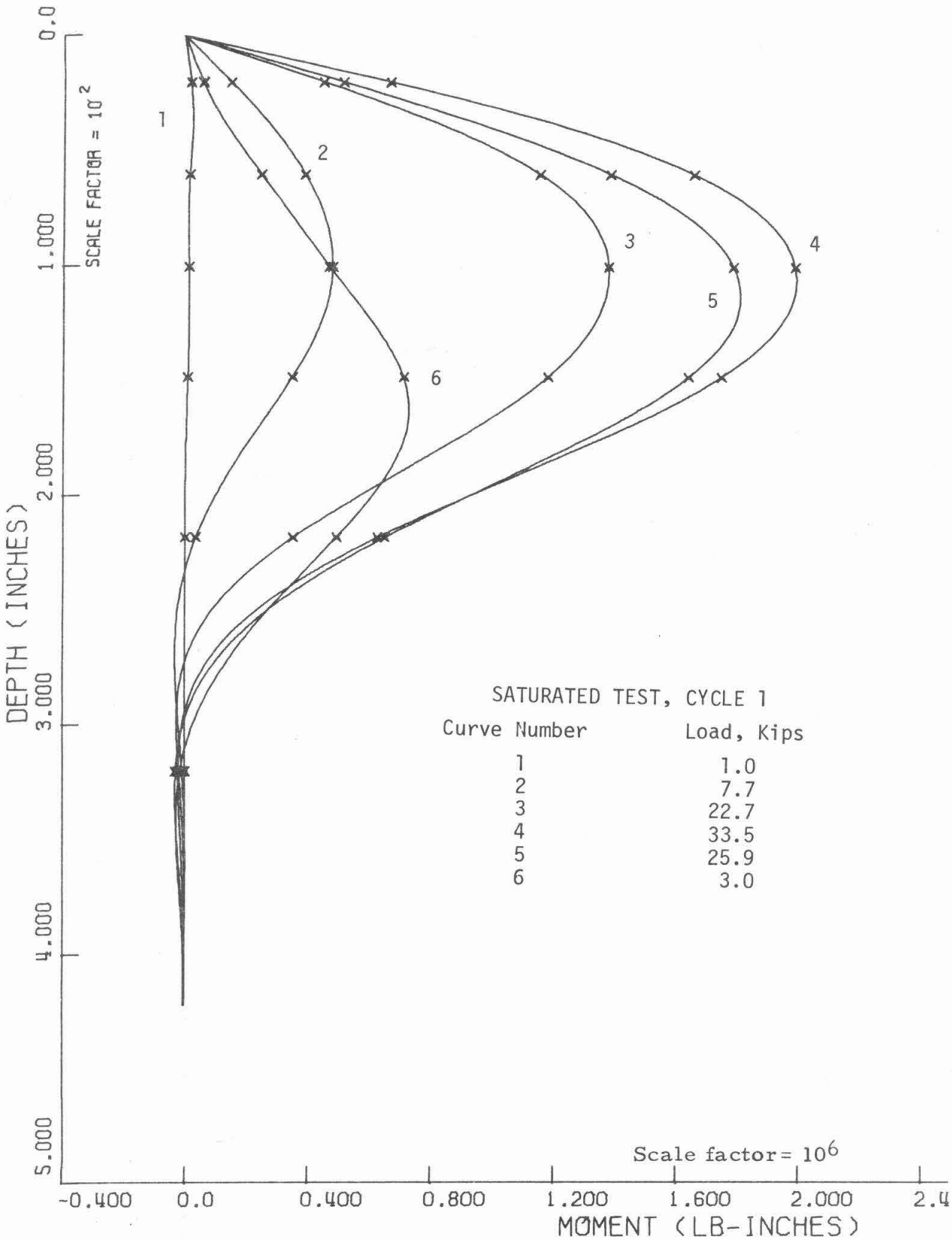

Fig. 4.1.5 Moment curves for test in saturated soil, first cycle of load-unload

digitizing the original data, samples of the strain-gauge outputs were taken at frequent intervals, at equivalent prototype loads only a kip or two apart. When these data were plotted by the computer, it was found that a confusing mass of moment curves resulted. As a result, the computer was instructed to plot only every 5th set of digitized strain-gauge readings. Thus, the values selected were arbitrary. Although this process conveniently gave the results shown in the figures here, it had the disadvantage that neither the moment distribution at zero load nor the moment distribution at the instant of maximum load were, in general, selected by the computer for plotting. In particular, there results the situation shown in Figure 4.1.2, where the selection of every 5th data set in a region of the test near the maximum load has resulted in the plotting of two curves virtually on top of each other, at loads of 34.4 and 35.4 kips, respectively. This plotting procedure will be modified at a later date.

For analysis purposes, it is desirable to have moment expressed or shown as continuous functions of depth. If this can be achieved, the curves may be integrated and differentiated to give further results of interest in the sequence:

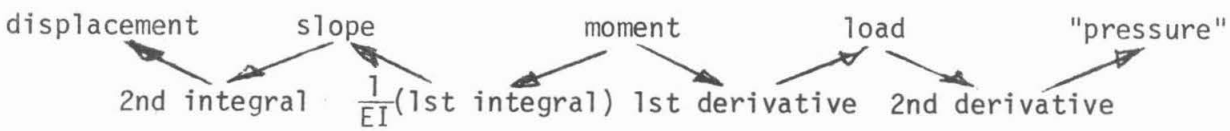

In general, even if the data points for any load are relatively crudely fitted by a curve, say by hand sketching, the first and second integrals will give a reasonably accurate picture of the slope and displacement along the pile's length. However, differentiation is a different matter. Any

unevenness in the selected curve through the moment values will be reflected in abrupt changes in the slope. Load in and soil pressure on the pile will be obtained very inaccurately as a consequence. This difficulty has been remarked on by other pile experimenters. It could be resolved if, in the test, field or laboratory, soil pressure on the pile could be measured as well as the moments in the pile. All other quantities could then be obtained by integration. This has not yet been attempted, and efforts have been concentrated, therefore, on moment-curve fitting methods.

After some study, the most appropriate technique was found to be the spline-fitting method. It proceeds as follows. A polynomial function with constant coefficients is selected (third order, fourth order, or other) for application to each pair of experimental points in the moment-depth diagram. Different coefficients are assumed to hold in the interval between each pair of points. The function will be made to match the points at each end of the interval. In addition the successive derivatives of the function in one interval will be forced to equal the values of the equivalent derivatives of the functions in the intervals on each side, at the end points. The number of derivatives selected for matching determines the order of the spline function. If at each end of the interval it is required that the function matches the moment values and that the first derivatives equal the first derivatives of the adjacent functions, then there will be four constants involved in each interval and the spline will be a cubic (third order). If moment, first and second derivatives are to match at the ends of the interval, the spline must contain 6 constants and will therefore be of 5th order.

For two successive integrations the order of the spline function is of little concern, since the integrated values will be similar regardless of the function chosen. However, in the determination of pressure, two differentiations are needed and here the order is important. Two differentiations of a cubic spline give straight lines, so that the pressure variation with depth would appear as a series of linear segments between the depths at which the moment values had been established by the experiment. Clearly, this would not be correct, and a higher order spline is required. The calculational complexities are minimized if only the next higher suitable order--the fifth--is chosen. This was done for the figures here. Two problems only remain in the fitting process: What to do below the last data point and at ground surface?

For all the loadings studied so far, the moment in the lowest or 6th strain gauge has been very small, so the first question was resolved by assuming another point below that one and spaced a distance from it equal to the distance between the 5th and 6th strain gauges. At this lowest point, the moment and all derivatives were taken to be zero. Resulting calculations would be little changed by small variations of this zero point.

At the top of the pile with the loading adopted, the moment is zero, but its first derivative at ground surface is equal to the applied lateral load, to which the first spline function derivative at the end of the top interval may be matched. The soil pressure against the pile at ground surface depends on the soil present. In the case of the tests conducted, the soil was sand, and the pressure exactly at ground surface can therefore be taken as zero, to which the second spline function derivative at that

end can be equated. Were the soil an overconsolidated clay, however, the pressure would not be zero, and it is not clear how it might be established. Perhaps it could be gotten through the shearing strength of the soil and plasticity theory. For the present tests, the sand fitting conditions were employed.

For the dry and wet tests, the moment points and fitting curves are shown in Figures 4.1.2 and 4.1.5. It is emphasized that the points are original data from the tests, multiplied only by scaling factors to give prototype moments. The results of the two successive integrations and differentiations are given for these tests on Figure 4.1.6 (dry) and 4.1.7 (wet). In both tests the integrated pile-top displacements correspond extremely closely to the measured values, and it is therefore reasonable to assume that the displacements given as a function of depth down the pile also match the actual values well. With the fitting requirement of known lateral load at the pile top, it follows that the distribution of load along the pile (first derivative) is also close to the test values. For the reasons given earlier, it is harder to be sure that the picture of soil pressure on the pile (second derivative) is also accurate. Presumably, however, it is not far from the truth over much of the pile length and is qualitatively correct, apart from the region near the surface.

In all the second derivative curves shown, there is a region in the top few inches of the pile where the soil pressure changes sign. Since the pile displacement, as can be seen from the displacement (second integral) curves, is largest at the top, it is obvious that this kink in the curve is not correct. It would be expected that the sand pressure on the

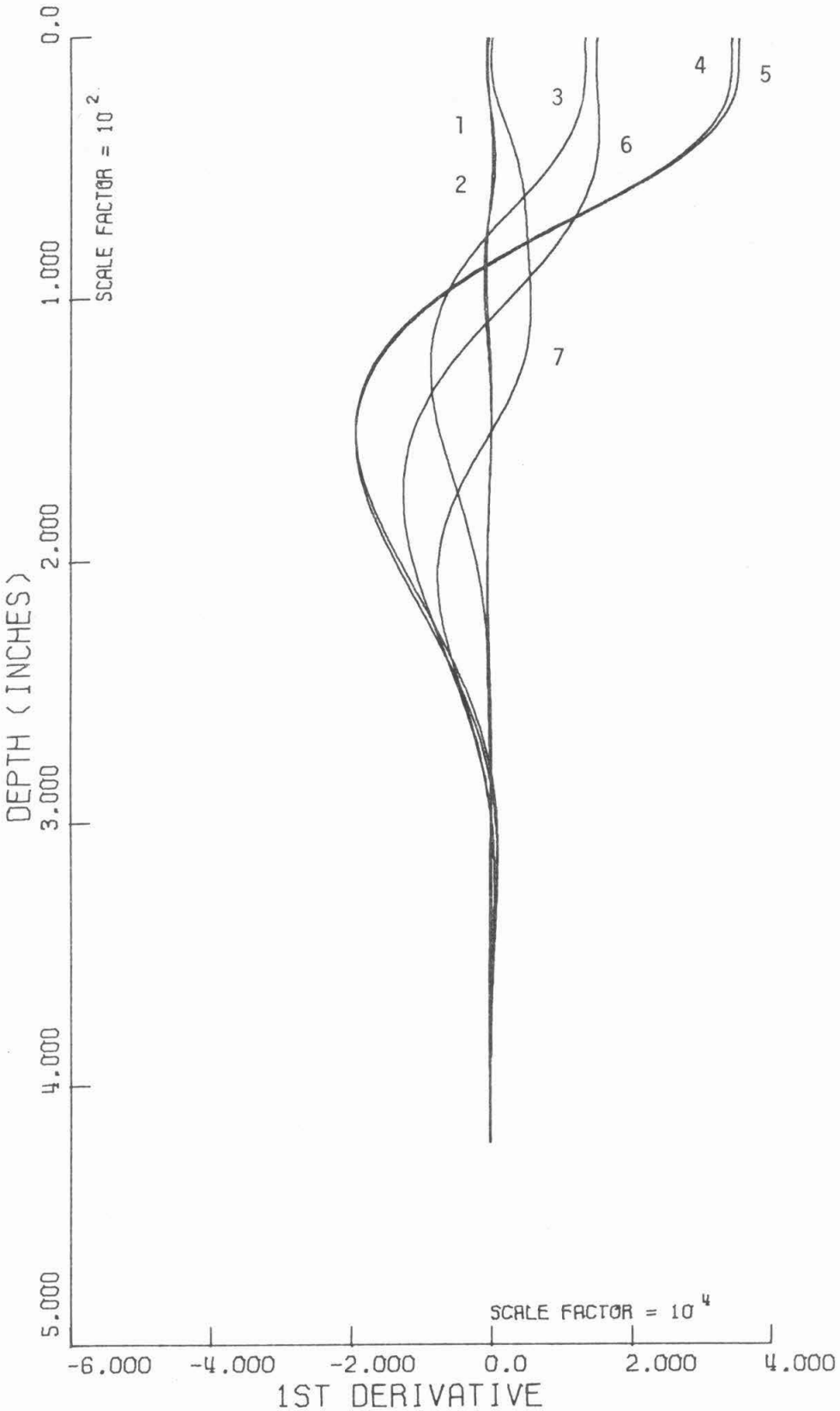

Fig. 4.1.6 Derivatives and integrals of moment curves: first cycle dry soil: (a) first derivative, shear force in pile

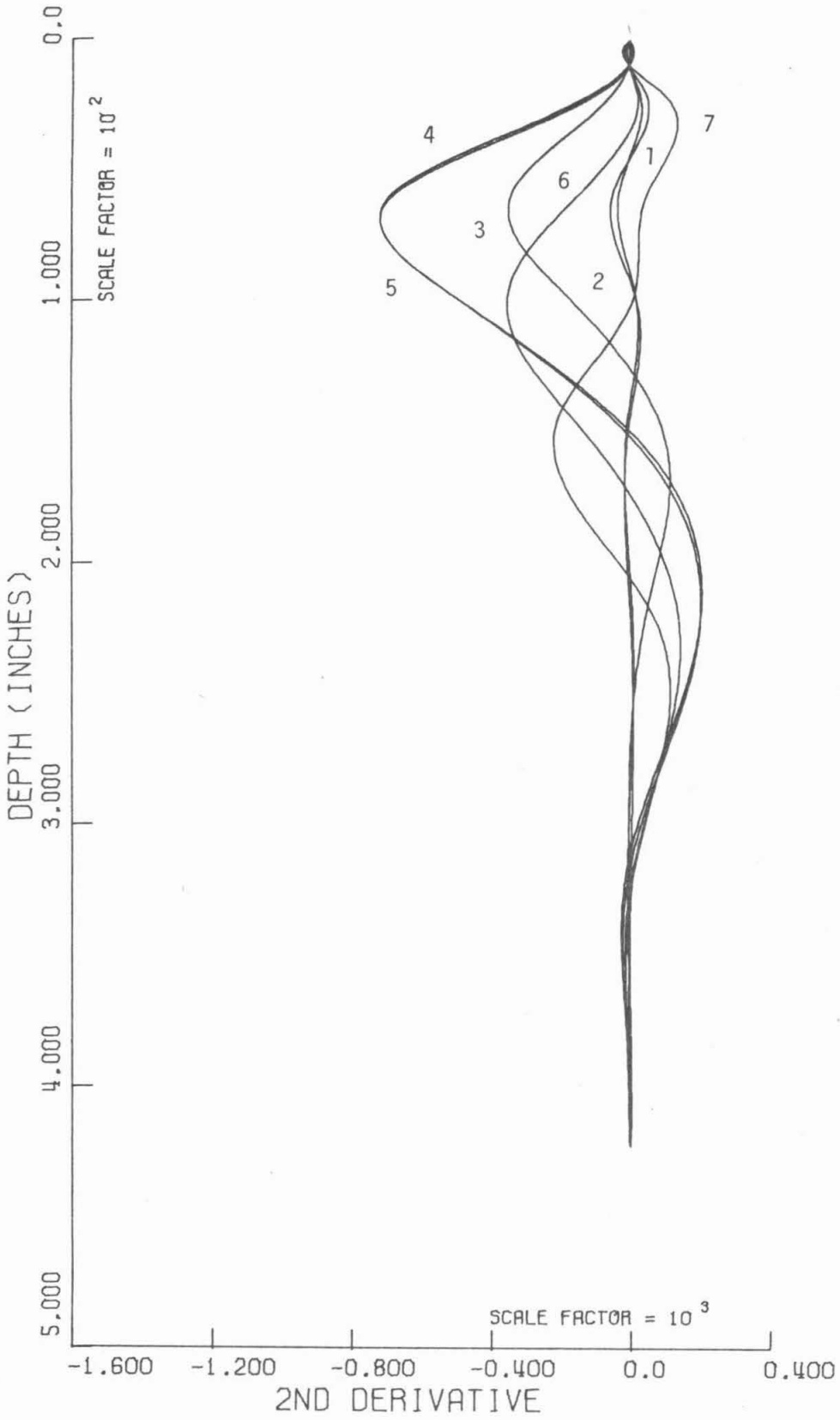

Fig. 4.1.6 (b) second derivative, soil reaction on pile

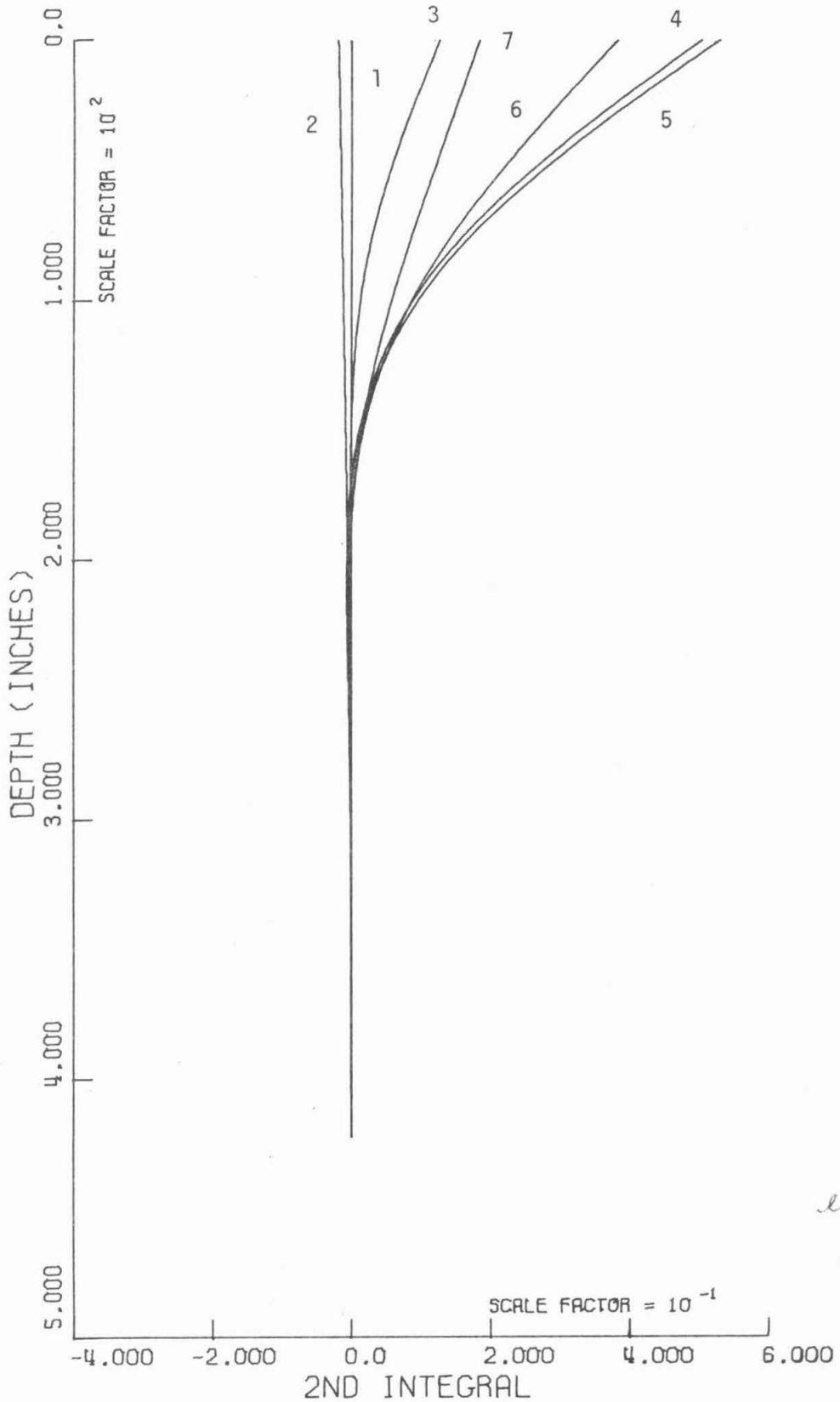

exchange figures (c) and (d)

Fig. 4.1.6 (c) first integral (÷EI), pile slope

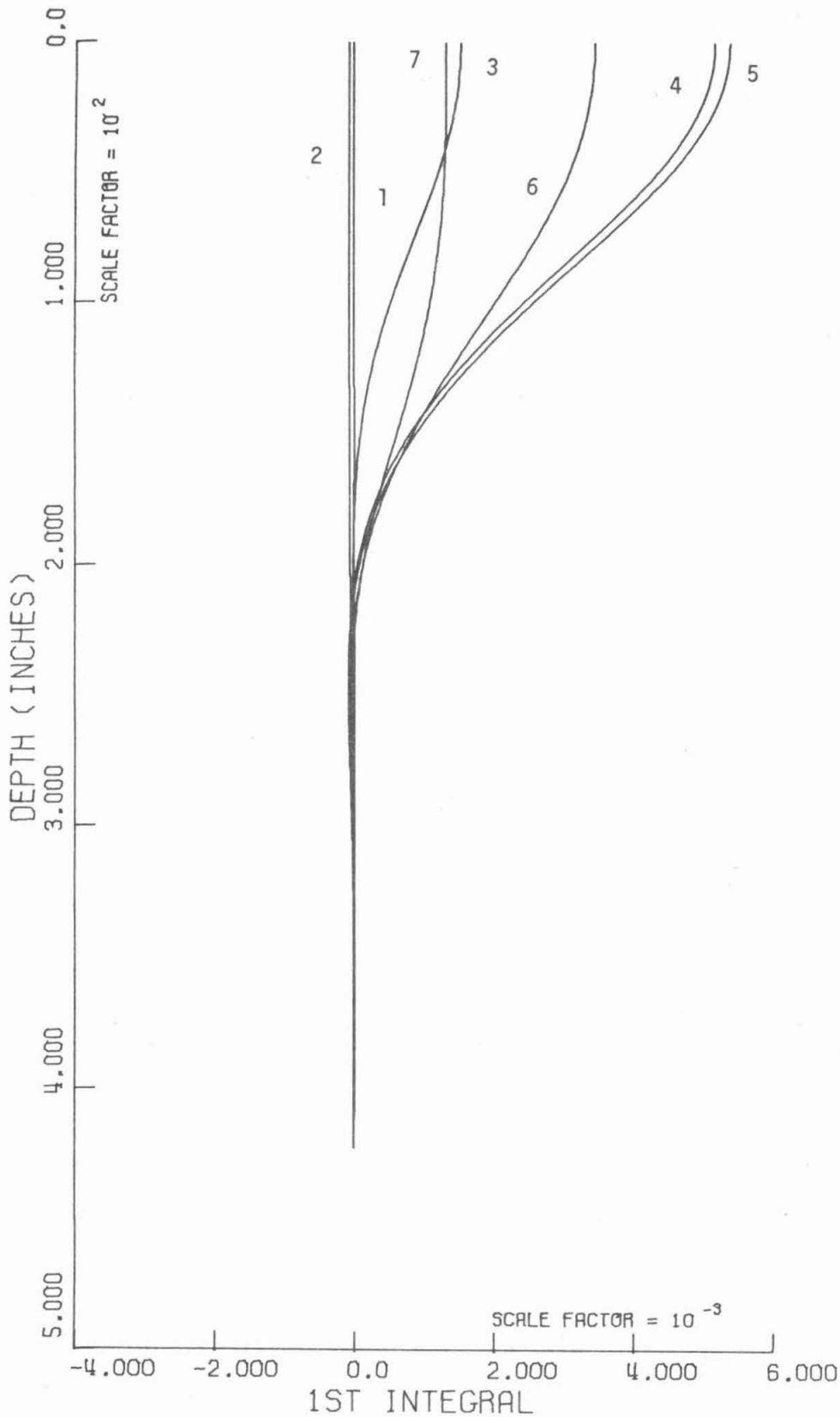

Fig. 4.1.6 (d) second integral, pile deflection

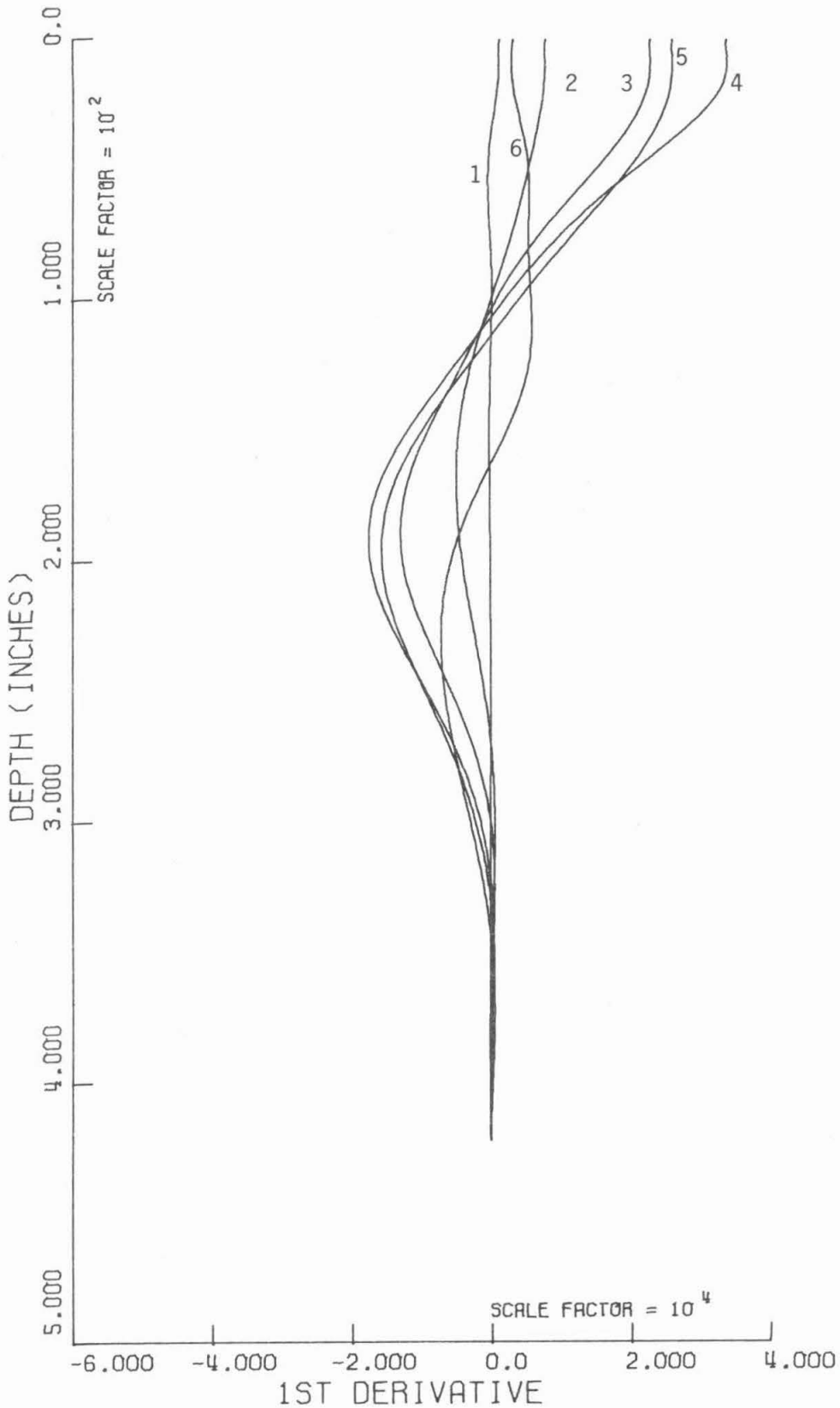

Fig. 4.1.7 Derivatives and integrals of moment curves: first cycle saturated soil: (a) first derivative, shear force

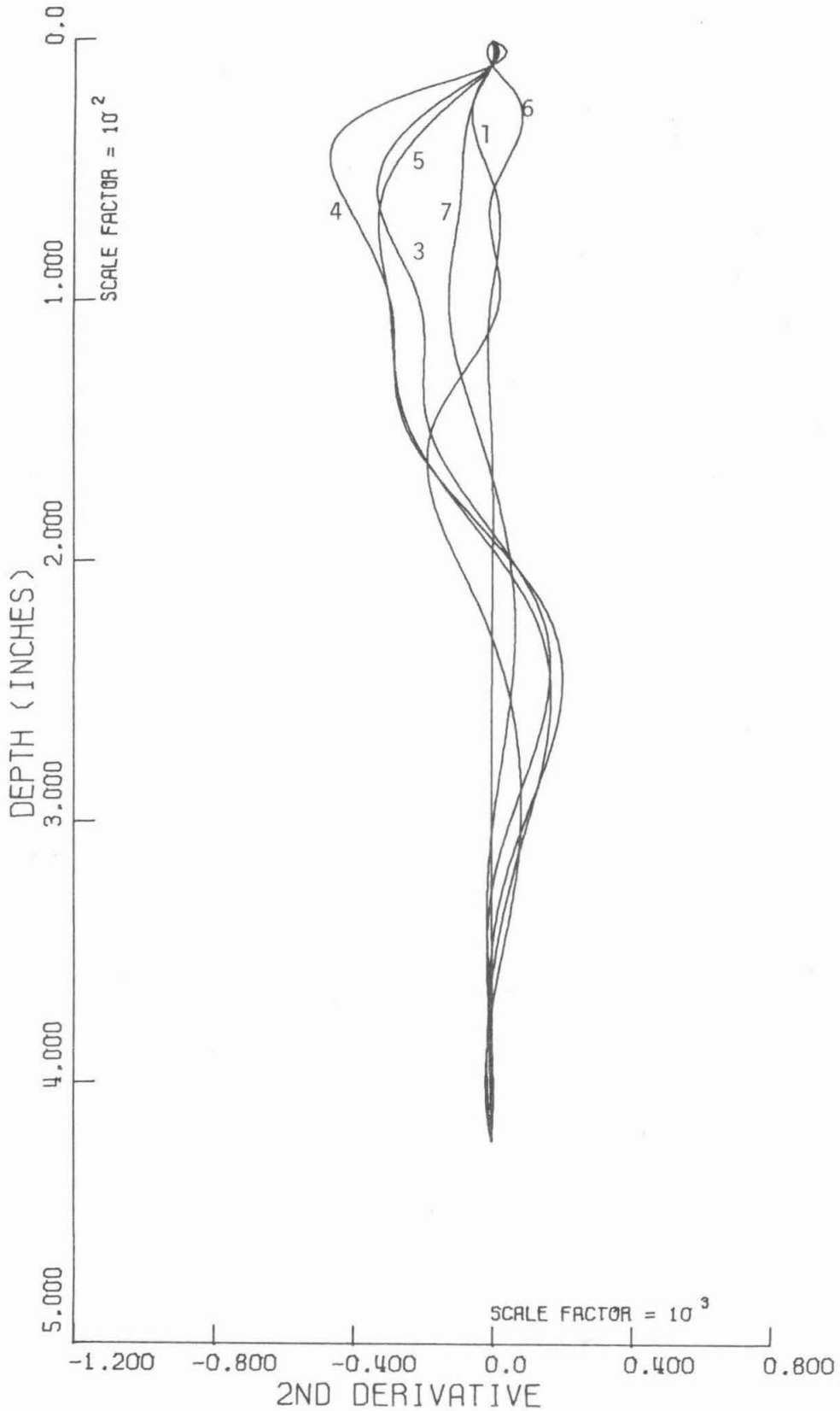

Fig. 4.1.7 (b) second derivative, soil reaction

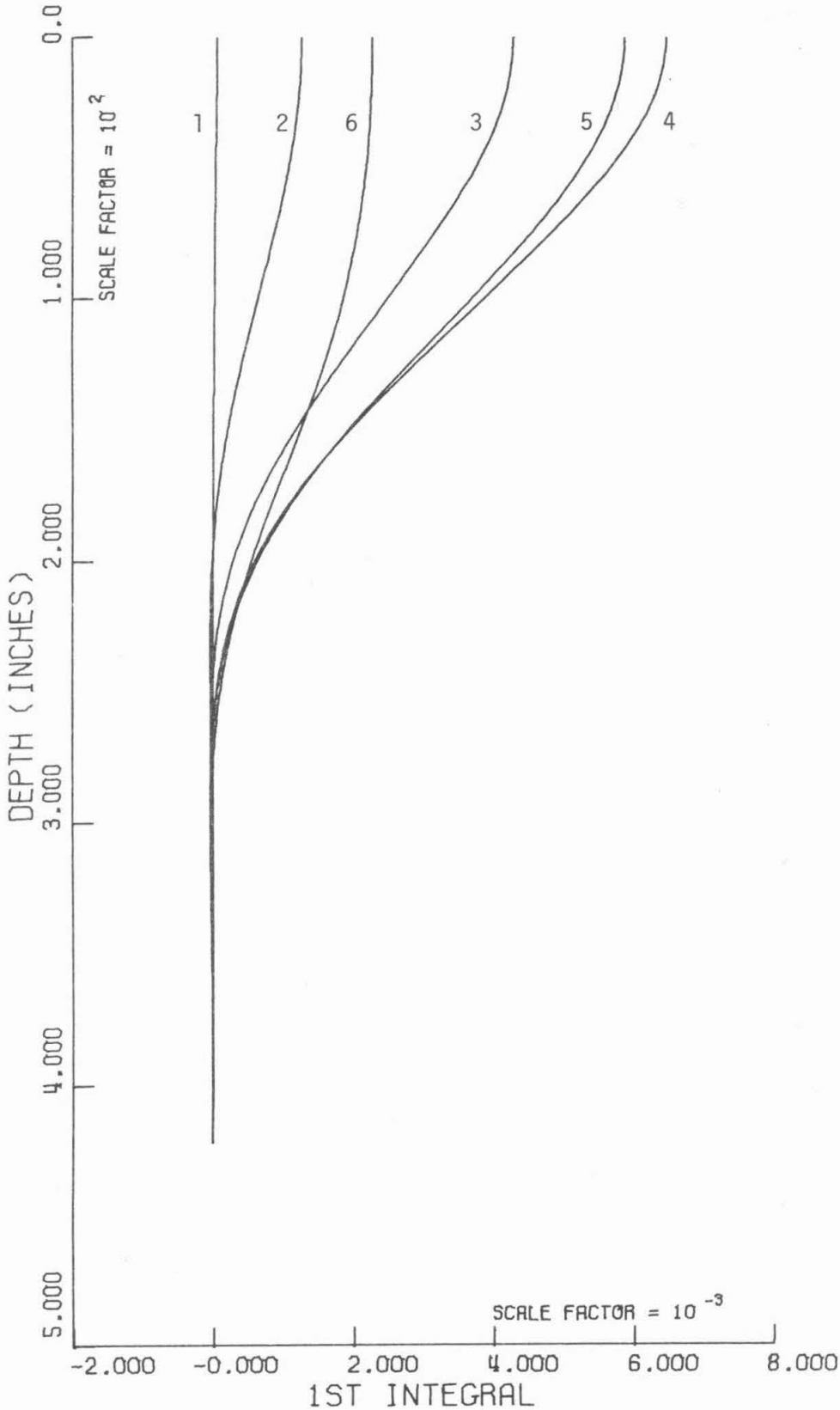

Fig. 4.1.7 (c) first integral ($\div EI$), slope

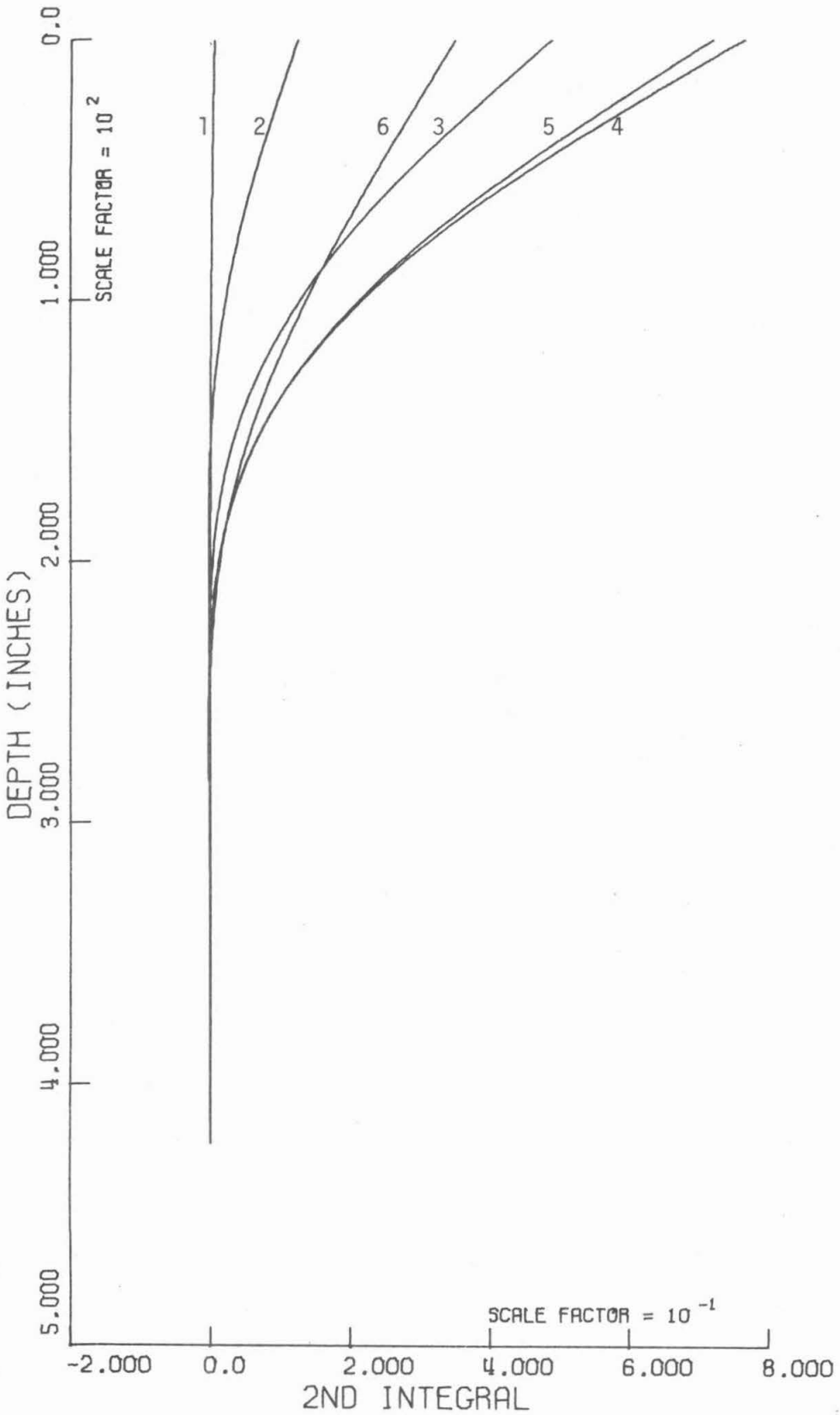

Fig. 4.1.7 (d) second integral, deflection

pile would increase smoothly from zero at ground surface to a maximum some distance down the pile.

The deviation from the behavior seen in the soil pressure figures is therefore a consequence of the fitting method and an inadequate number of strain gauges attached to the pile. Because of the smallness of the pile dimensions, it will be difficult to install more gauges. Other fitting techniques will be explored later in order to see if an improvement can be effected in the deduced pressure-depth relation at the pile top. Consideration is also being given to the installation of small pressure cells (which are, however, bigger and more expensive than the strain gauges) on the pile surfaces.

Ideally, at this stage it is desirable to plot soil pressure on the pile as a function of lateral displacement at several depths to see how the pressure-displacement function looks. Since this involves juxtaposing a second derivative and a second integral of the same quantity, it is doubtful if the result can be taken as more than a general picture of the relationships developed in the soil, at this stage.

The second derivative curves obtained from the moments are referred to here as "pressure," and reflect the interaction of soil and pile. They are not, obviously, the total soil pressure acting on the pile, which is composed of an initial, post-installation lateral pressure plus the pressure developed by the lateral movement of the pile. Since the "pressures" derive from the curvature of the pile, they are indicative of the stresses developed in the soil by the pile movement only. Simplifying the deformational pattern, this movement involves compressive straining of the soil in

"front" of the pile (the direction towards which the pile is moving), extensional straining of the soil "behind" the pile, and shear straining of the soil at each side of the rectangular model pile. The second derivative therefore reflects the pressure required in the pile to deform all the soil around it. Were the soil pressure increment to be measured in front of the pile during a test, it would not be found to be equal to the second derivative. Taking into account the mechanism of deformation and the soil properties, it is expected that the second derivative "pressure" would be two to three times the value of the pressure increment measured.

After the first cycle of loading, several more load/unload tests were performed at successively higher loads, to examine the effect of repeated loading, as shown in Figures 4.1.1 (dry sand) and 4.1.8 (wet). Not all of the results have been analyzed as yet and only the second loading cycle will be discussed here.

Two more sets of curves are given in Figures 4.1.9 (dry) and 4.1.10 (wet) for the second loading cycle of the pile in the dry and wet cases. In each case, the initial condition of the pile was zero applied load at the pile top after the first load-unload cycle. However, as seen in Figures 4.1.2 and 4.1.5, at this stage, substantial moments had been left in the pile. The second loading cycle then modified this initial moment distribution.

The peak loads in the first test cycle were 36 and 48, and in the second cycle were 34 and 43 kips for the dry and wet soil tests, respectively. The corresponding maximum and residual moments and other data are shown in the following table:

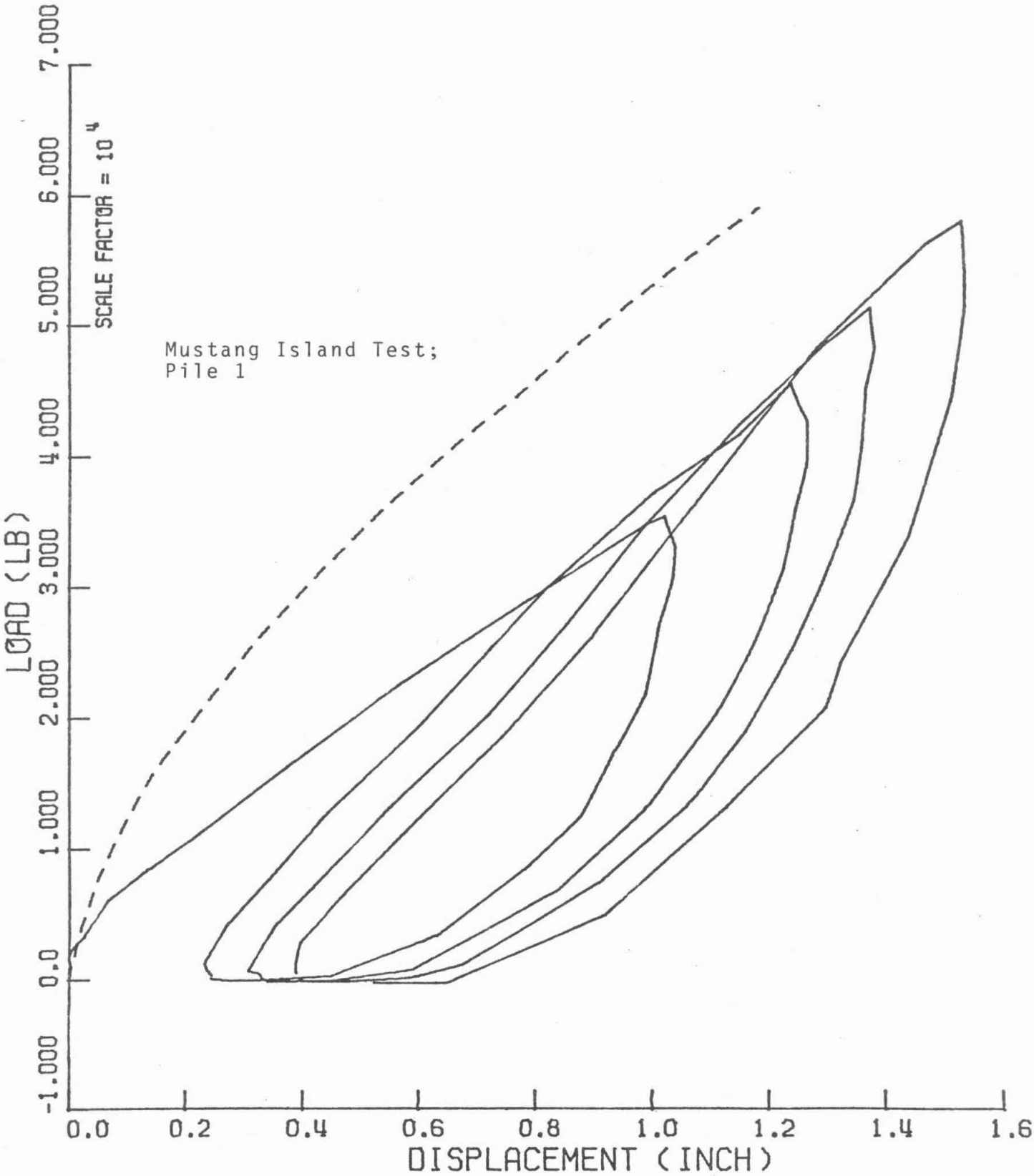

Fig. 4.1.8 Lateral load versus top displacement for saturated load-unload cyclic tests. Static Mustang Island Pile 1 prototype test also shown

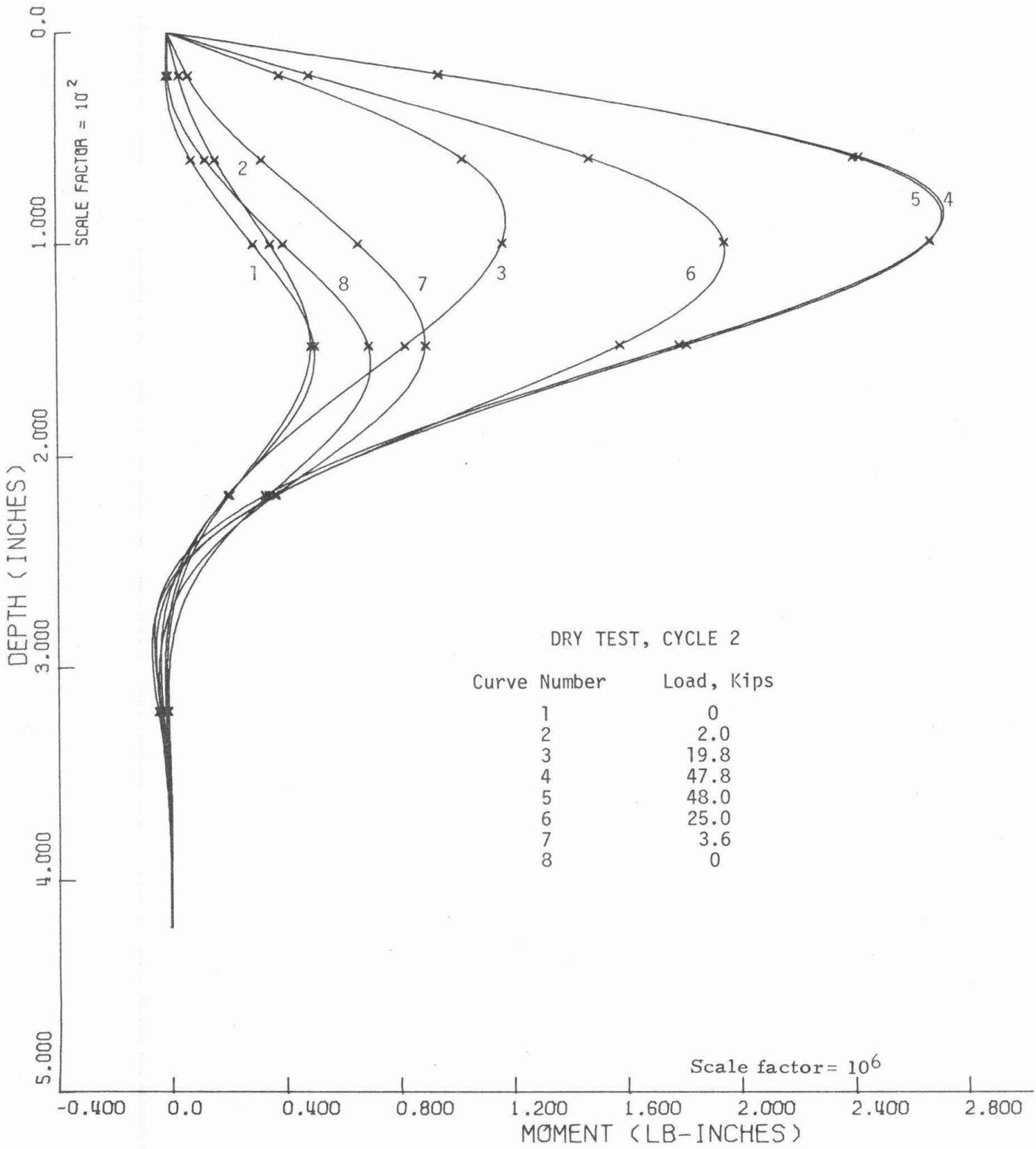

Fig. 4.1.9 Results of second load-unload cycle dry soil: (a) moment

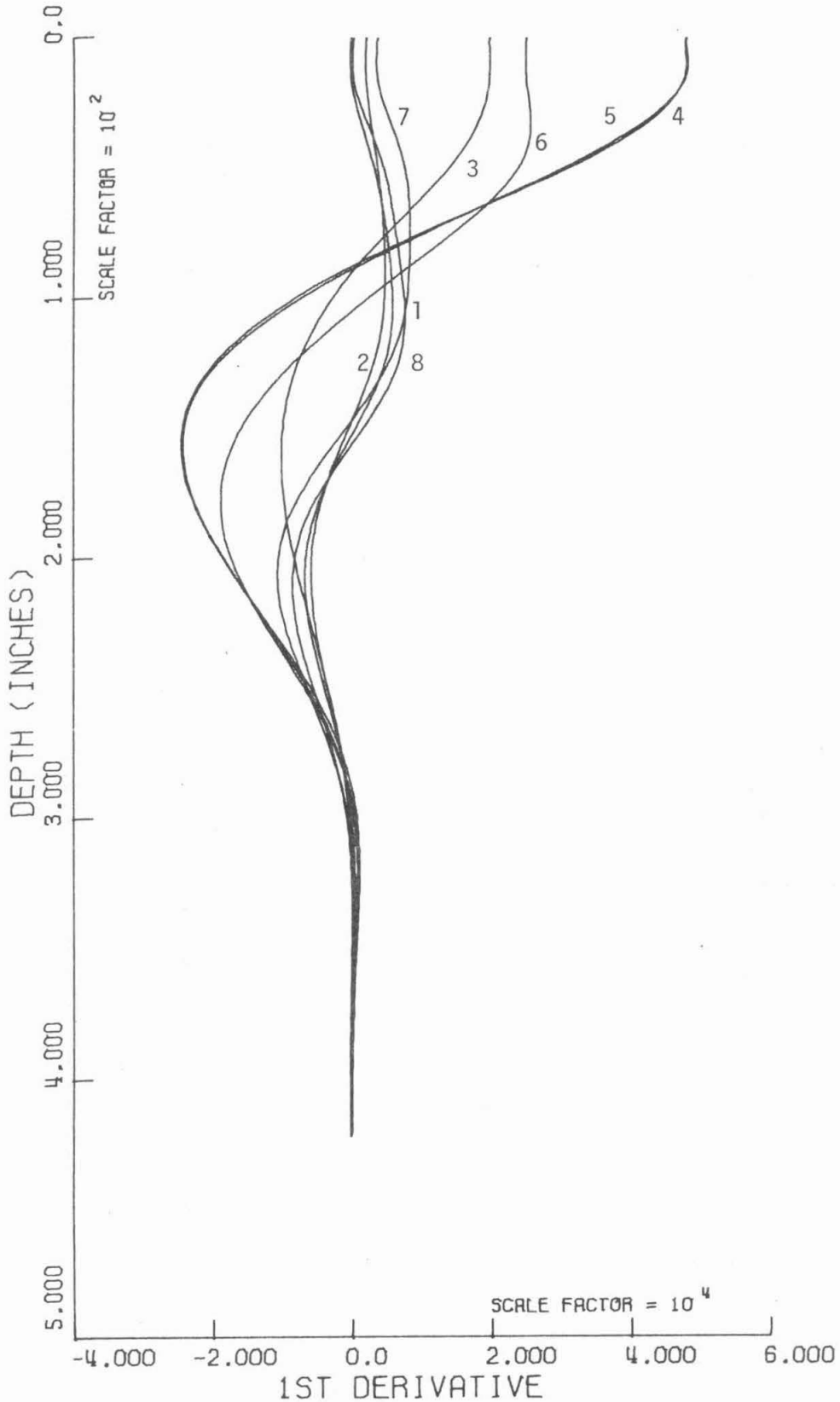

Fig. 4.1.9 (b) shear force

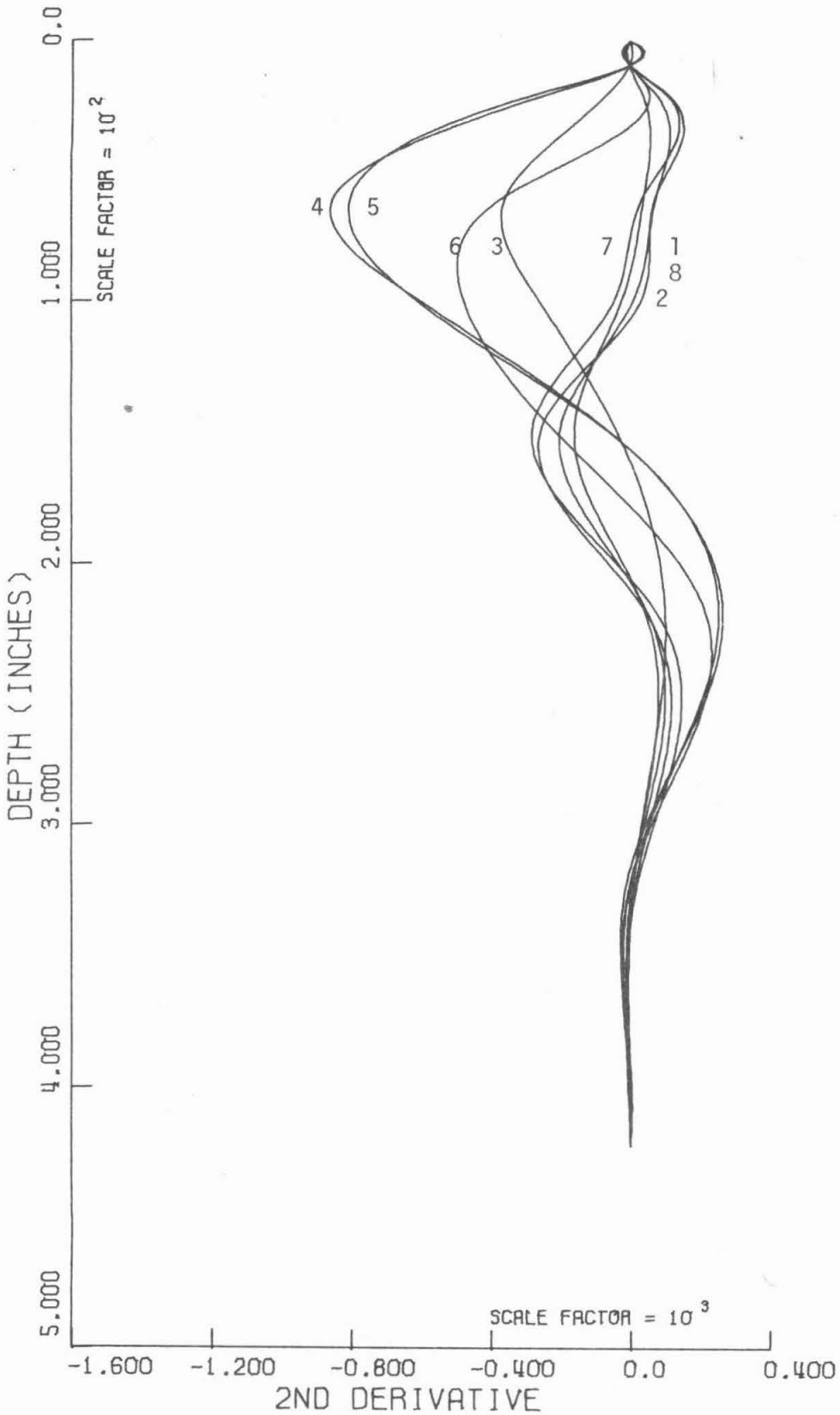

Fig. 4.1.9 (c) soil reaction

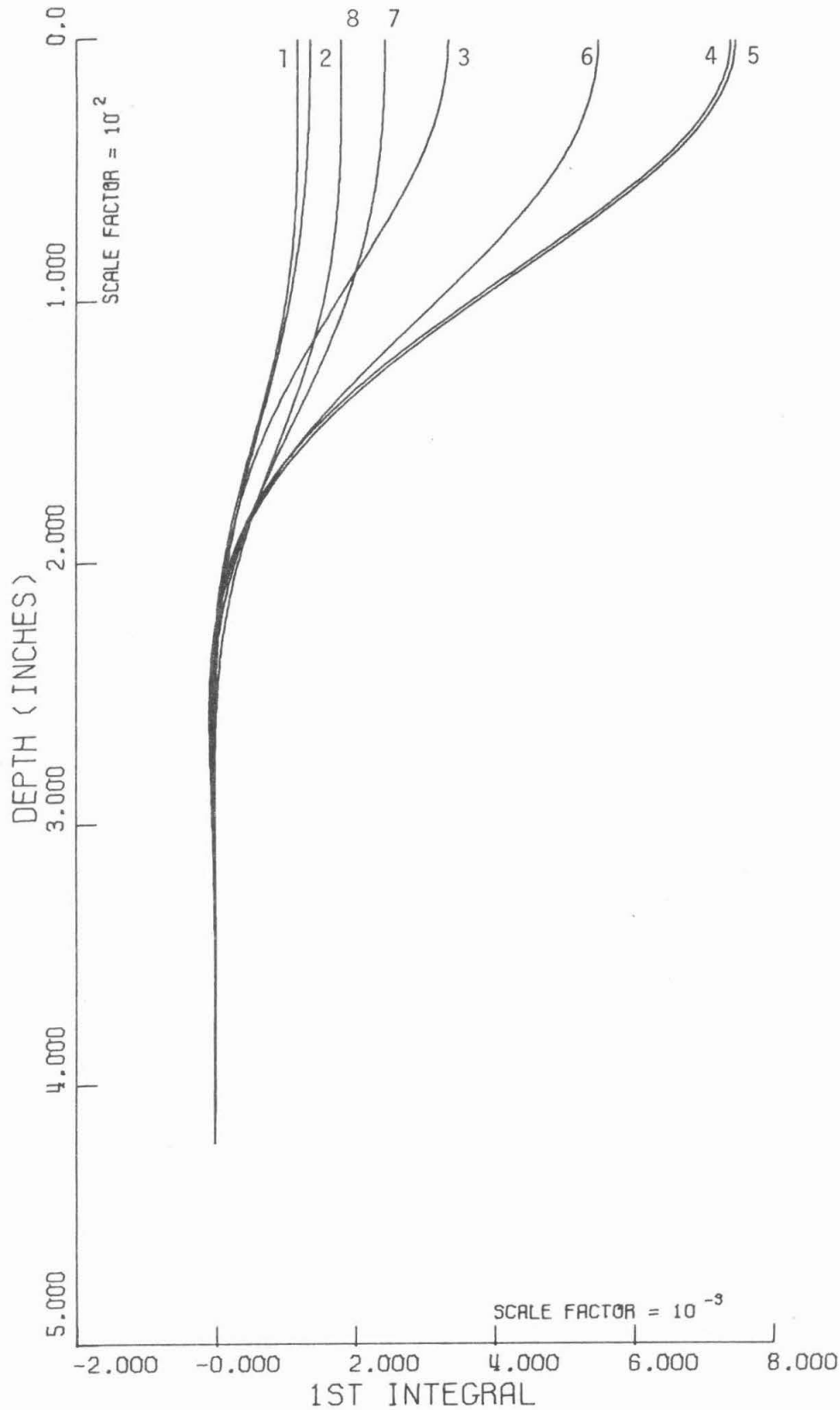

Fig. 4.1.9 (d) slope

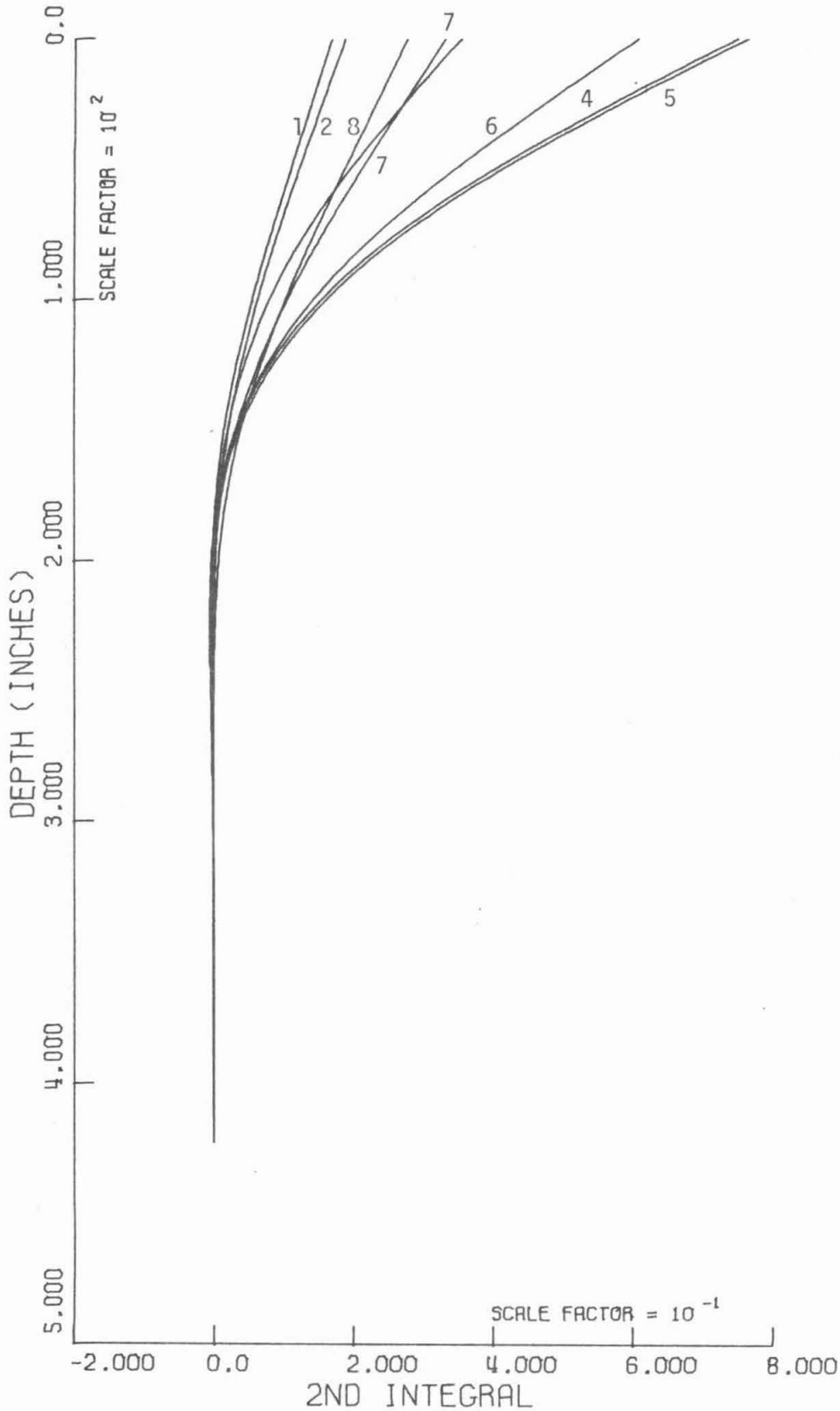

Fig. 4.1.9 (e) deflection

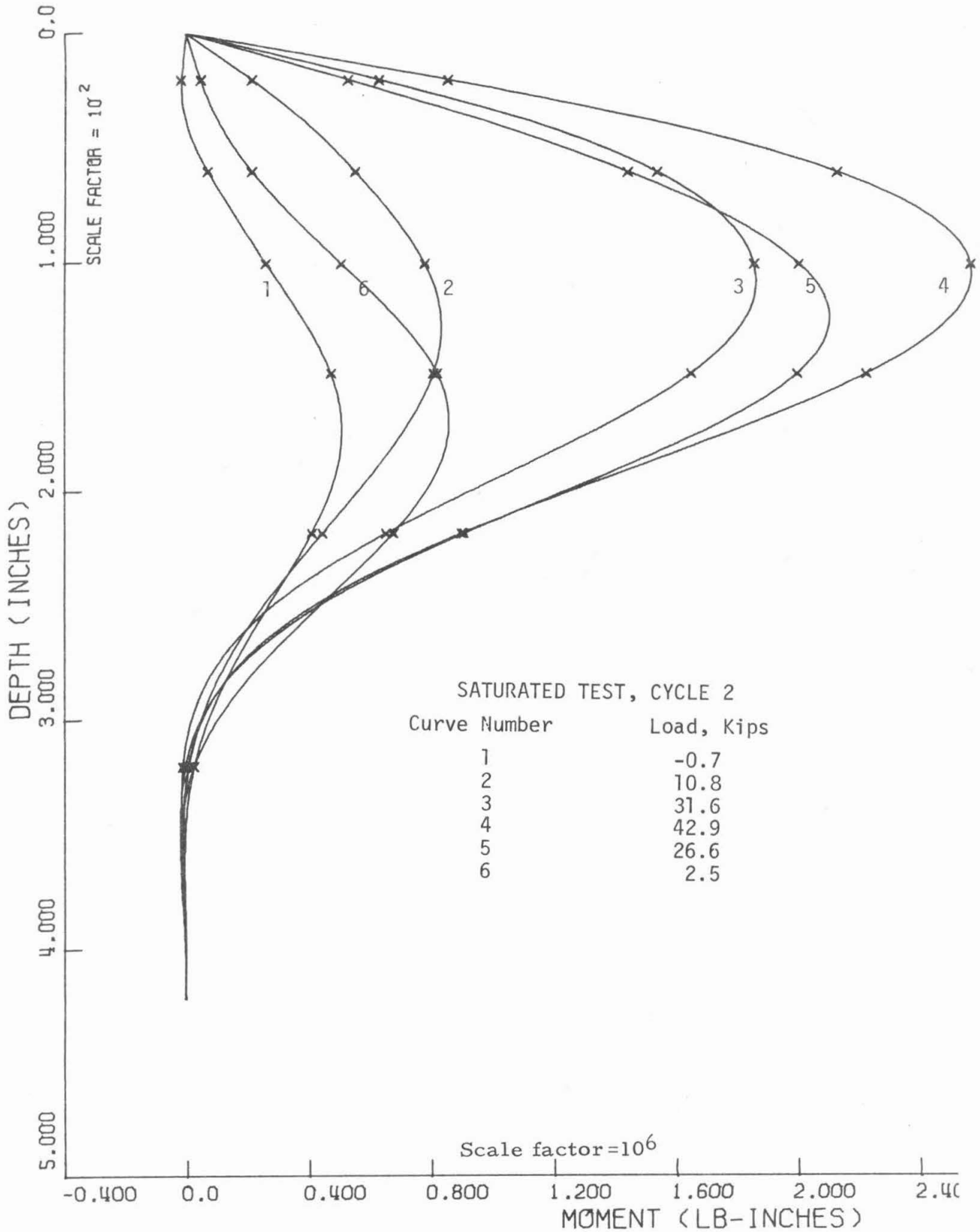

Fig. 4.1.10 Results of second load-unload cycle saturated soil: (a) moment

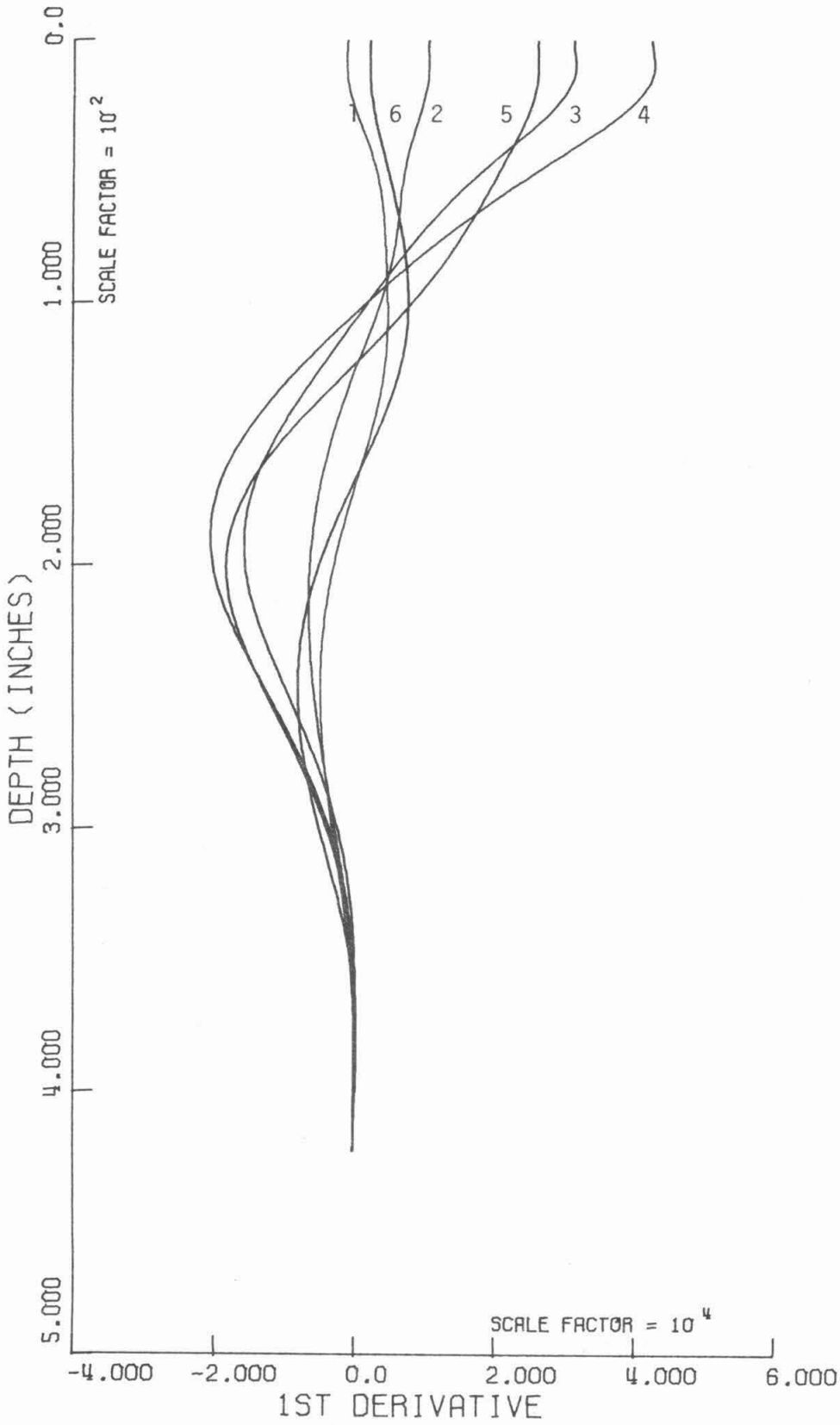

Fig. 4.1.10 (b) shear force

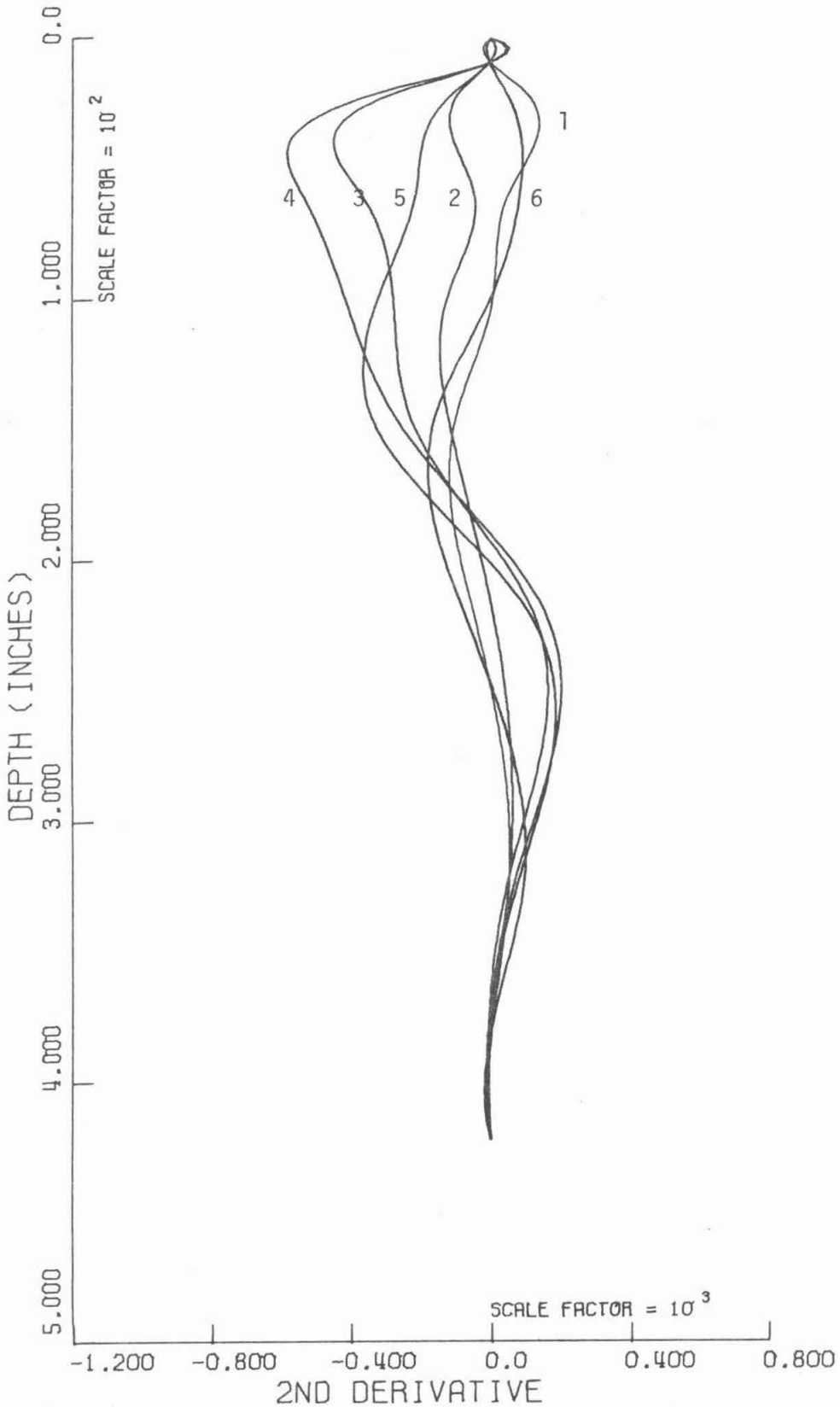

Fig. 4.1.10 (c) soil reaction

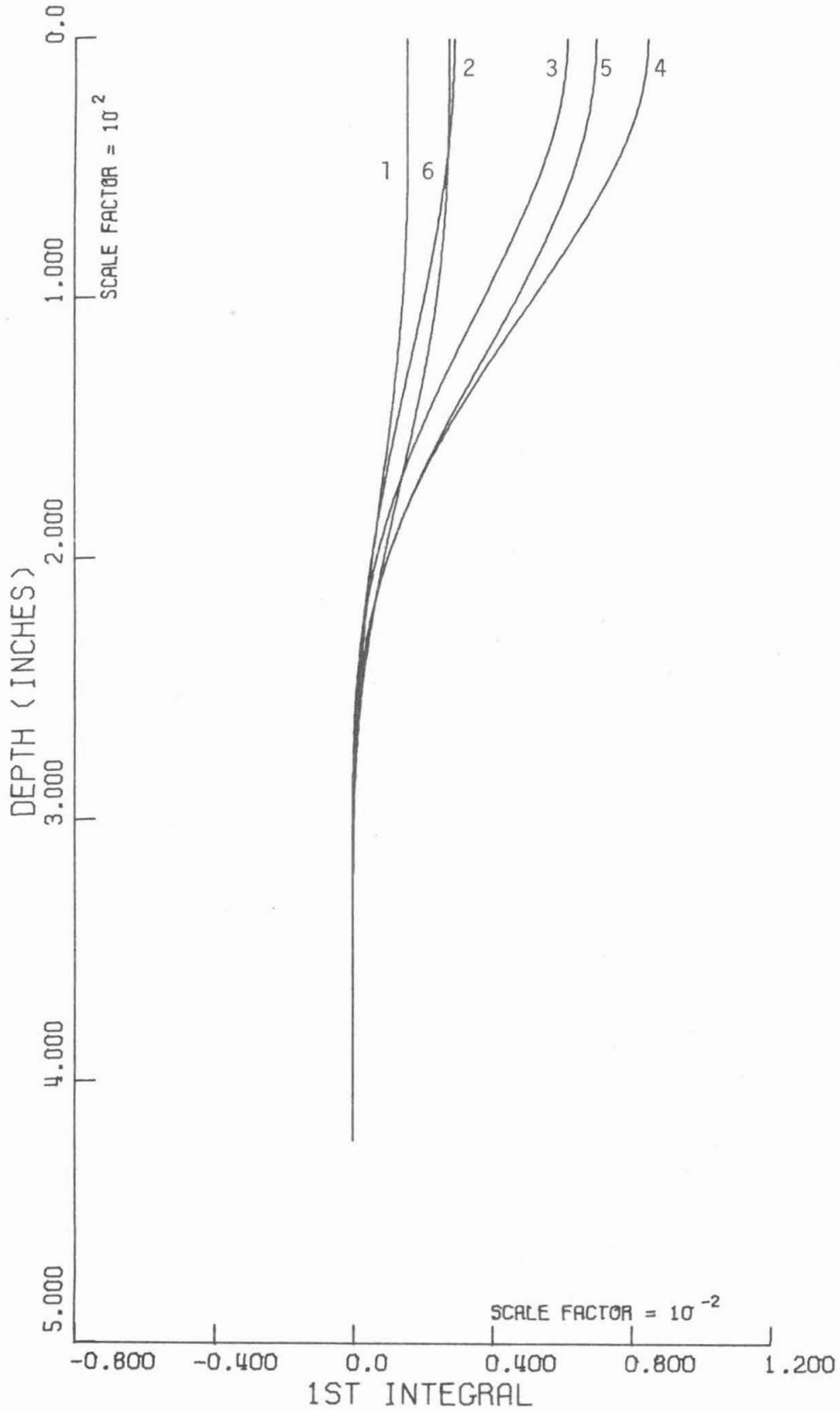

Fig. 4.1.10 (d) slope

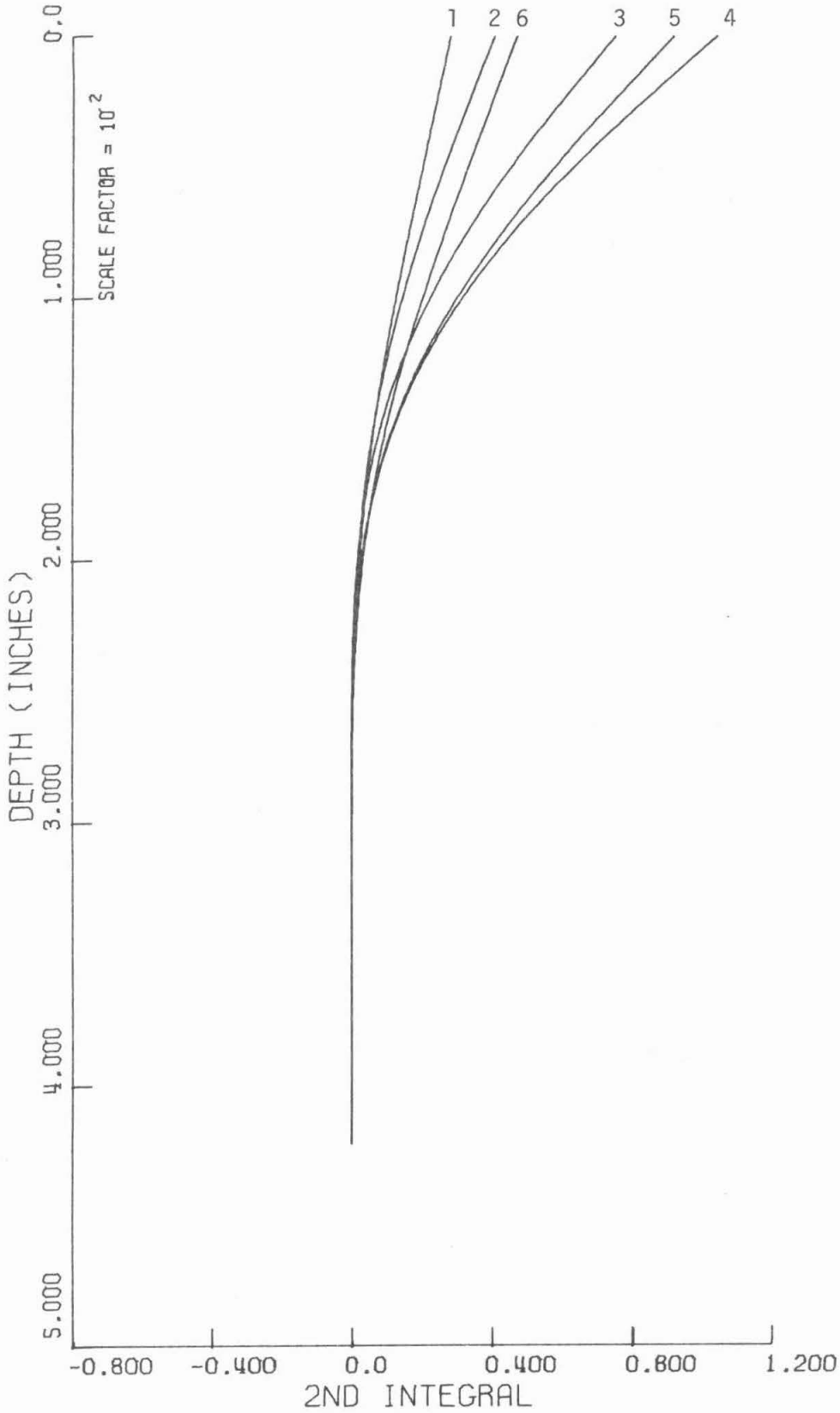

Fig. 4.1.10 (e) deflection

TABLE 4.1.1

Maximum Moments and Displacements in Cyclic Tests

	Dry Soil		Wet	
	Cycle 1	Cycle 2	Cycle 1	Cycle 2
Maximum Load, kips	36.	48.	34.	43.
Maximum Moment x 10^6 lb in	2.10	2.72	1.98	2.53
Depth of Maximum Moment, inches	85	90	105	110
Residual Moment (zero load) x 10^6 lb in	0.56	0.69	0.52	0.72
Maximum Displacement, inches	0.53	0.77	0.76	1.01
Residual Displacement, inches	0.17	0.27	0.26	0.45

From Table 4.1.1 it can be seen that the maximum moment generated in the pile is almost the same at the same load in the dry and wet tests, but that it occurs farther down the pile and at higher displacements in the wet soil. Larger residual displacements are left in the pile in wet soil upon unloading.

Figures 4.1.1 and 4.1.8 show the first four cycles of the cyclic load-unload displacement behavior of the pile in dry and saturated sand, respectively. For comparison on both figures is also drawn the load-displacement behavior of Pile 1, first loading, from the Mustang Island report. It can be seen that on first loading of the model pile it exhibits a load-displacement behavior that is more linear than the full-scale pile,

and that, after the first cycle of loading, it becomes progressively stiffer than the Mustang Island (MI) pile. On the other hand, Figure 4.1.8 on the model test in the saturated sand shows an initial behavior somewhat similar to the MI pile, but less stiff. Subsequent cycles of loading demonstrate a stiffening of the pile-soil system. It is apparent that at a load of about 70 kips the two piles, model and prototype, would exhibit a similar overall stiffness. The dry sand was relatively denser (91%) than the saturated sand (85%) in the model tests. With the given dry densities, the ratio of effective stresses in the saturated soil to those in the dry soil was about 0.62, so that it would be reasonable to expect that at any given value of deflection, the lateral load on the saturated-soil test would be about 0.62 of that in the dry soil. In contrast to the results reported on the preliminary test in the first API report of December 1977 (Figure 5.3 of that report), this time the behavior appears to be correct and substantiates the above conclusion.

Before discussing the tests further, it is convenient to present another figure, Figure 4.1.11, giving the maximum moment versus lateral load in the pile for both dry and wet tests for comparison with the MI test results (the maximum values from all cycles were used in the figure). In this case also, the model test behavior approaches a straight line more closely than the full-scale tests, and, indeed, the loading behavior is very close to linear. This is what would be expected in a linear soil model. However, although the behavior is nearly linear, it is not elastic, as is indicated by the moments shown for the first unloading from about 35 kips in both wet and dry soils. The residual moments of 0.5 to 0.6 X 10^3 inch-kips are apparent.

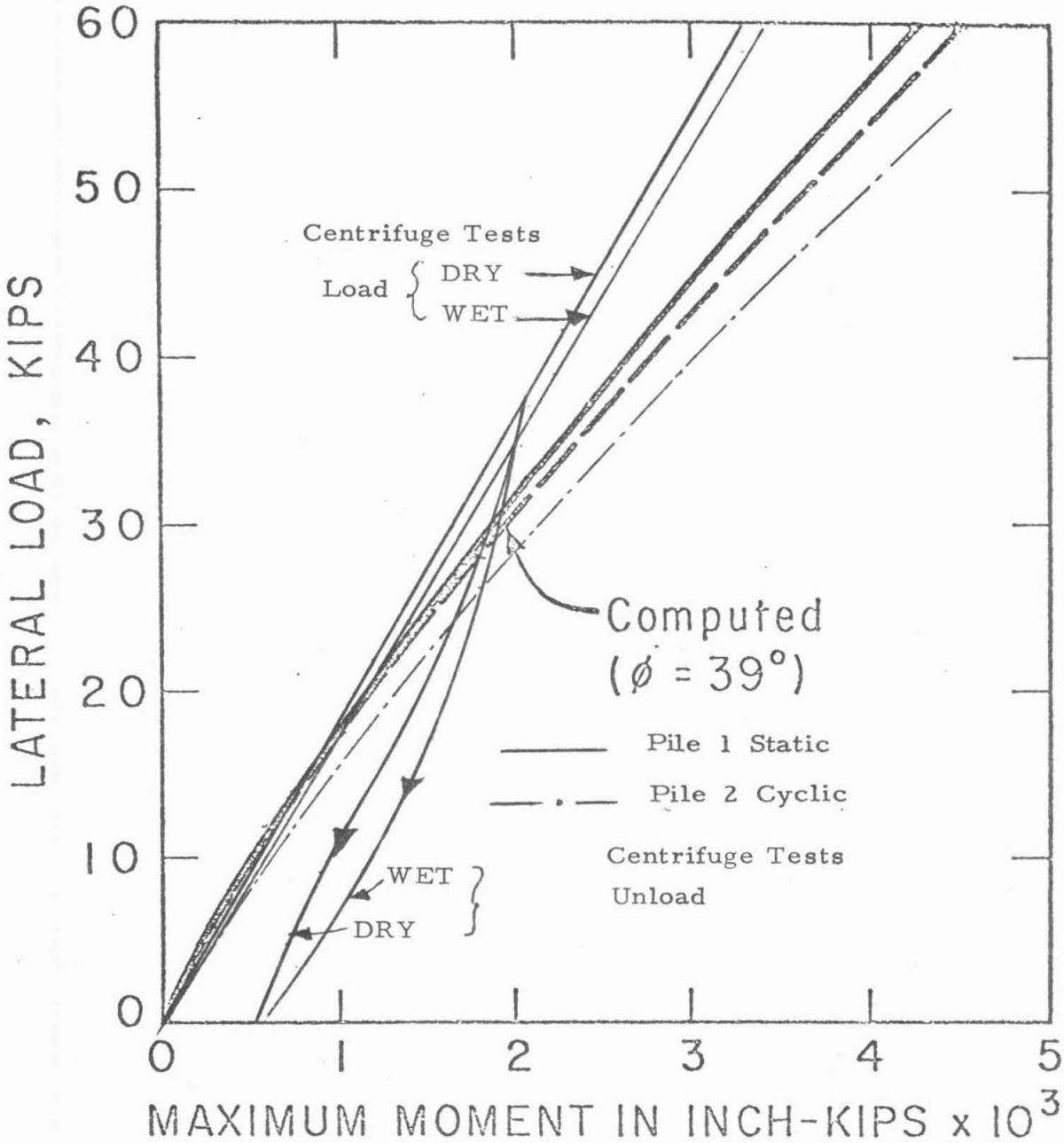

Fig. 4.1.11 Lateral load versus maximum pile moment for dry and saturated load-unload cyclic tests in centrifuge and Mustang Island prototype pile (amended from Ref. 7 of first API report).

It is obvious from both model and prototype tests that the maximum moment on loading is not very sensitive to the soil or pile properties. What happens, of course, is that the pile in the less dense soil (or saturated) deflects more and the maximum moment is generated at a greater depth. This effect can be seen by reference to the linearly elastic Winkler model with constant coefficient of lateral subgrade reaction, where the maximum moment, M_m, can be found to be

$$M_m = \frac{0.3224\ P}{\lambda} \qquad (4.1.1)$$

at a depth of $\lambda z = \pi/4$,

where

$$\lambda = \sqrt[4]{\frac{k}{4EI}} \qquad (4.1.2)$$

and the maximum deflection w_m occurs at the surface

$$w_m = \frac{2\lambda P}{k} \qquad (4.1.3)$$

In these equations, P is the applied lateral load at ground surface, k is the coefficient of subgrade reaction (= k_0 times the pile width), E is Young's modulus of the pile, I is its moment of inertia, and λ is a relative flexibility parameter with dimensions of L^{-1}.

The soil and beam properties enter the equation for maximum moment (4.1.1) only through λ which is seen to be weakly dependent on them, by the fourth root. However, the maximum displacement is related not only to λ, but to k directly. Thus, higher or lower values of k have a strong effect on the maximum deflection, but little impact on M_m.

From the results of the appendix, for the case where the subgrade reaction coefficient k increases linearly with depth

$$k = k_1 X \tag{4.1.4}$$

the maximum moment occurs at a depth of

$$\lambda_1 x = 1.34 \tag{4.1.5}$$

and has the value

$$M_m = 0.773 \frac{P}{\lambda_1} \tag{4.1.6}$$

where λ_1 is now given by the expression

$$\lambda_1 = \sqrt[5]{\frac{k_1}{EI}} \tag{4.1.7}$$

The maximum deflection in this case is

$$w_m = 2.4292 \frac{\lambda_1^2 P}{k_1} \qquad \frac{X_1^2 P}{K_1}$$

at the surface.

The unloading curve in Figures 4.1.1, 4.1.8, and 4.1.11 shows clearly that the soil behavior is not elastic, but it might be worth while to postulate the <u>loading</u> behavior of the soil elements as linear so that the above equations may be used to see if they describe the pile performance. At a load of 35.8 kips, in dry soil, the maximum moment in the pile is 2.08 X 10^6 inch-lb at a depth of 87.5 inches. The deflection of the pile top is 0.53 inches. Any one of the last three numbers can be used with the appropriate

equations above to establish values for λ and k or λ_1 and k_1. It is easiest to use the depth to the maximum moment. If this is employed to obtain λ and λ_1, the pile EI enables k and k_1 to be obtained. With these values, the maximum moment and deflection of the pile can be calculated to compare with the measured quantities. The results can be assembled in a table as follows:

					Predicted	
	λ	λ_1	k	k_1	M_m	w_m
Analysis Basis	$inch^{-1}$	$inch^{-1}$	lb/in^2	lb/in^3	lb-in x 10^6	inch
k = constant	8.98×10^{-3}	—	1298	—	1.29	0.495
$k = k_1 z$	—	1.531×10^{-2}	—	42.12	1.81	0.484
			Measured Values		2.08	0.53

It can be seen that, whereas both models indicate the deflection fairly well on this basis, the constant model does a poor job of estimating the maximum moment. The linear variation of k approach comes closer to giving the correct M_m. From this analysis, it is apparent that a model utilizing a subgrade reaction coefficient varying with depth to a power greater than unity might offer a better indication of maximum moment. With the limited data at hand, this approach will not be developed further at this time.

The appearance of the model test results in Figures 4.1.1, 4.1.8, and 4.1.11 compared to the prototype behavior may indicate that the model soil adjacent to the pile is being densified by the successive movements of the pile.

4.2 Vibration Tests

In Figure 3.3.1 is shown a tracing of the Visicorder output during a frequency sweep in a dynamic test on the model pile imbedded in saturated Nevada Sand. In the center of the diagram, the pile is seen to be resonating at the applied frequency, which, in this case, was about 38 Hz, or 0.38 Hz in the prototype. The direction of the sweep is from low to high frequency, or from right to left in the figure. The sharpness of the resonance response can be appreciated by observing how the signals attenuate on the left of the diagram, where the frequency has reached about 67 Hertz (0.67 Hertz, prototype).

This was the lowest mode found for this pile and, in confirmation, the length of the pile appears to be vibrating in phase with the top. The apparently opposite phase of strain gauge 5 is actually indicating a negative moment in phase with the upper gauges. This shows that care must be taken in the interpretation of moment readings in the vibrating pile. The motion appears to be close to sinusoidal in form, although there is some anomaly in the top displacement indication (second trace). This may be related to the characteristics of the optical system, but is more likely an indication of a more complicated vibrational movement in the pile head attachment structure (see Figures 3.1.3 and 3.1.4).

The maximum half-amplitude of strain shown in Figure 3.3.1 corresponds to a peak positive (or negative in the subsequent half cycle of movement) moment of about 1.9×10^6 lb-inches in the prototype pile just below ground surface. Comparing this with the statically-generated moments as shown in Figures 4.1.2 and 4.1.5, it is seen that the vibration test

equipment developed quite high and realistic moments in the pile. The load at the line of thrust of the coil required to give this moment was about 13 kips. Since the line of action was about 130 inches above ground surface, the pile moments and deflections were equivalent to those caused by a horizontal force of this magnitude (13 kips) and a moment of 13 x 130 x 1000 = 1.68 x 10^6 lb-inches at the ground surface. The prototype pile deflections at the maximum moment are estimated to be about 0.23 inches at ground surface and about 0.86 inches at the line of action of the force, 130 inches above ground level. These values are within the range of interest for prototype piles.

It appears from this preliminary study, therefore, that the vibration system developed is capable of producing realistic prototype-level moments and deflections in a pile-soil system.

The mass (145.5 gm) attached to the top of the model pile corresponds to a weight at the top of the prototype pile of 0.32 x 10^6 lb, and the weight of the prototype pile (15 gm) is 0.033 x 10^6 lb. Assuming that one-third of the pile mass can be added to the attached mass for vibration purposes, the total vibrating weight (mg) is then 0.331 x 10^6 lb. At the observed fundamental frequency, f, of 0.38 Hertz (prototype), the equivalent spring constant, K, of the vibrating system is found from the equation,

$$2\pi f = \sqrt{\frac{K}{m}}$$

to be about 5 kips/inch.

Further vibration tests on piles in wet sands and analyses of both dry and wet sands remain to be carried out.

5. Conclusions

The static and cyclic static centrifuge tests compare favorably with the prototype Mustang Island tests. There is still a question as to the comparative relative densities (RD) existing in model and prototype. The RD of the static cyclic model test in dry sand was 91%, and in the wet sand, slightly less, 85%, whereas in the prototype tests, the indicated relative density (wet soil) from 3 field tests was 100% (3 ft depth), 46% (7 ft), 75% (10 ft). The density increased below 10 feet depth. However, the field behavior seems to derive from a higher density than that evident in the top 10 feet where the maximum moments and deflections occurred. Since the presence of small amounts of clay and silt in the sand is noted in the Mustang Island report, it is possible that this material stiffened the sand somewhat. It is commonly difficult in soil engineering to identify mechanical soil properties (Young's modulus, etc.) with density, relative density, stiffness or hardness obtained by cone penetrometer or standard penetration test. The difference between the model and prototype tests may be ascribed to the usual scatter in behavior occurring as a result of largely unknown property differences. It does not appear to be due to a systematic scaling effect in the model tests, although this cannot be ruled out entirely.

There are, of course, a number of reasons why the model test results may depart from those of the prototype. Some of these are subject to control, others not. It is worth while listing them for clarity.

1. The model and prototype soils can never be made identical. Even if the prototype soil is actually used, its depositional history and structural

and depth variations cannot be simulated. This problem is further complicated by the questions associated with the field determination of the soil's relative density. It is difficult to say, with respect to Figure 5.1 of the first API report, whether or not the soil's density is correctly represented in the top 10 ft, which is the zone of greatest influence on lateral displacements and moments in the pile. Without accurate knowledge of the unit weight profile, simulations are necessarily limited.

2. It is difficult at the scales involved to build a model structure identical in geometry and properties to the prototype, even for such a simple element as a pile. The EI property of the pile appears, of course, in its behavior in the ground, and also in some of the computations which are based on the measured strains. Assuming the strains are measured correctly, the calculated slopes and displacements do not depend on the pile property, but the moments and loads do. For more complicated geometries, the task is even more difficult. One solution would be to perform tests at lower g-levels in a larger centrifuge machine, since a variety of tubes is available which might better simulate a prototype pipe pile.
3. The load in the model pile was applied at the ground surface, to simplify subsequent analysis of the data. However, in the field tests, the load was applied one foot above ground level, and this meant that the boundary conditions at zero elevation consisted of a horizontal force and a substantial moment. The comparison between model and MI prototype maximum moment is not strictly valid for this reason.

4. Lastly, there is the question of processes at work in the model which are not present, or are less important than in the prototype. They may concern the high stress or strain gradients in the model, or, in the saturated soil tests, pore pressure effects. It seems from the tests conducted that these scale effects, if present, are relatively less important than the other considerations above, of which the first, to do with soil simulation, is certainly the most significant.

The vibrating tests appear to be satisfactory (there are no prototype results as far as is known with which to compare them) when they are judged by the static tests. The vibration equipment works well, and develops stresses in the pile at a realistic prototype level. The tests will be continued and extended to encompass wet soils. It is intended to explore the possibility of generating random, earthquake-like excitations by the same means.

Because the Winkler model has been found to describe the behavior of beams and piles in soils reasonably well, but analytical solutions were not available to cases in which the soil subgrade reaction coefficient varies with depth, it was decided to examine analytical techniques for the solution of the latter class of problems. In the particular case of long, flexible piles where boundary conditions at the bottom end of the pile do not influence the solution, there are only two solutions to the fourth-order equation. This consequence enabled an analytical result to be obtained for the problem where the soil reaction coefficient increased linearly with depth. For other variations, a new numerical technique was found and used to solve a case where the soil property varied with the square root of depth. These results are described in the Appendix.

6. Acknowledgements

The tests and instrumentation were set up and operated by Caltech research engineer John Lee, who also contributed the instrumentation section of this report. John Lee digitized the test results. Michael Craig assisted in the preparation of the computer plots. The author would like to acknowledge again the support and cooperation of the API OSAPR advisory committee.

Carol Snyder typed this report.

APPENDIX

"The Solution of the Beam Equation with Variable Foundation Coefficients" by J. N. Franklin and R. F. Scott

THE SOLUTION OF THE BEAM EQUATION WITH VARIABLE FOUNDATION COEFFICIENT

By J. N. FRANKLIN and R. F. SCOTT

(Division of Engineering and Applied Science,

California Institute of Technology)

SUMMARY

The equation $w^{(4)}(x) + x^p w(x) = 0$ in the region $(0 < x < \infty)$ is of value in describing the behavior of loaded beams resting on, or imbedded (piles) in soils. Its solution when $p = 0$ is elementary, but for other values of p, solutions have formerly been obtained only by the finite difference method. Herein, an analytical solution is obtained and evaluated for the case of $p = 1$, and a numerical technique is developed for obtaining two of the solutions for other values of p. The solutions are those which tend to zero as x tends to infinity; they are of use in the case of the semi-infinite beam. In practice most piles in soil fall into this category.

THE SOLUTION OF THE BEAM EQUATION WITH VARIABLE FOUNDATION COEFFICIENT

By J. N. FRANKLIN and R. F. SCOTT

(Division of Engineering and Applied Science,
California Institute of Technology)

1. Introduction

In a wide variety of structural and foundation engineering problems consideration must be given to elastically supported beams. When the support is provided by a continuum, a solution in the form of the deflection of the beam as a function of its length is, in general, difficult to obtain. However, a satisfactory representation of the system, and one which is exact in some circumstances, can be achieved by considering the support of the beam to consist of springs continuously distributed along its length. In this case, it is customary to refer to the spring arrangement as the "foundation." The springs may in fact represent the reaction of soil surrounding the beam, when the latter lies on or is imbedded in such a foundation material. In this case the spring system may be considered as an approximation to an elastic half-space. In other circumstances, such as thin-walled shells and tubes, the foundation may describe the resistance to deformation of parts of a continuous elastic structure adjoining or supporting the beam.

There are conditions under which the behavior of a beam or slab on an elastic foundation is very closely described by the beam and spring system; an example is a floating ice sheet deflected by a surface load (5).

It cannot be said that the representation is exact, because the usual beam or slab equation is itself an approximation.

The concept of the spring foundation is usually attributed to E. Winkler (11) although it has been ascribed to Fuss (9) and to Euler (1). An historical summary and discussion of the approach is given by Hetenyi (4).

The continuous supporting spring system is frequently called a "Winkler foundation." In attempts to improve the identification of deflections and moments in a loaded beam or slab on a Winkler foundation with those in the same loaded beam on an elastic continuum, other foundation models have been proposed. These have been identified with the names of Wieghardt (10), Pasternak (8), Filonenko-Borodich (2), and Hetenyi (3). Sometimes, since the foundation material is represented by one constant in the Winkler model and by two or more in other systems, the different schemes are referred to as one-, two-, or more-parameter models. A systematization of these models was effected by Vlasov and Leontiev (9).

In the simplest case, which has still considerable practical importance, the beam and foundation have properties uniform along the length of the beam. For this circumstance analytical solutions in terms of elementary functions have long been available; tables for the convenient evaluation of the combinations of these functions have been presented in a variety of publications (3, 9). However, when beam or foundation properties vary in some fashion along the beam's length, closed-form analytical solutions have not obtained. Instead, series solutions, without evaluation and tabulation, have been proposed (3); these are time-consuming and inconvenient to use in practice. Alternatively, numerical, finite difference methods (7) have been employed; in general, a new calculation is required for each case studied.

Here we present closed-form solutions and tabulations of the solutions for the case of the uniform beam on a Winkler foundation whose coefficient varies linearly along the beam. With them, beam problems can be solved as readily as in the uniform-coefficient case. When the coefficient varies with distance along the beam in some fashion other than linearly, closed-form solutions have not been found. However, when practical circumstances require such a problem be evaluated, the geometry of the problem is usually different from the general case. A beam lying on or imbedded in the ground with its axis parallel to the ground's surface is frequently, in practice, finite, although on occasion it may reasonably be considered to be semi-infinite or infinite. For this horizontal beam a uniform, or linearly-varying Winkler foundation is a reasonable representation, and the closed-form solution mentioned above and presented herein can be employed.

On the other hand, a problem of considerable practical interest is the pile, which consists of a beam imbedded vertically, or near-vertically, in the ground, and loaded by a horizontal force or a moment at ground surface. In this case, it is usually not a reasonable assumption to take the foundation coefficient to be uniform with length (depth in the ground) along the beam. Most soils become stiffer with depth, in some cases linearly, in others with some other power of distance. Thus a solution to the beam problem with a general variation of foundation coefficient with length would be advantageous.

For the diameter and length of piles most frequently employed in practice, displacement, moment, and other quantities in this problem die out relatively rapidly with distance from the surface, so that the interesting

range of numerical values occurs near the loaded end. Conditions at the pile base or tip are unimportant, and the problem becomes a semi-infinite one. In this case, analysis can be simplified, and we present an approach to the solution leading to functions which need to be evaluated only once for each assumed variation of foundation coefficient with length.

2. Basic equations

The well-known simplified equation for a beam bending under the action of transverse forces q(x) is (3)

$$EIw^{(4)}(x) = q(x) \qquad (0 < x < \infty) \tag{1}$$

where E is the elastic modulus of the beam material, I the moment of inertia of the beam, w its deflection, and x the length coordinate taken along the beam's axis.

Where the beam is not loaded by external forces, the reaction q(x) is supplied by the foundation material pressing on the beam; it is the representation of this reaction which concerns us here.

In the case of the one-parameter or Winkler representation, we take

$$q(x) = -k(x)w \tag{2}$$

in which k is a spring coefficient, including the width of the beam, representing the elastic reaction of the foundation to the deflections of the beam. In the linear problem, it is taken to be independent of the deflection w. For the simplest equation, which has been most widely employed in practice, k(x) is taken to be a constant, k_1, independent of length x, whose substitution in (2) and (1) gives the beam-foundation equation

$$EIw^{(4)}(x) + k_1 w(x) = 0 \qquad (0 < x < \infty) \tag{3}$$

By introducing the parameter λ, with dimensions L^{-1}, where

$$\lambda^4 = \frac{k_1}{4EI} \tag{4}$$

equation (3) can be made dimensionless

$$w^{(4)}(x) + 4w(x) = 0 \tag{5}$$

where w and x are now taken to be dimensionless displacement and distance quantities.

The solution of (4) is most conveniently expressed in the form

$$w = (C_1 \cos x + C_2 \sin x)e^{x} + (C_3 \cos x + C_4 \sin x)e^{-x} \tag{6}$$

where the four C's are constants to be obtained from two boundary conditions at each end of the beam. It is seen that in (6) two of the four solutions for w increase exponentially, and two decrease exponentially with x. Thus, in the case of the semi-infinite beam or pile, for example, C_1 and C_2 would be taken to be zero, and the other two constants calculated from the load and displacement conditions at the beam end or pile top (x = 0). Thus, although other formulations of the solution are possible, the form of (6) is especially well-suited to the pile problem. It would be convenient, therefore, to obtain solutions to variations of (3) or (5) with k(x) a function of length, in the same form; that is to say, with two components increasing in more-or-less exponential fashion, and the other two decreasing with distance.

When k(x) is a linear function of x, say k_2x, the dimensionless beam equation becomes

$$w^{(4)}(x) + xw(x) = 0 \quad (0 < x < \infty) \tag{7}$$

when the substitution

$$\lambda^5 = \frac{k_2}{EI} \tag{8}$$

is made. With a replacement of variables and alteration of (8), (7) also describes the problem where in general, $k(x) = k_1 + k_2x$.

If k(x) is a power function of x, say k_3x^p, where $p \geq 0$, the dimensionless equation is

$$w^{(4)}(x) + x^p w(x) = 0 \quad (0 < x < \infty) \tag{9}$$

if λ is taken in the form

$$\lambda^{p+4} = \frac{k_3}{EI} . \tag{10}$$

In the case where it is felt that a two-parameter model can better fit the known practical problem conditions, the reaction-loading expression is

$$q(x) = -k(x)w(x) + S(x)w^{(2)}(x) \tag{11}$$

in which all the terms have the same meaning as before, and S is an additional foundation material constant. The substitution of this equation in (1) gives the two-parameter beam equation

$$EIw^{(4)}(x) - S(x)w^{(2)}(x) + k(x)w(x) = 0 \quad (0 < x < \infty) \tag{12}$$

With equation (4) as before, the dimensionless form of (12), when both S and k are independent of x, with symbols S_1, and k_1 respectively, is

$$w^{(4)}(x) - \frac{4S_1\lambda^2}{k_1} w^{(2)}(x) + 4w(x) = 0 \qquad (13)$$

For cases of practical interest $S_1^2 < 4k_1EI$ and four solutions to this equation have the same form as before, with two increasing exponentially and two decreasing exponentially with distance.

When both S and k vary with distance, appropriate dimensionless equations analogous to (7) and (9) can be established. In practical applications such as beams and piles, where the reaction is provided by the ground, information is lacking on the material properties which would lead to the development of beam-foundation equations with more than two parameters.

In the following sections, we consider first the contour-integral solution of equation (7), and later the generalized solution technique for equations of the form of (9).

3. Contour-integral solutions

First, we consider the differential equation (7) given previously

$$w^{(4)}(x) + xw(x) = 0 \qquad (0 < x < \infty) . \qquad (7)$$

We can obtain solutions to (7) as contour integrals.

Referring to Figure 1, where five contours C_k are drawn in the ζ-plane, we see that contour C_k appears in the sector

$$\pi - 2k\pi/5 > \arg \zeta > \pi - 2(k+1)\pi/5 \qquad (14)$$

We suppose that arg ζ varies between these limits as ζ moves along C_k.

Define the five integrals

$$w_k(x) = \int_{C_k} \exp(\zeta x + \zeta^5/5)d\zeta \quad (k = 0, \ldots, 4) . \tag{15}$$

The integrals converge because ζ^5 tends strongly to $-\infty$ at both ends of C_k. We will show that these integrals are solutions of the differential equation (7).

Differentiate $w_k(x)$ four times; the result is

$$\int_{C_k} \zeta^4 \exp(\zeta + \zeta^5/5)d\zeta .$$

By integration by parts, this equals

$$-x\int_{C_k} \exp(\zeta x + \zeta^5/5)d\zeta$$

since the integrated part vanishes at both ends of C_k. Thus, as asserted

$$w_k^{(4)}(x) = -xw_k(x) .$$

The five solutions $w_0, \ldots, w_4$ must be dependent. In fact, by the way the contours C_k are drawn,

$$\sum_{k=0}^{4} w_k(x) = 0 . \tag{16}$$

We note also that, since x is real,

$$w_0(x) + \overline{w}_4(x) = 0 \quad \text{and} \quad w_1(x) + \overline{w}_3(x) = 0 \ . \tag{17}$$

Thus, we can obtain these four real-valued solutions:

$$\mathrm{Re}w_0(x) \ , \quad \mathrm{Im}w_0(x) \ ; \quad \mathrm{Re}w_1(x) \ , \quad \mathrm{Im}w_1(x) \ . \tag{18}$$

We will obtain asymptotic forms for the complex-valued solutions $w_0(x)$ and $w_1(x)$. These asymptotic forms will show that the four real-valued solutions (18) are linearly independent; and they will show that, as $x \to +\infty$, the real and imaginary parts of $w_0(x)$ tend to 0 while both the real and the imaginary parts of $w_1(x)$ become unbounded.

The independence of the four solutions (18) can also be deduced from their initial conditions. First look at $w_0(x)$. If the contour C_0 is made to follow the edges of the sector, we find

$$\begin{aligned} w_0(x) &= \int_0^\infty \exp(-tx - t^5/5)dt \\ &\quad + \int_0^\infty \exp(e^{3\pi i/5} tx - t^5/5)dt \ . \end{aligned} \tag{19}$$

For $x = 0$ we can write the value of the j^{th} derivative by means of a gamma function:

$$w_0^{(j)}(0) = 5^{(j-4)/5}\left[(-1)^j + e^{(j+1)3\pi i/5}\right] \Gamma\left(\frac{j+1}{5}\right). \tag{20}$$

Similarly, we can write

$$w_1(x) = -e^{\pi i/5}\int_0^\infty \exp(e^{3\pi i/5}tx - t^5/5)dt + e^{\pi i/5}\int_0^\infty \exp(e^{\pi i/5}tx - t^5/5)dt \ . \tag{21}$$

And at x = 0 we find the initial conditions

$$w_1^{(j)}(0) = 5^{(j-4)/5}\left[-e^{(j+1)3\pi i/5} + e^{(j+1)\pi i/5}\right]\Gamma\left(\frac{j+1}{5}\right) \ . \tag{22}$$

Let $\underset{\sim}{w}_k(x)$ be the vector whose components are the four derivatives $w_k^{(j)}(x)$ (j = 0, ..., 3). From (20) and (22) we can form the four real initial vectors

$$\mathrm{Re}\underset{\sim}{w}_0(0) \ , \quad \mathrm{Im}\underset{\sim}{w}_0(0) \ , \quad \mathrm{Re}\underset{\sim}{w}_1(0) \ , \quad \mathrm{Im}\underset{\sim}{w}_1(0) \ . \tag{23}$$

It can be verified that the Wronskian determinant whose columns are these four vectors is non-zero; this proves the independence of the four solutions (18).

Since $\cos(3\pi/5) < 0$, the complex solution $w_0(x) \to 0$ as $x \to +\infty$, as we see from (19). Similarly, since $\cos(\pi/5) > 0$, the complex solution $w_1(x)$ is unbounded, as we see from (21).

4. Asymptotic behavior

If x is a positive constant, we can make the change of variable $\zeta = sx^{1/4}$ in the contour integral for $w_k(x)$. We then find

$$w_k(x) = x^{1/4}\int_{C_k} \exp[\lambda(s + s^5/5)]ds \tag{24}$$

where $\lambda = x^{5/4}$. We are permitted to leave the contour C_k with the same form, since the change of variable is just a stretching by a positive constant multiplier.

Now we can use the saddle-point method. We want to obtain the asymptotic behavior of the integral (24) as $\lambda \to +\infty$. The saddle points are the roots of $1 + s^4 = 0$. From Figure 1, we see that a curve of the form C_0 passes through the saddle point $\exp(3\pi i/4)$, while a curve of the form C_1 passes through the saddle point $\exp(\pi i/4)$. In the saddle-point method we choose these curves so that

$$\mathrm{Im}(s + s^5/5) = \text{constant on } C_k \,. \tag{25}$$

Then $\mathrm{Re}(s + s^5/5)$ begins at $-\infty$, increases to its maximum at the saddle point, and decreases to $-\infty$.

This is the standard formula obtained from the saddle-point method:

$$\int_C e^{\lambda f(s)} ds = \left(\frac{2\pi}{\lambda |f''(s_0)|}\right)^{\frac{1}{2}} e^{\lambda f(s_0)} \left(e^{i\alpha} + O\left(\frac{1}{\lambda}\right)\right) \tag{26}$$

where α is the argument of the tangent to C at the saddle point s_0, namely

$$\alpha = \pm \frac{\pi}{2} - \tfrac{1}{2} \arg f''(s_0) + 2n\pi \,. \tag{27}$$

We must now consider the integrals for $w_0(x)$ and $w_1(x)$ separately.

For $w_0(x)$ we have

$$\begin{aligned} s_0 &= e^{3\pi i/4} \quad , \quad f(s_0) = s_0 + s_0^5/5 \\ &= -\frac{2}{5}\sqrt{2}\,(i - i) \end{aligned} \tag{28}$$

To compute α, we first compute $\arg f''(s_0) = 9\pi/4$. From (27), we take

$$\alpha = -\frac{\pi}{2} - \frac{1}{2}\frac{9\pi}{8} + 2\pi = \frac{3\pi}{8}. \tag{29}$$

Then the asymptotic form (26) becomes

$$\left(\frac{\pi}{2\lambda}\right)^{\frac{1}{2}} \cdot \exp\left[-\frac{2}{5}\sqrt{2}\,(1-i)\lambda + \frac{3\pi i}{8}\right] \cdot \left(1 + O\left(\frac{1}{\lambda}\right)\right). \tag{30}$$

If we multiply this by $x^{1/4}$ and use $\lambda = x^{5/4}$, we get the asymptotic form

$$w_0(x) = (\pi/2)^{\frac{1}{2}} x^{-3/8} \cdot \exp\left[-\frac{2}{5}\sqrt{2}\,(1-i)x^{5/4} + \frac{3\pi i}{8}\right] \cdot (1 + O(x^{-5/4})). \tag{31}$$

If we do the same things for $w_1(x)$, we find

$$\begin{gathered} s_0 = e^{\pi i/4}, \quad f(s_0) = \frac{2}{5}\sqrt{2}\,(1+i) \\ \arg f''(s_0) = 3\pi/4, \quad \alpha = \frac{\pi}{2} - \frac{3\pi}{8} = \frac{\pi}{8}. \end{gathered} \tag{32}$$

Now (24) and (26) give

$$w_1(x) = (\pi/2)^{\frac{1}{2}} x^{-3/8} \cdot \exp\left[\frac{2}{5}\sqrt{2}\,(1+i)x^{5/4} + \frac{\pi i}{8}\right] \cdot (1 + O(x^{-5/4})). \tag{33}$$

From (31) we see that the real and the imaginary parts of $w_0(x)$ tend to zero and are linearly independent. From (33), the real and imaginary parts of $w_1(x)$ are unbounded and are linearly independent. Therefore, the four functions

$$\mathrm{Re}w_0(x), \quad \mathrm{Im}w_0(x), \quad \mathrm{Re}w_1(x), \quad \mathrm{Im}w_1(x)$$

are a basis for the solutions of the fourth-order equation $w^{(4)} + xw = 0$.

5. Computations

Equations (7) and (9) were written in expanded form and the real and imaginary components and their first three derivatives expressed. The resulting integrals were evaluated numerically in the range $0 < x < 6$ in which most practical interest is centered. Figures 2 and 3 display the solutions obtained.

6. Asymptotic solutions of a more general equation

If p is ≥ 0, we consider the differential equation (9) given previously:

$$w^{(4)}(x) + x^p w(x) = 0 \quad (0 < x < \infty) . \tag{9}$$

As a question of practical interest, we would like to compute the solutions that tend to zero as $x \to +\infty$. We have just solved this problem analytically for $p = 1$, and the problem is trivial for $p = 0$. In the next section we will discuss a numerical method for the general equation (9).

The numerical method will depend on the asymptotic behavior of the solutions. We shall need to know this: the equation (9) has two linearly independent solutions that tend to zero, and it has two independent solutions that are unbounded. We have just proved this for $p = 1$. For $p = 0$, we have these two solutions that tend to zero:

$$w(x) = \exp(e^{\pm 3\pi i/4} x) \tag{34}$$

and we have these two solutions that are unbounded:

$$w(x) = \exp(e^{\pm \pi i/4} x) . \tag{35}$$

For general $p \geq 0$ the fourth-order WKB method gives solutions of the asymptotic form

$$w_k(x) = \exp\left[c_k\left(\int_0^x \xi^{p/4}d\xi\right)(1 + o(1))\right] \quad k = 1, \ldots, 4) \tag{36}$$

where $c_k = \exp[(2k+1)\frac{\pi i}{4}]$ and when the term $1 + o(1)$ occurs in the exponent and tends to 1 as $x \to +\infty$. Since Re $c_k < 0$ for $k = 1, 2$, the solutions $w_1(x)$ and $w_2(x)$ tend to zero as $x \to \infty$; the solutions $w_3(x)$ and $w_4(x)$ are unbounded [see (6), pp. 186, 187].

For $p = 1$ we found solutions of the form

$$(\pi/2)^{\frac{1}{2}}x^{-3/8}(1 + O(x^{-5/4}))\exp(c_k\tfrac{4}{5}x^{5/4}) . \tag{37}$$

These solutions have the form (36) if $p = 1$ therein: the logarithm of the expression (36) equals

$$c_k\tfrac{4}{5}x^{5/4}(1 + o(1)) \tag{38}$$

while the logarithm of the expression (37) equals

$$\tfrac{1}{2}\log(\tfrac{\pi}{2}) - \tfrac{3}{8}\log x + O(x^{-5/4}) + c_k\tfrac{4}{5}x^{5/4} \tag{39}$$

and the expressions (38) and (39) are asymptotically equal.

7. A numerical method

For $p > 0$, we will solve examples of the equation

$$w^{(4)}(x) + x^p w(x) = 0 \quad (0 < x < \infty) \tag{9}$$

by a numerical method that applies to general linear boundary value problems in which the desired solutions tend to zero as $x \to \infty$. Now we will

describe the numerical method and indicate the general conditions for its validity.

First state the problem as a first-order system:

$$\underset{\sim}{w}'(x) = A(x)\underset{\sim}{w}(x) \qquad (0 < x < \infty) \ . \tag{40}$$

For the example (9), the first-order system (40) uses

$$\underset{\sim}{w} = \begin{pmatrix} w \\ w' \\ w'' \\ w''' \end{pmatrix} \ , \qquad A = \begin{pmatrix} 0 & 1 & 0 & 0 \\ 0 & 0 & 1 & 0 \\ 0 & 0 & 0 & 1 \\ -x^p & 0 & 0 & 0 \end{pmatrix} \ . \tag{41}$$

Let B be an $m \times n$ matrix, and suppose that the differential equation (40) has one and only one solution $\underset{\sim}{w}(x)$ to the boundary-value problem

$$B\underset{\sim}{w}(0) = \underset{\sim}{g} \ , \qquad \underset{\sim}{w}(x) \to \underset{\sim}{0} \quad \text{as} \quad x \to \infty \tag{42}$$

where $\underset{\sim}{g}$ is any given vector with m components. For instance, for the example (9) we might prescribe

$$\begin{aligned} w''(0) &= g_1 \\ w'''(0) &= g_2 \end{aligned} \ . \tag{43}$$

$$\begin{pmatrix} w \\ w' \\ w'' \\ w''' \end{pmatrix} \to \begin{pmatrix} 0 \\ 0 \\ 0 \\ 0 \end{pmatrix} \quad \text{as} \quad x \to \infty \ .$$

Here $m = 2$, and B is the matrix

$$B = \begin{pmatrix} 0 & 0 & 1 & 0 \\ 0 & 0 & 0 & 1 \end{pmatrix} . \tag{44}$$

This is the numerical method: Pick a fairly large number $a > 0$. Let $\underset{\sim}{w}_1(x), \ldots, \underset{\sim}{w}_m(x)$ be any vector solutions of the differential equation (40) that take prescribed values at $x = a$:

$$\underset{\sim}{w}_j(a) = \underset{\sim}{h}_j \quad (j = 1, \ldots, m) \tag{45}$$

where $\underset{\sim}{h}_1, \ldots, \underset{\sim}{h}_m$ are linearly independent vectors that are independent of a. Thus, the vector $\underset{\sim}{w}_j(x)$ is computed as the solution of an initial-value problem as x decreases from a to 0. We then compute the required solution $\underset{\sim}{w}(x)$ as a linear combination

$$\underset{\sim}{w}(x) = c_1\underset{\sim}{w}_1(x) + \ldots + c_m\underset{\sim}{w}_m(x) \tag{46}$$

where the m coefficients $c_1, \ldots, c_m$ are chosen to satisfy the boundary condition (42) at $x = 0$:

$$c_1 B\underset{\sim}{w}_1(0) + \ldots + c_m B\underset{\sim}{w}_m(0) = \underset{\sim}{g} . \tag{47}$$

Example. Consider the boundary-value problem

$$w''(x) - w(x) = 0 \quad (0 < x < \infty) \tag{48}$$

$$w(0) = 1 \quad w(x) \to 0 \quad \text{as} \quad x \to \infty . \tag{49}$$

Of course, the solution is e^{-x}. Let us apply the general method and see if it works.

Here $m = 1$. At $x = a$, let the solution $w_1(x)$ be determined by

$$\underset{\sim}{w}_1(a) = \underset{\sim}{h}_1 \tag{50}$$

then we look for the vector solution $\underset{\sim}{w}(x)$ in the form

$$\underset{\sim}{w}(x) = c_1 \underset{\sim}{w}_1(x) \tag{51}$$

where c_1 satisfies the condition $w(0) = 1$.

If $\underset{\sim}{h}_1 = (h_1, h_1')^T$, then (50) gives

$$w_1(x) = h_1 \cosh (x-a) + h_1' \sinh (x-a) . \tag{52}$$

Now c_1 must satisfy $c_1 w_1(0) = 1$:

$$c_1(h_1 \cosh a - h_1' \sinh a) = 1 . \tag{53}$$

This gives the computed solution for $0 \le x \le a$:

$$w(x) = c_1 w_1(x) = \frac{h_1 \cosh (x-a) + h_1' \sinh (x-a)}{h_1 \cosh a - h_1' \sinh a} . \tag{54}$$

In this fraction the denominator equals

$$\tfrac{1}{2}(h_1 - h_1')e^a + O(e^{-a}) \tag{55}$$

while the numerator equals

$$\tfrac{1}{2}(h_1 - h_1')e^{a-x} + O(e^{x-a}) . \tag{56}$$

Unless $h_1 = h_1'$, the quotient equals

$$e^{-x} + O(e^{x-2a}) \quad (0 \le x \le a) \tag{57}$$

Thus we see that for large a the approximation (54) is good in the whole interval $0 \le x \le a$: the error is uniformly $O(e^{-a})$.

Note that the method fails if $h_1 = h_1'$. Thus, an unlucky choice of the vector $\underset{\sim}{h}$ causes the method to fail. Such an unlucky choice is possible but very improbable.

The example shows why the method usually succeeds. We are looking for a solution $\underset{\sim}{w}(x)$ that tends to zero as x increases from 0 to a; then $\underset{\sim}{w}(x)$ blows up as x decreases from a to 0. Conversely, the troublesome solutions that become unbounded as x increases are just the solutions that tend to zero as x decreases. Thus, we expect the solutions $\underset{\sim}{w}_j(x)$ to become large as x decreases from a to 0; and for x near zero we may expect these solutions to lie almost within the m-dimensional linear space of solutions that tend to zero as $x \to +\infty$. Finally, when we impose the initial condition (47), we may expect to damp out the unwanted components on the whole range $0 < x < a$. In particular, we may expect $\underset{\sim}{w}(a)$ to be practically zero.

In general, let F(x) be a fundamental matrix solution:

$$F'(x) = A(x)F(x) \quad , \quad \det F(x) \neq 0 \ . \tag{58}$$

We suppose that the differential equation (40) has m linearly independent solutions

$$\underset{\sim}{w}(x) = \underset{\sim}{f}_1(x), \ \ldots, \ \underset{\sim}{f}_m(x) \tag{59}$$

that tend to zero as $x \to \infty$. (In the example (9), m = 2.) Further, we suppose that (40) has n-m independent unbounded solutions

$$\underset{\sim}{w}(x) = \underset{\sim}{f}_{m+1}(x), \ \ldots, \ \underset{\sim}{f}_n(x) \tag{60}$$

We may suppose that F(x) has the n columns $\underset{\sim}{f}_j(x)$ (j = 1, . . . , n).

It is convenient to partition F(x) into its bounded and unbounded parts. We write

$$F(x) = [F_0(x) \quad , \quad F_1(x)] \tag{61}$$

where $F_0(x)$ has the m columns (59), and $F_1(x)$ has the n-m columns, (60).

The solutions of (40) that tend to zero as $x \to \infty$ are the linear combinations of the columns of $F_0(x)$:

$$\underset{\sim}{w}_0(x) = F_0(x)\underset{\sim}{b}_0 \to 0 \quad \text{as} \quad x \to \infty . \tag{62}$$

Here $\underset{\sim}{b}_0$ is any constant vector with m components. The solution to the nonsingular boundary-value problem (42) must satisfy

$$BF_0(0)\underset{\sim}{b}_0 = \underset{\sim}{g} \tag{63}$$

The nonsingularity of the boundary-value problem is equivalent to the nonsingularity of the $m \times m$ matrix $BF_0(0)$:

$$\det (BF_0(0)) \neq 0 . \tag{64}$$

Let $\underset{\sim}{h}_1, \ldots, \underset{\sim}{h}_m$ be any m independent vectors in the n-dimensional vector space E^n. Choose a large number $a > 0$. Let the vector solutions $\underset{\sim}{w}_1(x), \ldots, \underset{\sim}{w}_m(x)$ solve the initial-value problems

$$\underset{\sim}{w}_j(a) = \underset{\sim}{h}_j \quad , \quad \underset{\sim}{w}_j'(x) = A(x)\underset{\sim}{w}_j(x) \quad (a > x > 0) . \tag{65}$$

Now compute $\underset{\sim}{w}(x)$ as the linear combination (46) that satisfies the boundary condition (47). Now we wish to show that the computed solution $\underset{\sim}{w}(x)$ is close to the true solution $\underset{\sim}{w}_0(x)$, which is defined by (62) and (63).

Every solution $\underset{\sim}{w}_j(x)$ has the form $F(x)\underset{\sim}{k}_j$, where

$$\underset{\sim}{w}_j(a) = F(a)\underset{\sim}{k}_j = \underset{\sim}{h}_j \quad (j = 1, \ldots, m) . \tag{66}$$

Let k be the n × m matrix whose columns are $\underset{\sim}{k}_1, \ldots, \underset{\sim}{k}_m$:

$$K = [\underset{\sim}{k}_1, \ldots, \underset{\sim}{k}_m] . \tag{67}$$

Similarly, let $H = [\underset{\sim}{h}_1, \ldots, \underset{\sim}{h}_m]$. Then (66) says

$$F(a)K = H . \tag{68}$$

If we partition F(x) as in (61), the last equation becomes

$$F_0(a)K_0 + F_1(a)K_1 = H \tag{69}$$

where K_0 is the m × m matrix formed from the first m rows of K, and K_1 is the (n-m) × m matrix formed from the last n-m rows of K. Though H was chosen independently of a, the matrices K_0 and K_1 do depend on a.

We want to show that $K_1(a)$ is small compared with $K_0(a)$. In (69) we expect $F_0(a)$ to be small and $F_1(a)$ to be large. Let P be some matrix with n rows and n-m columns that are independent and are orthogonal to all the columns of H. If we multiply (69) by P^T, we get

$$P^T F_0(a)K_p(a) + P^T F_1(a)K_1(a) = 0 . \tag{70}$$

Note that P depends only on H and not on a. We suppose that the square matrix $P^T F_1(a)$ is large and nonsingular. More precisely, we suppose that the norm of its inverse is small:

$$\epsilon_1(a) \equiv \|(P^T F_1(a))^{-1}\| \ll 1 . \tag{71}$$

And we suppose that the matrix $P^T F_0(a)$ is small:

$$\epsilon_0(a) \equiv \|P^T F_0(a)\| \ll 1 \tag{72}$$

Now (70) implies

$$K_1(a) = -(P^T F_1(a))^{-1} \cdot P^T F_0(a) \cdot K_0(a) \tag{73}$$

and (71) and (72) give

$$\|K_1(a)\| \leq \epsilon_1(a)\epsilon_0(a)\|K_0(a)\| \ . \tag{74}$$

If $\underset{\sim}{c}$ is any vector in E^m, equation (73) implies

$$\|K_1(a)\underset{\sim}{c}\| \leq \epsilon_1(a)\epsilon_0(a)\|K_0(a)\underset{\sim}{c}\| \ . \tag{75}$$

In particular, let $\underset{\sim}{c}$ solve the boundary condition (47). Since $\underset{\sim}{w}(x) = F(x) K \underset{\sim}{c}$, the condition (47) says

$$BF(0)K\underset{\sim}{c} = \underset{\sim}{g} \tag{76}$$

or

$$B(F_0(0)K_0\underset{\sim}{c} + F_1(0)K_1\underset{\sim}{c}) = \underset{\sim}{g} \ . \tag{77}$$

Since the true solution satisfies (63), we deduce

$$\underset{\sim}{k}_0 + (BF_0(0))^{-1}BF_1(0)\underset{\sim}{k}_1 = \underset{\sim}{b}_0 \tag{78}$$

where we define

$$\underset{\sim}{k}_0 = K_0(a)\underset{\sim}{c} \ , \quad \underset{\sim}{k}_1 = K_1(a)\underset{\sim}{c} \ . \tag{79}$$

Now (75) says

$$\|\underset{\sim}{k}_1\| \leq \epsilon_1(a)\epsilon_0(a)\|\underset{\sim}{k}_0\| \tag{80}$$

and so

$$\|(BF_0(0))^{-1}BF_1(0)\underset{\sim}{k}_1\| \leq \gamma\epsilon_1(a)\,\epsilon_0(a)\|\underset{\sim}{k}_0\| \tag{81}$$

where γ = constant = $\|(BF_0(0))^{-1}BF_1(0)\|$. The identity (78) now implies

$$\|\underset{\sim}{k}_0 - \underset{\sim}{b}_0\| \leq \gamma\,\epsilon_1(a)\,\epsilon_0(a)\|\underset{\sim}{k}_0\| \ . \tag{82}$$

Since $\|\underset{\sim}{k}_0\| \leq \|\underset{\sim}{k}_0 - \underset{\sim}{b}_0\| + \|\underset{\sim}{b}_0\|$, this implies

$$\|\underset{\sim}{k}_0 - \underset{\sim}{b}_0\| \leq \epsilon(a)\|b_0\| \tag{83}$$

where, for large a,

$$\epsilon(a) \equiv \gamma\,\epsilon_1\epsilon_0(1 - \gamma\,\epsilon_1\epsilon_0)^{-1} < 2\gamma\,\epsilon_1\epsilon_0 \ . \tag{84}$$

Thus, $\underset{\sim}{k}_0(a)$ is practically equal to $\underset{\sim}{b}_0$. Now (80) implies

$$\|\underset{\sim}{k}_1\| \leq 2\,\epsilon_1(a)\epsilon_0(a)\|b_0\| \tag{85}$$

if a is large. And so $\underset{\sim}{k}_1(a)$ is practically equal to zero.

The computed solution is

$$\underset{\sim}{w}(x) = F(x)K\underset{\sim}{c} = F_0(x)\underset{\sim}{k}_0 + F_1(x)\underset{\sim}{k}_1 \ . \tag{86}$$

This solution depends not only on x but on a and the constants $\underset{\sim}{h}_1, \ldots, \underset{\sim}{h}_m$. The true solution is $\underset{\sim}{w}_0(x) = F_0(x)\underset{\sim}{b}_0$. The error is

$$\underset{\sim}{w}(x) - \underset{\sim}{w}_0(x) = F_0(x)(\underset{\sim}{k}_0 - \underset{\sim}{b}_0) + F_1(x)\underset{\sim}{k}_1 \ . \tag{87}$$

Now (83) and (85) give this upper bound for $0 \le x \le a$:

$$\|\underset{\sim}{w}(x) - \underset{\sim}{w}_0(x)\| \le c\,\epsilon_1(a)\,\epsilon_0(a)\|\underset{\sim}{b}_0\|(\|F_0(x)\| + \|F_1(x)\|) \ . \tag{88}$$

where $c = 2(1 + \gamma)$. We assume that the following product is bounded for $0 \le x \le a$ as $a \to \infty$:

$$\epsilon_1(a)\|F_1(x)\| \equiv \|(P^T F_1(a))^{-1}\|\,\|F_1(x)\| = O(1) \ . \tag{89}$$

Under this assumption, the error (88) is uniformly of the order $\epsilon_0(a)$ for $0 \le x \le a$. This shows that <u>the computed solution</u> (86) <u>is good on the whole interval</u> $0 \le x \le a$.

We end this discussion by looking again at the simple example (48). We recall that the method failed if we made an unlucky choice for the vector $\underset{\sim}{h}_1$. In terms of the general discussion, what went wrong? Here

$$F(x) = [F_0(x),\ F_1(x)] = \begin{pmatrix} e^{-x} & e^{x} \\ -e^{-x} & e^{x} \end{pmatrix}$$

$$H = \underset{\sim}{h}_1 = \begin{pmatrix} h_1 \\ h_1' \end{pmatrix} \ , \quad P = \begin{pmatrix} -h_1' \\ h_1 \end{pmatrix} \ . \tag{90}$$

Therefore,

$$P^T F_1(a) = (-h_1' + h_1)e^a \ . \tag{91}$$

In the general formula (71), we assumed

$$\epsilon_1(a) \equiv \|(P^T F_1(a))^{-1}\| \ll 1$$

and this is correct for the example (91) unless $h_1 = h_1'$. If $h_1 \neq h_1'$, we have $\epsilon_1(a) = O(e^{-a}) \ll 1$.

8. Computations

The case of $p = 1/2$ was chosen as being one of some practical interest. A trial solution with the initiation point $x = 5$ indicated that errors in the solution were unacceptably large in the region $3 < x < 5$, and a subsequent solution was prepared beginning at $x = 10$. The initial values were chosen as follows for the two required convergent solutions:

Function	First Solution	Second Solution
$w(10)$	0	0
$w'(10)$	0	0
$w''(10)$	0.1	0
$w'''(10)$	0	0.1

The values of the functions were calculated and recorded for $0 < x < 10$ at intervals of $\Delta x = 0.01$ for both solutions. The results are displayed in Figure 4.

It should be noted that the same technique may be applied to the cases where the modulus of the beam varies with distance along the beam, and where both modulus and foundation reaction coefficient vary with distance.

Acknowledgments

We would like to thank A. Chang of the Booth Computing Center of the California Institute of Technology for his assistance in evaluating the integrals of section 4, and in computing the functions by the method of section 7. A portion of this work was supported by a grant from the American Petroleum Institute.

REFERENCES

1. L. Euler, Novi Comm. Acad. Petropolit., Tom XVIII, St. Petersburg, (1774) 289-329.

2. M. M. Filonenko-Borodich, Uchenye Zapiski MGU 46 (1940) 3-18.

3. M. Hetenyi, Beams on Elastic Foundation (University of Michigan Press, 1946).

4. M. Hetenyi, App. Mech. Rev. 19 (1966) 95-102.

5. A. D. Kerr, Jour. App. Mech 3 (1964) 491-498.

6. C. Lamberto, Asymptotic Behavior and Stability Problems in Ordinary Differential Equations, 3rd Edition (Springer-Verlag, New York 1971).

7. H. Matlock and L. C. Reese, Proc. ASCE 86, Jour. SMFD, SM5 (1960) 63-91.

8. P. L. Pasternak, Gos. Izd. Lit. po Stroit. i Arkh. (Moscow 1954).

9. V. L. Vlasov and N. N. Leontiev, Beams, Plates and Shells on Elastic Foundations, Transl. from Russian (NTIS N67-14238 1966).

10. K. Wieghardt, Zeit für Angew. Math u. Mech. 2 (1922) 165-184.

11. E. Winkler, Theory of Elasticity and Strength (Dominicus Prague 1867).

FIGURE CAPTIONS

Figure 1 Complex plane

Figure 2 Solutions to equation $w^{(4)}(x) + xw(x) = 0$ $(0 < x < \infty)$.

(a) $w_1 = \text{Re } w_0(x)$ and derivatives.

(b) $w_2 = \text{Im } w_0(x)$ and derivatives.

Figure 3 Unbounded solutions to equation $w^{(4)}(x) + xw(x) = 0$ $(0 < x < \infty)$.

(a) $w_3 = \text{Re } w_1(x)$ and derivatives.

(b) $w_4 = \text{Im } w_1(x)$ and derivatives.

Figure 4 Numerical solutions to equation $w^{(4)}(x) + x^{\frac{1}{2}}w(x) = 0$ $(0 < x < \infty)$ tending to zero as x goes to infinity.

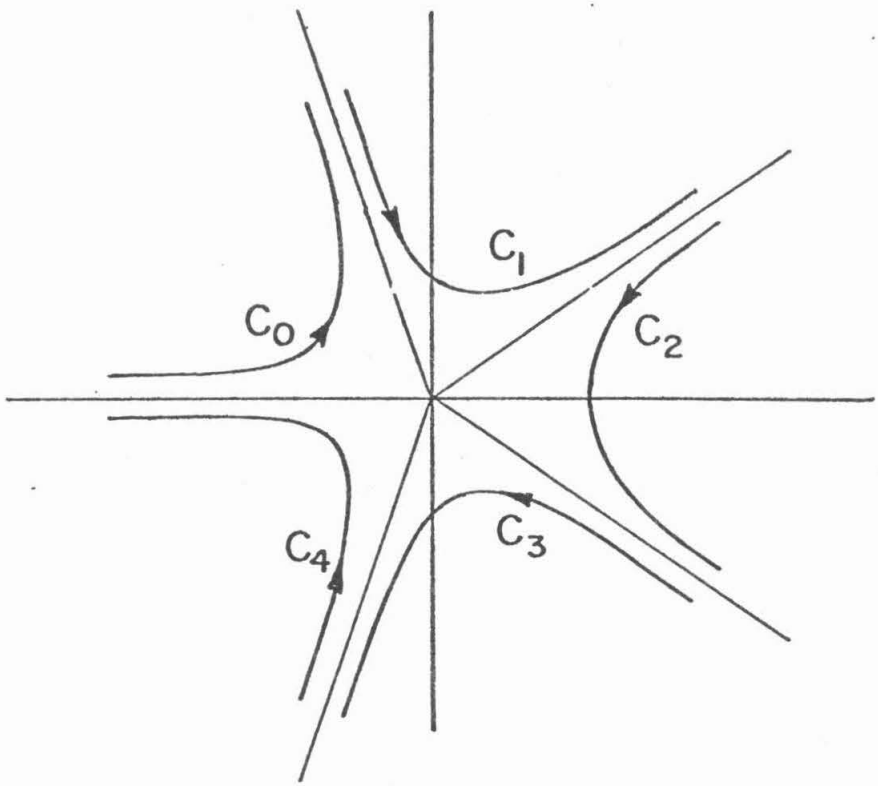

Figure 1

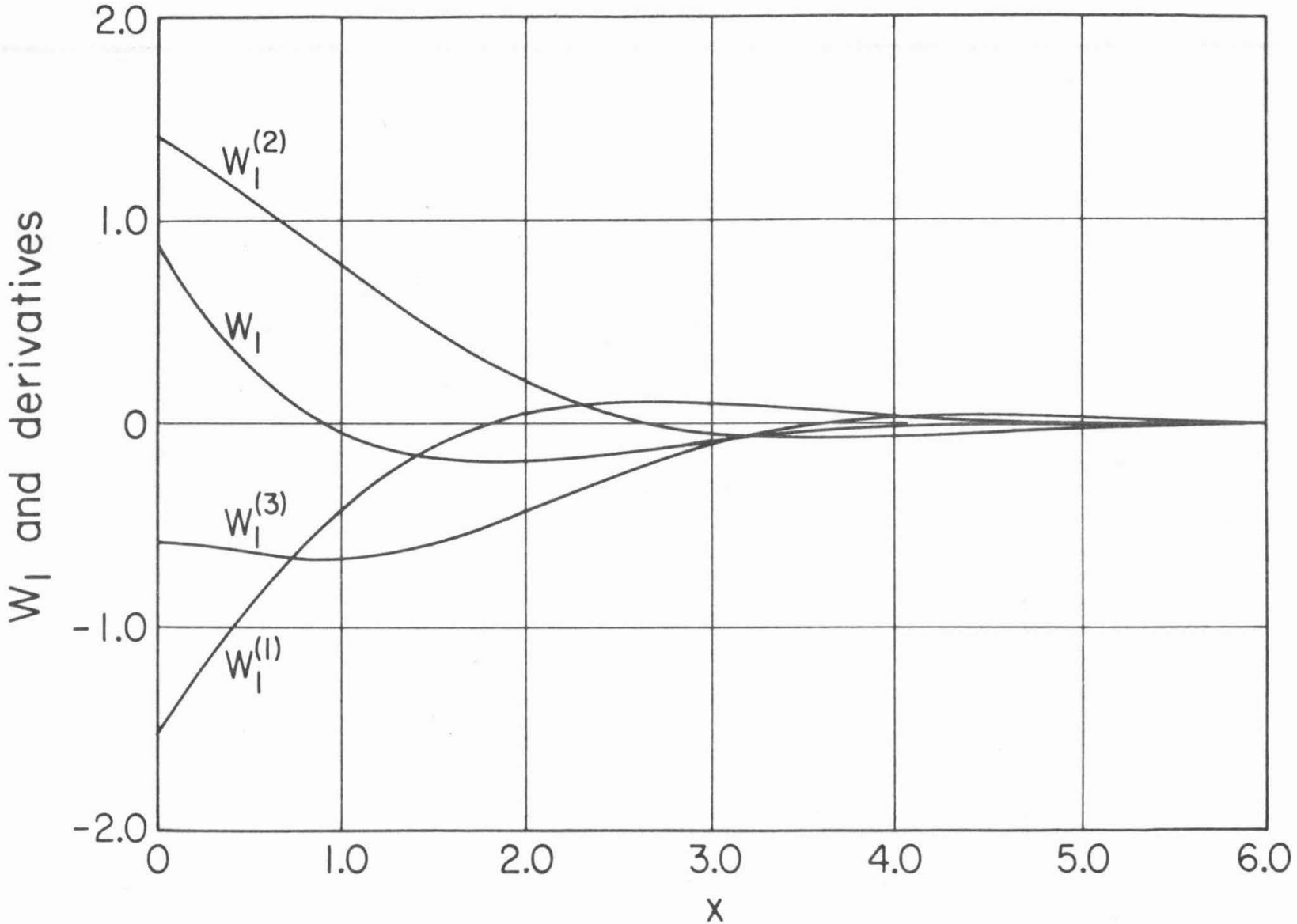
2.0
1.0
0
-1.0
-2.0
0
1.0
2.0
3.0
4.0
5.0
6.0
X
W_1 and derivatives
$W_1^{(2)}$
W_1
$W_1^{(3)}$
$W_1^{(1)}$

Figure 2(a)

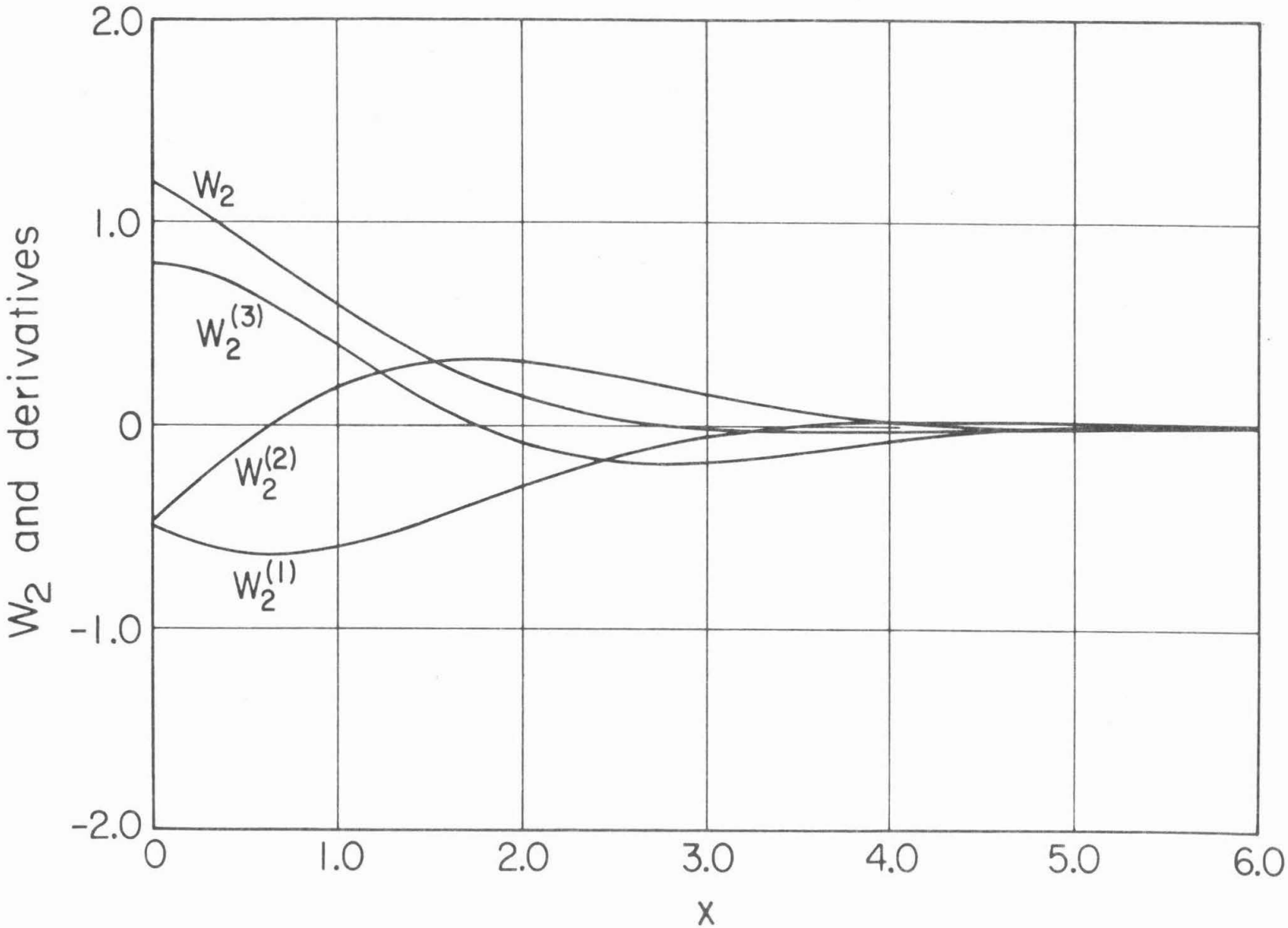
2.0
1.0
0
-1.0
-2.0
0
1.0
2.0
3.0
4.0
5.0
6.0
X
W2 and derivatives
W2
W2(3)
W2(2)
W2(1)

Figure 2(b)

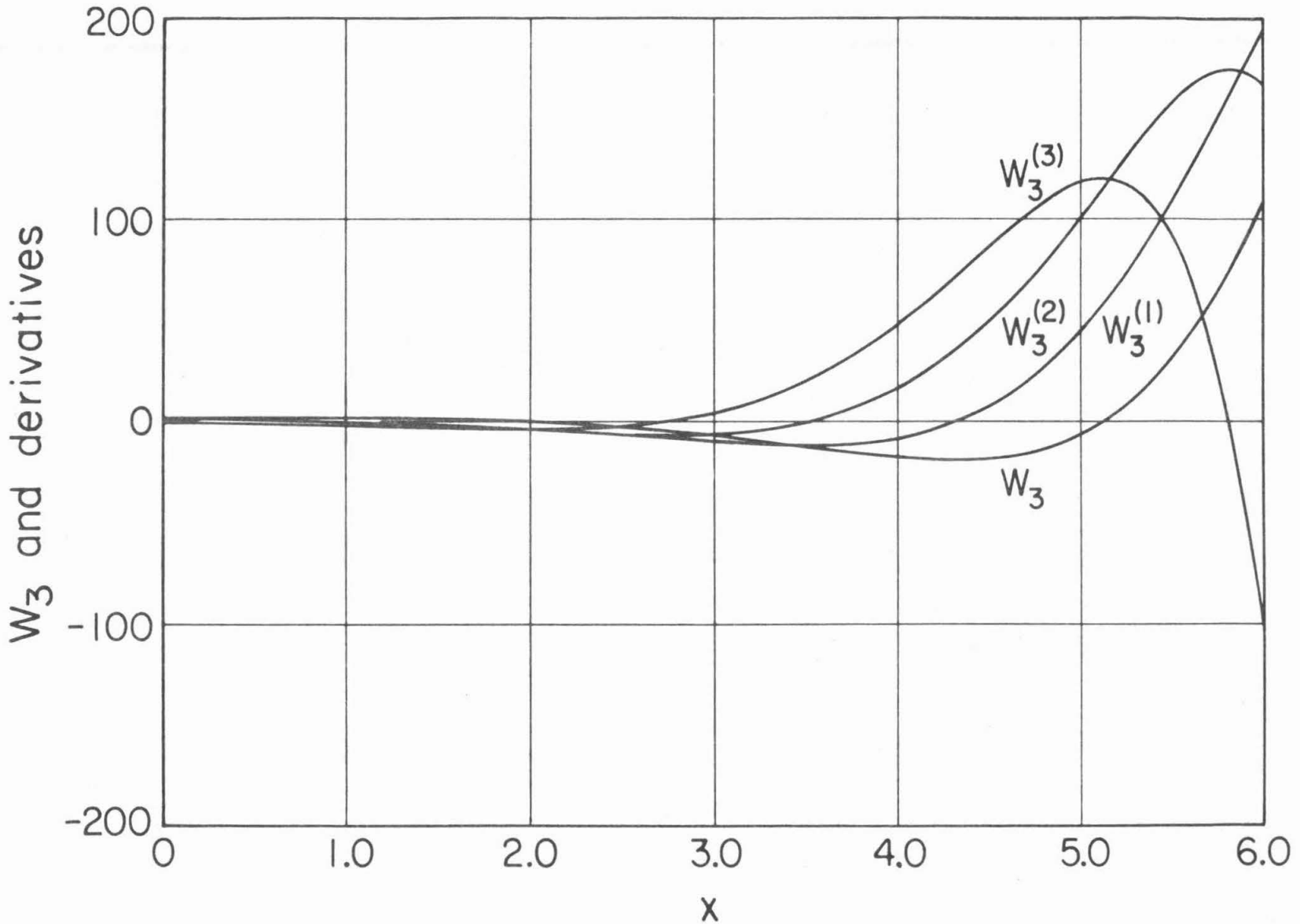
200
100
0
-100
-200
0
1.0
2.0
3.0
4.0
5.0
6.0
X
W3 and derivatives
W3(3)
W3(2)
W3(1)
W3

Figure 3(a)

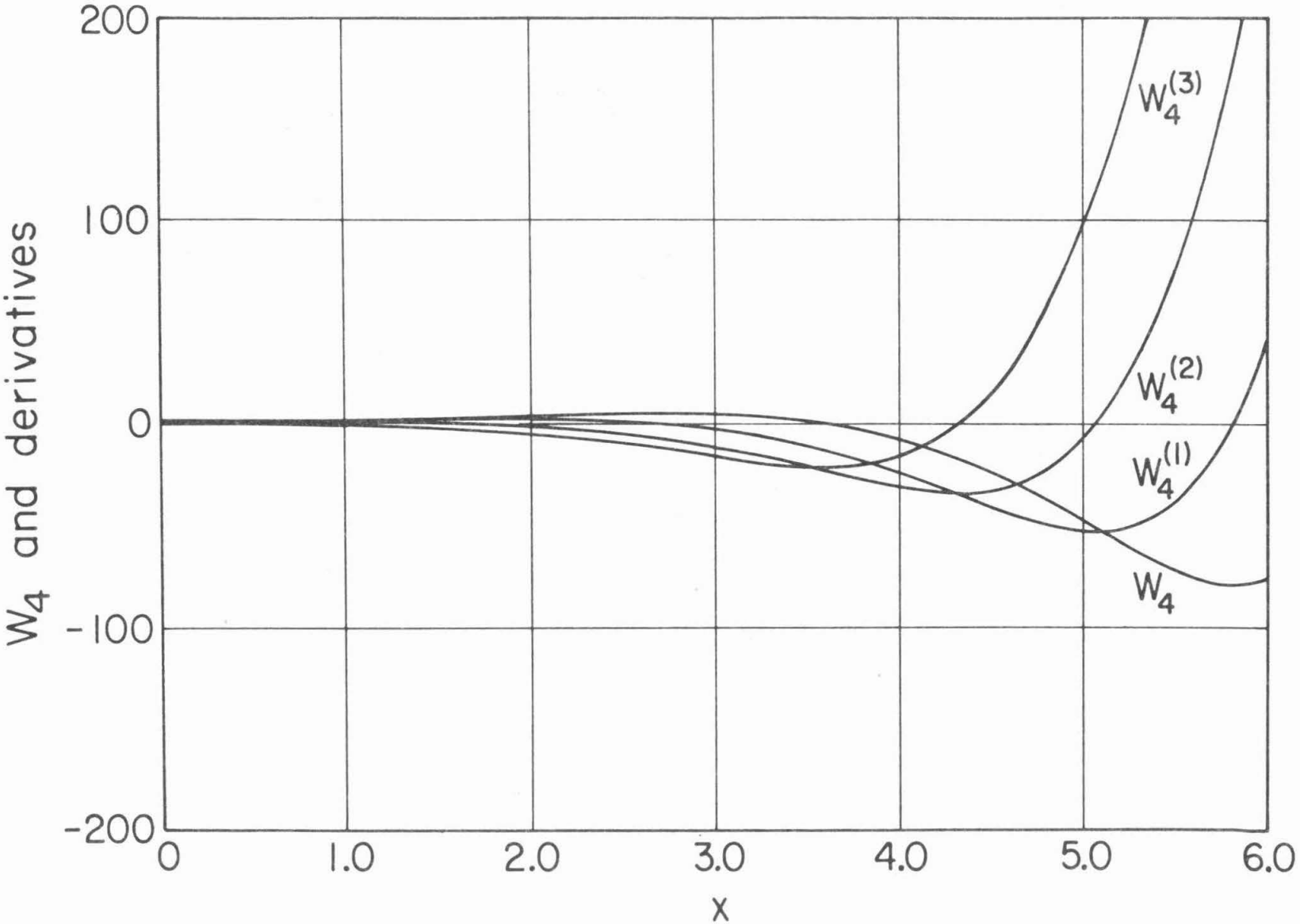
200
100
0
-100
-200
0
1.0
2.0
3.0
4.0
5.0
6.0
X
W4 and derivatives
W4(3)
W4(2)
W4(1)
W4

Figure 3(b)

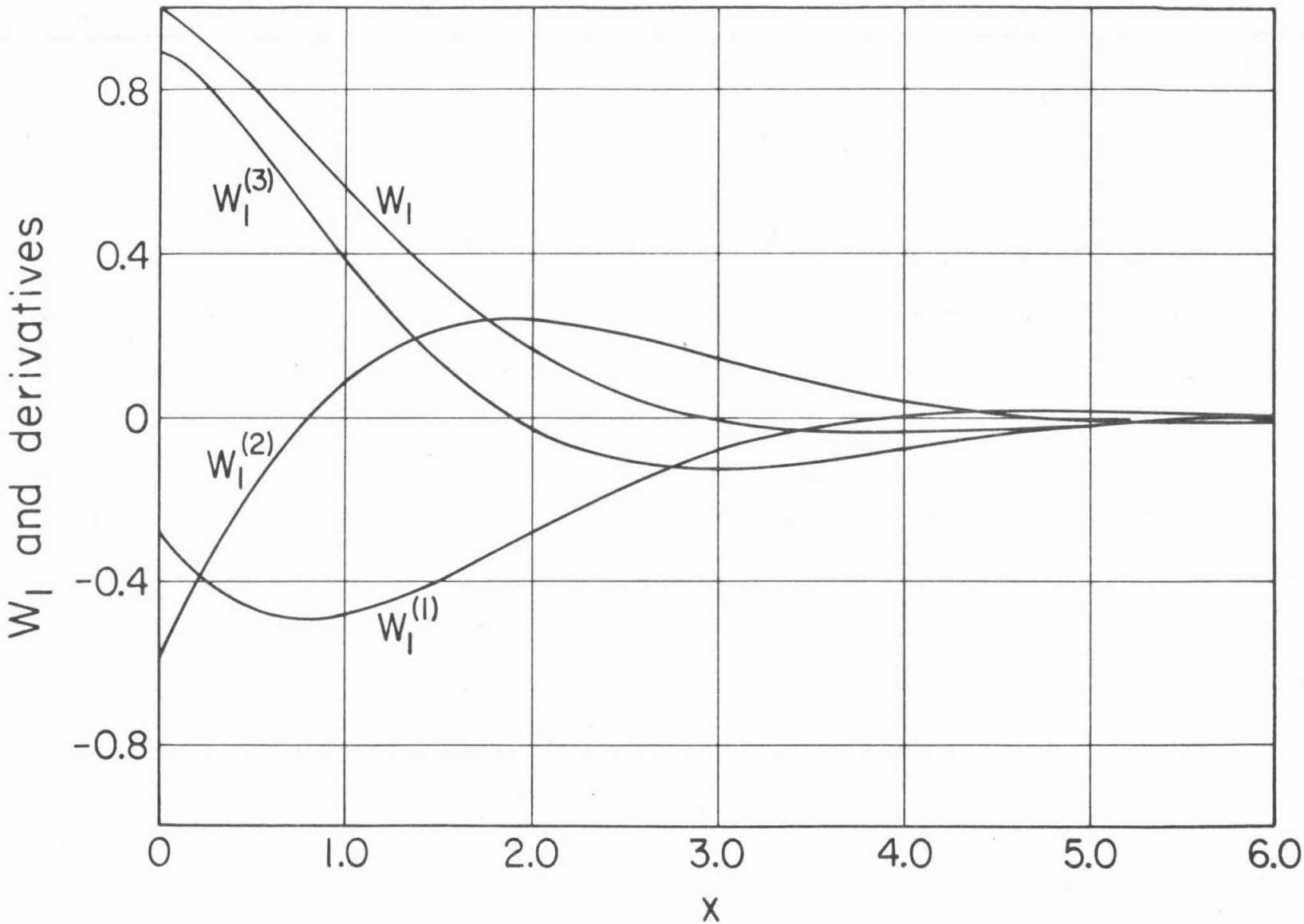
0.8
0.4
0
-0.4
-0.8
W_1 and derivatives
$W_1^{(3)}$
W_1
$W_1^{(2)}$
$W_1^{(1)}$
0
1.0
2.0
3.0
4.0
5.0
6.0
X

Figure 4(a)

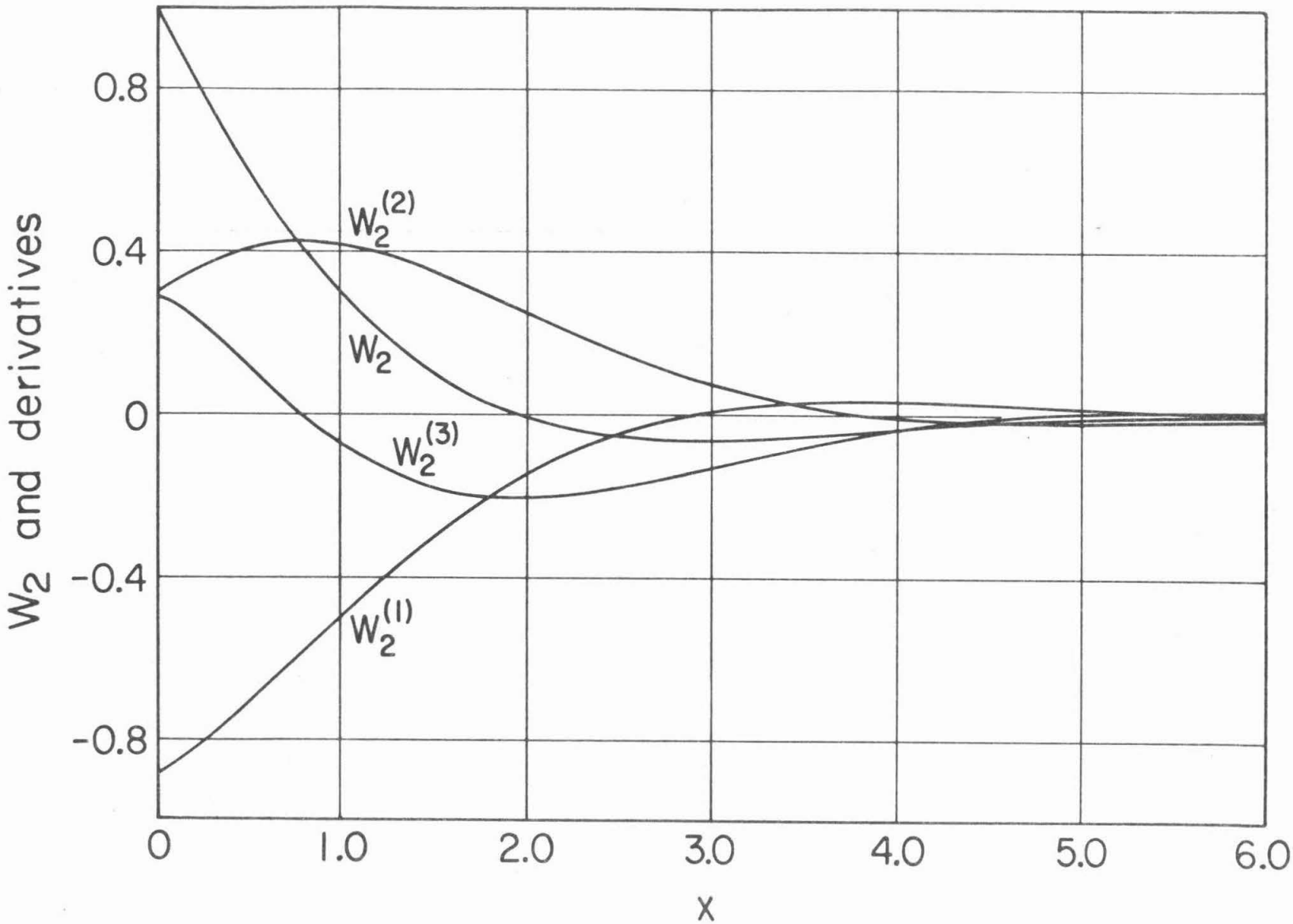
0.8
0.4
0
-0.4
-0.8
W_2 and derivatives
$W_2^{(2)}$
W_2
$W_2^{(3)}$
$W_2^{(1)}$
0
1.0
2.0
3.0
4.0
5.0
6.0
X

Figure 4(b)